Quantum Ergodicity in the Many-Body Localization Problem

Felipe Monteiro de Amorim

Coordenação de Física Teórica

Centro Brasileiro de Pesquísas Físicas

January 2024

"QUANTUM ERGODICITY IN THE MANY-BODY LOCALIZATION PROBLEM"

FELIPE MONTEIRO DE AMORIM

Tese de Doutorado em Física apresentada no Centro Brasileiro de Pesquisas Físicas do Ministério da Ciência Tecnologia e Inovação. Fazendo parte da banca examinadora os seguintes professores:

Tobias Micklitz - Orientador/CBPF

Reinaldo Faria de Melo e Souza – UFF

Thiago Rodrigues de Oliveira – UFF

Marcello Barbosa da Silva Neto – UFRJ

Fernando da Rocha Vaz Bandeira de Melo – CBPF

Rio de Janeiro, 12 de janeiro de 2024.

Acknowledgements

I extend my heartfelt gratitude to my parents, Helena Monteiro and Flávio Amorim, with special mention to my mother, for not only always supporting my (questionable) decision to pursue a career in Physics, but also for all the long-term financial and emotional support that such decision requires.

My life partner, Júlia Sanges, deserves a world of thanks. Júlia has been my rock in all the brightest and darkest moments, always with an open heart and unwavering support. Her joy in my successes, even when I dismissed them as trivial or mere flukes, has been a source of constant encouragement. Whatever I learned during this PhD pales in comparison to what she has taught me about being a loving and kind person.

I am immensely grateful to my supervisor, Tobias Micklitz. Tobias is possibly the best advisor one could hope for. His knowledge and passion for physics are only matched by his willingness to share his expertise. Beyond academic guidance, his valuable advice on career and life has been invaluable. I deeply appreciate his patience and unwavering belief in me.

A special thanks to Fernando de Melo, who not only deepened my understanding of quantum mechanics and quantum information but also showed what an engaging lecture truly looks like.

To my friends—Guilherme Brando, Luiz Filipe, Pedro Caneda, Filipe Batista—thank you for providing the lighter moments of graduate life. The times spent at Bigode, sharing beers and laughter, are certainly among the most cherished memories of this journey.

Lastly, I am thankful to CNPQ for the essential financial support.

Abstract

We investigate the possible existence of a phase of non-ergodic extended states in random many-body systems. On one hand, a direct analysis of the spectral and wave function statistics indicates that there is a wide range of values where the states conform to the classification of 'non-ergodic extended.' However, upon further analysis of the entanglement entropy, we suggest an alternative description where non-localized many-body wave functions remain ergodic in an orthodox sense—uniform coverage of a shell of constant energy in Fock space.

Resumo

Investigamos a possível existência de uma fase de estados estendidos não ergódicos em sistemas de muitos corpos com desordem. Por um lado, uma análise direta das estatísticas espectrais e de função de onda indica que há uma ampla gama de valores onde os estados correspondem à classificação de 'estendidos não ergódicos'. No entanto, após uma análise mais aprofundada da entropia de emaranhamento, sugerimos uma descrição alternativa onde as funções de onda de muitos corpos não localizadas permanecem ergódicas em um sentido ortodoxo—cobertura uniforme de uma casca de energia constante no espaço de Fock.

List of Publications

The following publications form the basis for this thesis. My contributions included implementing and diagonalizing relevant Hamiltonians, analyzing numerical data, and interpreting results along with collaborators. I also participated in discussions on the overall research findings and contributed with writing the text of the papers.

Chapter 4 of this thesis consists of Ref. [1], co-authored with Tobias Micklitz and Alexander Altland.

Chapter 5 consists of Ref. [2], co-authored with Tobias Micklitz, Masaki Tezuka, and Alexander Altland.

Chapter 6 consists of Ref. [3], co-authored with Masaki Tezuka, Alexander Altland, David A. Huse, and Tobias Micklitz.

Table of contents

1 General Introduction **1**

2 Background Material **5**

2.1 Quantum Chaos and Random Matrix Theory 5

2.1.1 Eigenvalue distribution 6

2.1.2 Structure of Many-Body Eigenstates 8

2.1.3 Matrix Elements of Operators 11

2.1.4 Quantum Chaos and Entanglement 12

2.2 Thermalization in Quantum Systems and the Eigenstate Thermalization Hypothesis 13

2.3 Many-body Localization 16

2.4 Non-Ergodic Extended States 17

3 Model and Methods **19**

3.1 The Sachdev-Ye-Kitaev Model 19

3.2 The "extended" SYK Model 20

3.3 Numerical Methods 22

4 Non-ergodic extended states in the SYK model **27**

5 A minimal model of many body localization **33**

6 Quantum ergodicity in the many-body localization problem 53

7 Closing Remarks 61

References 65

Appendix A Supplementary Material to: "Non-ergodic extended states in the SYK model" 69

A.1 SUSY Matrix integral in a nutshell 69

Appendix B Supplementary Material to: "A minimal model of many body localization" 75

B.1 Derivation of the action (**??**) 75

B.2 The operator $\mathcal{P}$ 76

B.3 Saddle point equations 77

B.4 Effective matrix theory 79

B.5 Wave function and spectral statistics from matrix model 81

B.6 Localization criterion 86

Appendix C Supplementary Material to: "Quantum ergodicity in the many-body localization problem" 89

C.1 Entanglement entropy and local density of states 89

C.2 Entanglement entropy in regimes II/III 92

C.3 Exact diagonalization 94

C.4 Generalization 96

Chapter 1

General Introduction

One of the main assumptions in quantum statistical mechanics is that systems are in thermal equilibrium. However, this is far from trivial when considering closed systems, that is, those completely decoupled from a bath. In recent years, there has been a lot of focus on answering the question of what happens to a closed quantum system in the long time limit. Major results find that systems that are not integrable, which we will refer to as generic systems, can fit into two possible cases: those that do, in fact, reach thermal equilibrium, and those that fail to thermalize through many-body localization [4, 5].

Despite existing mathematical proof establishing the stability of the MBL phase in 1d systems [6], possible loopholes in the proof related to the role of correlations allow for some wiggle room. This is reflected in recent controversies surrounding the existence of the MBL phase, and whether the localization transition is observable in numerical simulations or experiments. In [7], the authors argue that, when approaching the transition point from the ergodic side, the critical value for disorder found from numerical simulation scales extensively with system size. If valid, this would imply that the MBL phase is not stable in the thermodynamic limit. However, in [8] the authors warn that one should not extrapolate scaling analysis done deep in the ergodic

regime to strong disorder regimes. For example, they show how a similar analysis as done in [7] but now applied to the well-established Anderson transition in the random regular graph model (a single-particle model that serves as a toy-model for the MBL problem) would lead to a (false) conclusion that the transition does not exist due to the same scaling of the critical disorder with system size.

Another point of contention regarding the localization transition, which we will address in this work, is whether there exists an intermediate phase, sandwiched between the thermal and localized. In this purported intermediate phase, states are extended, like in the thermal phase, but have theirs amplitudes distributed non-ergodically, thus differing from fully thermal states. After two decades since the prediction of many-body localization (MBL), there is still no strong consensus about possible intermediate phases (or regimes) between the MBL and thermal [9–12].

The lack of definitive answers for these questions, much like the rest of theoretical physics, is due to the challenge in treating complex quantum many-body systems, be it analytically, numerically, or experimentally. One reason this option comes into focus only now is that standard tools in diagnosing chaos are too coarse to resolve spatial structure of quantum states in Fock space.

The typical phase diagram obtained numerically for the MBL transition is shown in Fig. 1.1. Here we can see that as disorder strength h increases, the states at all energies ϵ eventually change from the ergodic (dark region in figure) to localized behavior (light region).

One way to try to make progress is to study systems that are complex enough to display the desired properties, but still amenable to analytical and numerical analysis. In this work, we will focus on two modified versions of the Sachdev-Ye-Kitaev (SYK) model [13, 14]. The SYK model, which we will describe in more details further below, is known to be fully ergodic [15–17], so we introduce modifications of the form

$\hat{H} = \hat{H}_2 + \hat{H}_4$, where $\hat{H}_4$ is the regular SYK Hamiltonian, and $\hat{H}_2$ is a term that induces localization. Specifically, we will use two versions of this $\hat{H}_2$ term, each parametrized with some disorder strength parameter h that will control the localization transition. In recent years, the SYK model has become the paradigm for many-body quantum chaos, and has attracted a lot of attention, specially because it can be used to obtain closed form solutions for many questions in strongly interacting systems. This is because the SYK model is a confined many-body system with strong long-range interactions, meaning that all of its single-particle states are coupled, which in turn facilitates analytical treatment of several physical quantities.

Thus, the main question we wish to address is whether wave functions in regimes prior to the onset of strong localization in the modified SYK model satisfy an ergodicity principle. An implication of this purported phase of non-ergodic extended states is that one cannot rely solely on spectral statistics to classify a system as ergodic or localized, in contrast to the common practices in the field. The existence of non-ergodic extended states complicates the use of spectral statistics as a sole tool for classification. Non-ergodic extended (NEE) states are special states that are neither localized nor ergodic, but rather exhibit characteristics of both. They are extended in space, but their dynamics are not completely chaotic, and they can display time-dependent revivals of localization. Further, the distribution of the components of these states differs from the usual distribution for fully ergodic states, which would point to a possible non-ergodicity. However, as we will discuss below, while these NEE states are indeed more localized than regular ergodic states, they are better understood as still being ergodic, albeit in a vanishing fraction of Hilbert space determined by their energy shell.

Additionally, the existence of this intermediate regime could shift the value of the critical disorder necessary to localize the system after finite-size scaling analysis, which could help settle some controversies regarding the MBL phase transition.

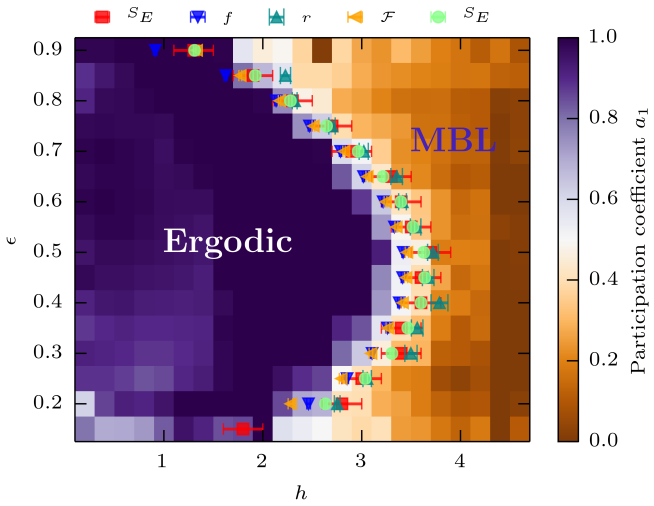

Fig. 1.1 Phase diagram of the random field Heisenberg spin chain. The vertical axis is normalized energy density. Horizontal axis is disorder strength. Figure extracted from ref. [18], see there for more details.

Outline of the thesis

In what follows, we go over some necessary background material in Chapter 2. Then, in Chapter 3, we discuss the models used in the research and some quantities analyzed. Chapters 4, 5, and 6 are a compilation of published papers. Finally, Chapter 7 contains general concluding remarks.

Chapter 2

Background Material

In this chapter, we will provide an overview of the essential background material necessary to understand the main results presented in later chapters. We begin by discussing fundamental results from Random Matrix Theory (RMT) and its connection to quantum chaos, serving as a foundation for our study. Subsequently, we will introduce a more general description of ergodic systems, particularly through the Eigenstate Thermalization Hypothesis (ETH). Finally, we will explore how certain systems can deviate from ETH, with a specific focus on the phenomenon of many-body localization (MBL).

2.1 Quantum Chaos and Random Matrix Theory

Random Matrix Theory (RMT), initially developed by Wigner and subsequently expanded upon by Dyson, was designed to characterize the energy spectra of large, complex atomic nuclei. Since its inception, RMT has evolved into a comprehensive theory, finding applications across various domains in physics, as well as in diverse fields such as mathematics and statistics.

Wigner's original insight was the realization that, rather than attempting to precisely determine the exact energy levels and corresponding eigenstates of a large, complex quantum system, a more pragmatic approach would be to first understand their statistical properties. To develop this statistical model, he proposed that by focusing on states located far from the edges of the spectrum, within a sufficiently small energy window where the density of states remains constant, and by choosing a "generic" basis, the Hamiltonian could be approximated as a matrix with random entries. This approximation rests on the assumption that the matrix has no discernible structure beyond the minimum required by the symmetries inherent to the problem.

When constructing a random matrix, a crucial question to address is the choice of distribution for the matrix entries. Two critical criteria guide this decision. Firstly, the matrix entries should be independent random variables, allowing the joint probability distribution of the matrix to be expressed as a product of individual distributions:

$$p(H) \propto \prod_i p(H_{ii}) \prod_{i<j} p(H_{ij}). \tag{2.1}$$

Secondly, the probability measure $p(H)$ should exhibit rotational invariance, remaining unchanged under similarity transformations of the matrix H. Remarkably, the only distribution that fulfills both these requirements is the Gaussian distribution for the matrix entries. This defines the Gaussian ensemble in RMT, which can then be further classified into three distinct classes: the Gaussian Orthogonal Ensemble (GOE), Gaussian Unitary Ensemble (GUE), and Gaussian Symplectic Ensemble (GSE), each corresponding to different symmetry properties of the system.

2.1.1 Eigenvalue distribution

We now delve into what is arguably the most distinctive feature of RMT systems: their spectral statistics. Our focus will particularly be on the statistical properties of

level spacings, providing insight into the behavior and characteristics of eigenvalue distributions within these systems.

To guide our discussion, consider the case of a 2×2 real symmetric matrix H. The diagonal elements of H follow a Gaussian distribution with zero mean and unit variance. Meanwhile, the off-diagonal elements follow a Gaussian distribution still with zero mean, but now with a variance $1/2$. This choice often simplifies analytical calculations, which will become clear in what follows. The matrix H can thus be written as

$$H = \begin{pmatrix} H_{11} & H_{12} \\ H_{12} & H_{22} \end{pmatrix}. \tag{2.2}$$

The eigenvalues are then

$$\lambda_{1,2} = \frac{H_{11} + H_{22}}{2} \pm \frac{\sqrt{(H_{11} - H_{22})^2 + 4H_{12}^2}}{2}. \tag{2.3}$$

We now wish to find the probability distribution for the difference between the eigenvalues, $s = \lambda_2 - \lambda_1$, where we take $\lambda_2 > \lambda_1$.

$$p(s) = \frac{1}{2\pi^{3/2}} \int_{-\infty}^{\infty} \mathrm{d}H_{11}\, \mathrm{d}H_{22}\, \mathrm{d}H_{12}\, e^{-\frac{H_{11}^2 + H_{22}^2 + 2H_{12}^2}{2}} \delta\left(s - \sqrt{(H_{11} - H_{22})^2 + 4H_{12}^2}\right). \tag{2.4}$$

The integrals can be calculated through a change of variables, yielding

$$p(s) = \frac{s}{2} e^{-\frac{s^2}{4}}. \tag{2.5}$$

This distribution, known as the Wigner-Dyson distribution, characterizes the spacings between energy levels of a matrix sampled from the GOE. One can verify that this

distribution is normalized. Further, it is customary in the literature to rescale this distribution such that the mean level spacing is set to one, $\langle s \rangle = 1$. The distribution then takes the form

$$\bar{p}(s) = \frac{\pi s}{2} e^{-\frac{\pi s^2}{4}}. \tag{2.6}$$

While here we have obtained this results for a 2×2 matrix, it turns out that while there does not exist a closed form solution for finite matrix size N, the result for finite N is qualitatively and quantitatively similar to Eq. (2.5).

One important takeaway from these results is that the eigenvalues of the random matrix are not independent. In fact, they present *level repulsion*, meaning that the probability to find a degenerate energy level is zero.

The same reasoning applies if we now use a Hermitian random matrix, that is, one sampled from the GUE. The normalized distribution for energy spacing, with mean level spacing set to one, now reads

$$p(s) = \frac{32 s^2}{\pi^2} e^{-\frac{4 s^2}{\pi}}. \tag{2.7}$$

Note that for the GUE level repulsion is stronger than for GOE. In comparing the results for GOE and GUE, we can observe a notable difference in their level repulsion. Namely, in the small s limit, the probability for GUE behaves as $p(s) \sim s^2$, and thus displays stronger level repulsion than GOE, where $p(s) \sim s$.

2.1.2 Structure of Many-Body Eigenstates

Due to the invariance of the Gaussian ensemble to unitary transformations, the eigenvectors are only constrained by their normalization. Therefore, it is straightforward to write the joint distribution for their components.

The Gaussian ensemble's invariance under similarity transformations implies that the eigenvectors are solely constrained by normalization. Therefore, we can directly derive their joint distribution. Specifically, if ψ is an eigenvector of H, the joint probability density function of its components ψ_i can be expressed as:

$$P(\psi_1, \psi_2, \ldots, \psi_N) \propto \delta\left(1 - \sum_{i=1}^{N} |\psi_i|^2\right), \tag{2.8}$$

where $\delta(x)$ is the Dirac delta function, ensuring the normalization $|\psi| = 1$. This is a uniform distribution on the unit sphere in $\mathbb{C}^N$. This uniform distribution highlights the lack of preferred direction for the eigenvectors in the high-dimensional complex space, reiterating the fundamental property of unitary invariance in the Gaussian ensemble.

For $N \times N$ within the GUE ensemble, the eigenvectors ψ will generally have complex components. Consequently, the joint distribution for the components ψ_n, $n = 1 \ldots N$, is given by

$$p_{\mathrm{GUE}}\left(\{\psi_n\}\right) = \mathcal{N}\delta\left(1 - \sum_{n=1}^{N} |\psi_n|^2\right), \tag{2.9}$$

where $\mathcal{N}$ is a normalization constant. A convenient change of variables to the amplitudes $y_n = |\psi_n|^2$ simplifies the expression to,

$$p_{\mathrm{GUE}}\left(y\right) = (N-1)(1-y)^{N-2}, \tag{2.10}$$

where we also substituted the value for the normalization constant. Similarly, for matrices within the GOE ensemble, the joint distribution for eigenvector amplitudes $y_n = |\psi_n|^2$ is given by

$$p_{\mathrm{GOE}}\left(y\right) = \frac{1}{\sqrt{\pi}} \frac{\Gamma(N/2)}{\Gamma((N-1)/2)} \frac{(1-y)^{(N-3)/2}}{\sqrt{y}}. \tag{2.11}$$

In both scenarios, the average intensity is $\langle y \rangle = 1/N$. By rescaling to $\eta = yN$ and considering the limit $N \to \infty$, the distributions converge to

$$p_{\mathrm{GUE}}(\eta) = \frac{1}{\sqrt{2\pi\eta}} e^{-\eta/2}, \tag{2.12}$$

$$p_{\mathrm{GOE}}(\eta) = e^{-\eta}. \tag{2.13}$$

These are known as the Porter-Thomas distributions, which describe the behavior of the (squared) components of eigenvectors in RMT. This result is crucial in applications such as quantum chaos, where the distribution of eigenstate components can provide insights into the underlying physical phenomena.

In the previous analysis, we made an implicit assumption about the independence of distinct eigenvectors, treating them as statistically independent. However, this assumption is only an approximation, since eigenvectors corresponding to different eigenvalues of a Hermitian matrix must be orthogonal. Nevertheless, this assumption is justified for large enough dimension N, since orthogonality is the only constraint on the N components. Thus, for two distinct eigenvectors, their inner product will be a random variable with a narrow distribution, converging to zero as $N \to \infty$.

The moments $I_q = \langle y^q \rangle$ of the Porter-Thomas distribution also play an important role in RMT. Specifically, the second moment, known as the inverse participation ratio (IPR), is commonly used as a measure of localization. For ergodic systems, the IPR scales as

$$I_2 = 2N^{-1}, \tag{2.14}$$

where N is the dimension of the Hamiltonian matrix.

It is crucial to note that this scaling behavior is consistent across all generic bases for ergodic systems. On the other hand, localized systems exhibit a different behavior:

there exists a unique basis, the one that diagonalizes the disorder, where the IPR remains constant, not affected by system size. This characteristic serves as marker of localization in such systems.

Note that in what follows we will use N to denote the number of fermions, such that the dimension of Hilbert space is $D = 2^N$. In this case, the IPR can be written as $I_2 = 2N^{-1}$.

2.1.3 Matrix Elements of Operators

For a system described by RMT, we now consider computing the average value of matrix elements for a certain observable O, considering the eigenvectors of the RMT Hamiltonian. Let $\{|\psi^m\rangle, m = 1 : D\}$ be these eigenvectors, with D the Hamiltonian's dimension. We express the ensemble average of the matrix elements of the operator O between eigenvectors m, n as:

$$\langle \langle \psi^m | O | \psi^n \rangle \rangle = \sum_{jk} O_{jk} \left\langle (\psi_j^m)^* \psi_k^n \right\rangle, \tag{2.15}$$

where the average is over the different sets of eigenvectors of matrices in the ensemble. Since different eigenvectors of the same matrix are approximately independent, and eigenvectors of different realization of the matrix are independent, this ensemble averaging process amounts to averaging over the Porter-Thomas distribution Eq. (2.12). We can then show that the expectation value of the product of components j, k of eigenvectors m, n, to first order in $1/D$, is $\left\langle (\psi_j^m)^* \psi_k^n \right\rangle \sim \frac{1}{D} \delta_{mn} \delta_{jk}$. This leads to the following expression for the matrix element of O:

$$\langle \langle \psi^m | O | \psi^n \rangle \rangle = \frac{1}{D} \sum_j O_{jj} \delta_{mn} = \overline{O} \delta_{mn}, \tag{2.16}$$

where we have defined $\overline{O} = \frac{1}{D} \operatorname{tr} O$.

Further, can can obtain the fluctuations around this mean value by considering the variance of the matrix element:

$$\begin{aligned}\langle \langle \psi^m|O|\psi^n\rangle \langle \psi^n|O|\psi^m\rangle\rangle - \langle \langle \psi^m|O|\psi^n\rangle\rangle^2 &= \sum_{jkpq} O_{jk}O_{pq}\left\langle \psi_j^{m*}\psi_k^n\psi_p^{n*}\psi_q^m\right\rangle - \overline{O}^2\delta_{mn} \\ &= \frac{1}{D}\overline{O^2}, \end{aligned} \tag{2.17}$$

where we have used Wick's theorem to rewrite $\left\langle \left|\psi_j^a\right|^4\right\rangle = 2\left\langle \left|\psi_j^a\right|^2\right\rangle$.

Consequently, the matrix elements of any observable within the RMT framework can be written as

$$\langle \psi^m|O|\psi^n\rangle \simeq \overline{O}\delta_{mn} + \sqrt{\frac{\overline{O^2}}{D}}R_{mn}, \tag{2.18}$$

where R_{mn} is a random number, with mean zero and variance equal to one.

Note that the fluctuations around the mean are suppressed by a factor $1/D$, becoming negligible in the thermodynamic limit. Hence, this result should hold for eigenvectors of a single realization of a RMT ensemble, that is a single Hamiltonian, provided the dimension is large enough.

2.1.4 Quantum Chaos and Entanglement

In this section, we now discuss the seminal result by Page [19] regarding the average entanglement entropy in subsystems of ergodic systems. Specifically, that for such systems the entanglement entropy grows with a "volume law" with regard to the subsystem size, in contrast to the "area law" of localized systems. Thus, the character of entropy growth serves as a marker of ergodicity/localization.

Consider a quantum system with Hilbert space dimension D, partitioned into two subsystems, A and B, each with Hilbert space dimensions D_A and $D_{B=D/D_A}$,

respectively. The entanglement entropy of subsystem A is defined as the von Neumann entropy of the reduced density matrix

$$S_A(\rho_A) = -\operatorname{tr} \rho_A \log \rho_A, \quad \rho_A = \operatorname{tr}_B \rho. \tag{2.19}$$

If the whole system is prepared in a pure state, $\rho = |\psi\rangle\langle\psi|$, it is possible to compute the average entropy over all possible initial states

$$\langle S_A \rangle = \log D_A - \frac{D_A}{2D_B}. \tag{2.20}$$

This result shows that when subsystem A is small enough relative to the entire system, $D_A \ll D$, the entanglement entropy closely approximates the thermodynamic microcanonical entropy, $S_{\text{th}} = \log D_A$. This suggests that the complement of subsystem A acts as a thermal bath to A.

2.2 Thermalization in Quantum Systems and the Eigenstate Thermalization Hypothesis

Consider a closed system with $N \gg 1$ degrees of freedom, described by a Hamiltonian H with a discrete energy spectrum, $H|n\rangle = E_n|n\rangle$. We prepare this system in a generic initial state $|\psi(t)\rangle = \sum_n c_n e^{-iE_n t}|n\rangle$, characterized by a mean energy $\langle E \rangle = \sum_n |c_n|^2 E_n$. Here, the term "generic" means that the initial state resides within the bulk of the spectrum, with its energy lying far above the ground state as well as far below the most excited state.

Similar to our prior exploration of RMT, we now consider on the matrix elements of an operator, only now relative to the initial state $|\psi(t)\rangle$. The time-averaged expectation

value of the observable O is given by

$$\begin{aligned}\overline{\langle O\rangle} &= \lim_{t\to\infty}\frac{1}{t}\int_0^t \mathrm{d}\tau\ \langle\psi(\tau)|O|\psi(\tau)\rangle \\ &= \sum_n |c_n|^2 O_{nn},\end{aligned} \tag{2.21}$$

where all the off-diagonal terms average to zero due to the oscillating exponential in the integral—a process known as dephasing.

Conversely, if the system reaches thermal equilibrium, the expectation value of measurements of the observable is given by the microcanonical ensemble,

$$\langle O\rangle_{\text{m.c.}} = \frac{1}{\mathcal{N}}\sum_{E\in\mathcal{S}} O_{nn}. \tag{2.22}$$

where $\mathcal{S}$ is the energy shell $[E, E+\Delta E]$ and $\mathcal{N}$ is the number of states within the shell. Thermalization of a system implies that a system initially prepared in the state $|\psi(t)\rangle$ will evolve, after sufficiently long time, to a state that is properly described by the microcanonical ensemble. For thermalization to be possible, it is then necessary to reconcile equations (2.21) and (2.22). This reconciliation is far from trivial, given that the time-averaged expectation value of the operator is solely determined by the initial state via the coefficients c_n, whereas the microcanonical expectation value depends only on the energy, allowing for several different on-shell initial state configurations being equivalent. Nonetheless, under a set of broad assumptions, it turns out to be possible to reconcile both expressions.

Referring back to the RMT matrix elements result Eq. (2.18), one can verify that for such a scenario, the time average and the microcanonical average are indeed equal, thereby indicating system thermalization. This convergence stems from the structure of the matrix elements in RMT, such that the diagonal elements are constant in time,

$O_{nn} = \overline{O}$. That is, using Eq. (2.18),

$$\overline{\langle O \rangle} = \sum_n |c_n|^2 O_{nn} = \overline{O} \sum_n |c_n|^2 = \overline{O}, \tag{2.23}$$

$$\langle O \rangle_{\text{m.c.}} = \frac{1}{\mathcal{N}} \sum_{E \in \mathcal{S}} O_{nn} = \overline{O} \frac{1}{\mathcal{N}} \sum_{E \in \mathcal{S}} 1 = \overline{O}. \tag{2.24}$$

However, this requirement that the diagonal elements of $\langle \psi^m | O | \psi^n \rangle$ be constant across the whole spectrum is too strict. We are then led to consider a more general expression that nevertheless still satisfies this notion of thermalization through equivalence between time and microcanonical averages. Specifically, it is sufficient to require that the diagonal elements depend smoothly on the energy. This generalization is the known as the Eigenstate Thermalization Hypothesis (ETH) ansatz [20–23], and can be expressed as

$$O_{mn} = \mathcal{O}(\bar{E})\delta_{mn} + \mathrm{e}^{-S(\bar{E})/2} f_O(\bar{E}, \omega) R_{mn}, \tag{2.25}$$

where the parameters are defined as $\bar{E} = (E_m - E_n)/2$, $\omega = E_m - E_n$, and R_{mn} is a Gaussian-distributed random number with zero mean and unit variance. The functions $\mathcal{O}(\bar{E})$ and $f_O(\bar{E}, \omega)$ remain constant within the energy shell, and $S(\bar{E})$ is the thermodynamic entropy. The ETH ansatz extends the RMT result, allowing for variability in the diagonal elements and Gaussian fluctuations in the off-diagonal, thus accommodating a broader class of systems, beyond those described by RMT.

A remarkable feature of ETH is that knowledge of a single eigenstate is sufficient to compute thermal averages, since within the microcanonical energy shell any eigenstate is interchangeable.

As shown, a system that satisfies the ETH evidently thermalizes. However, the converse—that thermalization implies ETH—remains an open question despite substantial numerical evidence. The direct numerical verification of ETH presents compu-

tational challenges because obtaining exact eigenstates for large quantum systems is computationally costly, and thus numerical simulations are limited to relatively small systems sizes, which limits their generalization to the thermodynamic limit.

A useful alternative formulation of the ETH is in terms of subsystems. In this case, the full system is in an eigenstate of energy E_n of the Hamiltonian, $\rho = |n\rangle\langle n|$. The state of a subsystem A is then $\rho_A = \mathrm{tr}_B\, \rho$. If the subsystem A is small enough, then the subsystem B acts as a bath, inducing thermalization in A. In this framework, the ETH implies that the reduced density matrix in the subsystem gets exponentially close to the microcanonical density matrix ρ_{th} in the energy shell defined by the initial state of the whole system.

2.3 Many-body Localization

ETH is not true for a broad class of systems, those that are many-body localized, or many-body localized (MBL). To understand localization in interacting many-body systems, it is helpful to have in mind the picture for single-particle localization.

To advance the discussion to MBL, let us now consider a spin-$\frac{1}{2}$ system,

$$H = \sum_i h_i \sigma_i^z + \sum_{ij} J_{ij} \sigma_i \cdot \sigma_j, \tag{2.26}$$

with h_i static random local field, and the interaction matrix J_{ij} is short range. We are then interested if the many-body eigenstates of this Hamiltonian obey the ETH. For $J = 0$, the many-body eigenstates are simply product states, and the system is fully localized. For finite $J \ll W$, states on different sites do not hybridize, so thermalization does not occur. As we decrease disorder strength W, there is a quantum phase transition in which the system thermalizes and all eigenstates obey ETH.

2.4 Non-Ergodic Extended States

As discussed in the introduction, open questions remain about the MBL transition. In particular, we are interested in the possibility of an intermediate phase. Some work in single-particle Anderson localization on hierarchical lattices points to the existence of a second transition, between ergodic and non-ergodic extended states [9, 12]. This would be a transition at a lower disorder strength than the transition to (non-ergodic) localized states. A single random matrix model that has this behavior is the Rosenzweig-Porter model. It is an ensemble of random Hermitian matrices with off-diagonal entries being random Gaussian numbers with variance $\left\langle H_{ij}^2 \right\rangle = \frac{1}{N^\gamma}$, and diagonal elements are random Gaussian numbers with unit variance. Here γ is the parameter that will control the "disorder strength". At $\gamma \leq 1$, we have regular RMT behavior, for $\gamma \geq 2$, regular Anderson localization. For $1 < \gamma < 2$, non-ergodic extended states.

Chapter 3

Model and Methods

3.1 The Sachdev-Ye-Kitaev Model

In recent years, the Sachdev-Ye-Kitaev (SYK) model quickly rose to become an influential model in research on quantum many-body systems [13, 14]. This rise is due to it being an exactly solvable model, which enables several analytical insights into the dynamics of complex quantum systems. In particular, it has been shown that the SYK model is fully ergodic [17] and equivalent to RMT at long time scales.

The SYK model describes a system of $2N \gg 1$ Majorana fermions χ_i, $\{\chi_i, \chi_j\} = 2\delta_{ij}$, with random all-to-all 4-body interaction. We express the Hamiltonian as

$$H_4 = \frac{1}{4!} \sum_{i,j,k,l=1}^{2N} J_{ijkl} \chi_i \chi_j \chi_k \chi_l, \tag{3.1}$$

where J_{ijkl} are random, Gaussian-distributed coupling constants, with zero mean and variance $\left\langle |J_{ijkl}|^2 \right\rangle = \frac{6J^2}{(2N)^3}$. The constant J defines the bandwidth of the system as $\gamma = (\frac{J}{2})(2N)^{1/2}$.

It is worth noting that when rewriting this Hamiltonian in terms of N complex fermions $\hat{c}_i = \frac{1}{2}(\hat{\chi}_{2i-1} + i\hat{\chi}_{2i})$, it becomes evident that the SYK model does not conserve

particle number. Consequently, the Hamiltonian incorporates terms such as $cccc$ and $c^\dagger c^\dagger c^\dagger c$, along with all possible similar combinations. However, due to the structure of these terms, fermion parity is still conserved. That is, states with even (odd) number of fermion are coupled only to other states with even (odd) number. This non-conservation of particle number, only of parity, is a distinguishing feature, making the SYK model analytically more tractable in contrast to systems with regular fermions.

Regarding other possible discrete symmetries, the SYK model's symmetry class is determined by the number of Majoranas $2N$. Specifically, for N odd, the system belongs to the GUE symmetry class and thus does not have time-reversal symmetry, while for N even it belongs to either GOE or GSE, depending on a certain periodicity modulo 4, and thus is symmetric under time-reversal. For more details, see [17].

3.2 The "extended" SYK Model

In order to investigate possible non-ergodic extended states, we have to include another term which will induce Fock space localization. To this end, we will investigate two possible perturbations. First, we will consider a perturbation H_{2a} which takes the form of a "1 to N" particle potential, where each occupation state $|n\rangle = |n_1, n_2, \ldots, n_N\rangle$, $n_i = 0, 1$ is coupled to every other occupation state through a random potential. Second, we will consider a more physical model, representing a single-particle contribution.

More specifically, for the first model we add to the Hamiltonian a term which is diagonal in Fock space with random coefficients,

$$H_{2a} = \gamma \sum_{n=1}^{2^N} v_n \, |n\rangle\langle n| \,, \tag{3.2}$$

where γ is the energy bandwidth of the SYK model, and the coefficients v_n are drawn from a random distribution. For the distribution in this case, we choose as a uniform

distribution with width Δ, but different choices would yield qualitatively similar results. This parameter Δ then sets the strength of the perturbation in units of the SYK bandwidth, and in the limit $\Delta \gg 1$ it induces localization in Fock space on states with energies v_n.

For the second model, we start from the single-particle Hamiltonian in terms of Majorana fermions,

$$H_{2b} = \sum_{i=1}^{2N} J_{ij}\chi_i\chi_j. \tag{3.3}$$

For the Hamiltonian to be Hermitian, J_{ij} is a random antisymmetric matrix, with elements drawn from a Gaussian distribution with variance $\left|J_{ij}^2\right| = \delta^2/2N$. The matrix iJ_{ij} is diagonalizable, with eigenvalues $\pm v_i$. This allows us to rewrite the Hamiltonian above, as

$$H_{2b} = \sum_{i=1}^{N} v_i\chi_{2i-1}\chi_{2i}. \tag{3.4}$$

This can further be rewritten in terms of regular fermionic operators,

$$H_{2b} = \sum_{i=1}^{N} v_i(2\hat{n}_i - 1). \tag{3.5}$$

The two models introduced, $H_{a/b} = H_4 + H_{2a/b}$, present two contrasting approaches to modifying the SYK model to probe the nature of non-ergodic extended states. Model H_a all-to-all interaction in Fock space provides an analytically simpler starting point to investigate the effects of a localization-inducing disorder on the ergodicity of the SYK model. In contrast, the model H_b retains the flavor of the original SYK model's interactions, simplified to single-particle terms. This model allows for a more physical interpretation of the dynamics and their contributions to the overall behavior of the

system. Together, these models serve as valuable tools for examining the delicate balance between interaction, disorder, and quantum chaos in many-body systems.

3.3 Numerical Methods

To analyze the models outlined above, we employ the exact diagonalization (ED) technique.

Exact diagonalization involves selecting an appropriate Hilbert space basis, expressing the Hamiltonian in its matrix form, and diagonalizing this matrix using standard numerical algorithms.

The ED method yields exact energies and eigenstates without the biases and approximations that other methods, such as Markov Chain Monte Carlo and variational methods, introduce. However, it is worth noting that the "exactness" of ED comes with a significant computational expense. The cost scales as $\mathcal{O}(D^3)$, where D is the dimension of matrix. In quantum systems, the Hamiltonian matrix size often grows exponentially with the particle count. Consequently, ED is typically constrained to smaller systems. As of now, the state-of-the-art for spin chains has a length of the order $L = 50$, although this makes extensive use of the systems symmetries to reduce the Hilbert space dimension [24]. This size limitation restricts the use of ED, especially when we are interested in the behavior of systems in the thermodynamic limit.

Much of the computation cost of ED can be alleviated if, instead of the entire spectrum of the Hamiltonian, we are interested only in the ground state and a few low-lying excitations. In this case, the Lanczos algorithm provides an efficient way to partially diagonalize the matrix, returning only a few energies and eigenstates, with a large gain in computational efficiency. The Lanczos algorithm is an iterative algorithm which leverages matrix-vector multiplication, in place of the more computationally

expensive matrix-matrix multiplication in regular diagonalization, to achieve a more efficient scaling with respect to matrix size.

If we are interested in states deep in the band, an alternative is the shift-invert method [25]. This method consists of defining the operator $G = (\hat{H} - \epsilon\hat{\mathbb{I}})^{-1}$, where ϵ is the target energy and $\hat{\mathbb{I}}$ is the identity matrix. The iterative Lanczos method is then applied to this new operator. This effectively transforms the problem of finding eigenvalues in the interior of the band to the extremal problem of finding the lowest (highest) eigenvalues of the operator G. However, computational efficiency is only gained when one requires just a few eigenpairs near the target energy. For analysis where one requires more eigenpairs, it might still be more efficient to perform full diagonalization.

The choice of basis is crucial, as it determines the complexity of the diagonalization process. Usually, the best approach is to opt for a basis that simplifies the matrix form of the Hamiltonian, for example by making it banded or sparse. This choice might also depend on the particular symmetries present in the system, as well as the physical properties that one wishes to investigate. As it pertains to the models described above, the natural basis to choose is that which diagonalizes the disorder potential, i.e. the H_2 term.

More specifically, in our work, we generate a family of Hamiltonians by fixing one random realization of the disorder potential H_2 and varying the random H_4. We then diagonalize each of these matrices, taking only energies and eigenstates in the center of the band, which we take to mean the middle 1/7th of the spectrum. This is a compromise between selecting a region small enough such that density of states is constant, but large enough such that there are enough states to obtain robust statistics. Taking into account the parity symmetry of the Hamiltonian, we can reorder the labeling of the basis such that the Hamiltonian is block-diagonal. We then split the eigenstates

into the different parity sectors, and treat them as effectively 2^{N-1}-dimensional vectors. This leads to some gain in computational efficiency while not influencing results for wave function statistics, but introducing a subtlety in calculating the entanglement entropy, which we will discuss below. The typical procedure of numerically analyzing spectral statistics involves, for each realization of the Hamiltonian in question, calculating the spacings $s_n = e_{n+1} - e_n$ between adjacent energy levels e_n. By performing these calculations across several realizations of disorder and pooling the resulting spacings, we are able to compile a histogram representing the distribution of spacings.

This distribution is subsequently compared with the theoretical distributions associated with ergodic or localized systems—specifically, the Wigner-Dyson or Poisson distributions, respectively [26]. This comparison serves as a conventional methodology for determining whether a system resides in one phase or the other, typically by assessing how well the numerical level statistics align with the anticipated distributions.

However, this seemingly straightforward calculation conceals a layer of complexity. The fluctuations in the level spacing derive from two distinct sources: a global dependence on energy density and local fluctuations in the energy levels [27]. To distinguish these contributions, it is necessary to "unfold" the spectrum, which involves normalizing the local level spacing by the average level spacing at a given energy. This unfolding process is non-trivial and has the potential to introduce additional finite-size effects.

A more convenient alternative was proposed by Oganesyan and Huse [28], who introduced an analysis based on the ratio of neighboring spacings, $r_n = s_n/s_{n-1}$. This ratio is advantageous as it circumvents the need for spectral unfolding, thereby enhancing the precision of statistical tests applied to the spectrum. It is worth noting that while the distribution of spacing ratios $P(r)$ for ergodic (localized) systems exhibits

quantitative differences from the conventional Wigner-Dyson (Poisson) distribution, qualitative similarities persist [29].

In our work, we chose to quantitatively compare the numerical and theoretical distributions for spacings ratio using the Kullback-Leibler divergence, defined as

$$D_{\mathrm{KL}}(P \parallel Q) = \sum P(r) \log\left(\frac{P(r)}{Q(r)}\right), \tag{3.6}$$

where $P(r)$ is the distribution obtained from the numerical histogram of spectrum data, and $Q(r)$ is the expected distribution for ergodic or localized systems. For wave function statistics, we exploit the parity symmetry inherent in the Hamiltonian to perform block-diagonalization, resulting in two distinct sets of eigenvectors. Each set corresponds to either even or odd parity and has a reduced dimension of 2^{N-1}. To further improve statistics, we can treat both sets of eigenvectors as different independent samples.

Upon gathering all the eigenvectors from various realizations of the Hamiltonian under investigation, we proceed to compute the second moment in order to obtain the inverse participation ratio (IPR), $\sum_n |\psi_n|^4$. The IPR serves as a measure of the localization of the wave functions.

We are particularly interested in observing how the IPR changes with varying strengths of disorder in the system. This analysis could potentially reveal transition points or regimes where the behavior of the system shifts, providing valuable information about the underlying physics of the system. The computation of the entanglement entropy involved calculating the reduced density matrix and the average entanglement entropy of eigenstates situated at the center of the energy band of the composite Hamiltonian $\hat{H} = \hat{H}_2 + \hat{H}_4$. The entanglement entropy was averaged across eigenstates that corresponded to energy levels within the central 1/7th of the spectrum. In the same way as for wave function statistics, the eigenstates of even and odd fermion

parity were considered as an independent samples. Considering the density matrix ρ defined by an eigenstate, which has definite parity, the partial trace leads to a block diagonal structure $\rho_A = \mathrm{tr}_B\, \rho = \begin{pmatrix} \rho^e_A & \\ & \rho^o_A \end{pmatrix}$, with matrices ρ^o_A and ρ^o_A acting in even and odd parity subspaces of subsystem A Hilbert space. A trace over the two-dimensional parity sector defines the normalized reduced density matrix $\mathrm{tr}_\mathrm{P}\, \rho_A = \rho^e_A + \rho^o_A$. This parity-traced density matrix then has the same entropy as the reduced density matrix of a pure state in the 2^{N-1} system with broken fermion parity conservation. This can be verified by comparing our results in the fully ergodic phase to Page's prediction for a Fock space of Dimension $D = 2^{N-1}$. We further improve the statistics by averaging over all $\binom{N}{N_A}$ Fock space bi-partitions.

Chapter 4

Non-ergodic extended states in the SYK model

The following consists of a reproduction Ref. [1], co-authored with Tobias Micklitz and Alexander Altland.

Nonergodic Extended States in the Sachdev-Ye-Kitaev Model

T. Micklitz and Felipe Monteiro
Centro Brasileiro de Pesquisas Físicas, Rua Xavier Sigaud 150, 22290-180, Rio de Janeiro, Brazil

Alexander Altland
Institut für Theoretische Physik, Universität zu Köln, Zülpicher Str. 77, 50937 Cologne, Germany

(Received 13 January 2019; revised manuscript received 28 April 2019; published 18 September 2019)

We analytically study spectral correlations and many body wave functions of a Sachdev-Ye-Kitaev model deformed by a random Hamiltonian diagonal in Fock space. Our main result is the identification of a wide range of intermediate coupling strengths where the spectral statistics is of Wigner-Dyson type, while wave functions are nonuniformly distributed over Fock space. The structure of the theory suggests that such manifestations of nonergodic extendedness may be a prevalent phenomenon in many body chaotic quantum systems.

DOI: 10.1103/PhysRevLett.123.125701

Introduction.—In recent years, classifications of many body quantum systems as either "ergodic" or "many body localized" (MBL) have become mainstream. This reflects the discovery of a growing number of systems supporting MBL phases [1–12] and naturally extends the distinction between single particle ergodic and Anderson localized systems to many body quantum disorder. However, recently, we are seeing mounting evidence [13–21] that the above dichotomy may be too coarse to capture the complexity of chaotic many body systems. Specifically, recent work has put the focus on the study of statistical properties of many body wave functions. It has been reasoned that, sandwiched between the extremes ergodic and many body localized, there might exist intermediate phases of nonergodic extended (NEE) states, i.e., quantum states different from localized in that they have unbounded support, and different from ergodic in that their amplitudes are not uniformly distributed. One reason why this option comes into focus only now is that standard tools in diagnosing chaos—spectral statistics applied to systems of small size of $\mathcal{O}(10^1)$ physical sites—are too coarse to resolve the spatial structure of quantum states in Fock space. Indeed, the above indications are indirect in that they are based on numerical and analytic work on disordered graphs with high coordination numbers, artificial systems believed to share key characteristics with genuine random Fock spaces. The complexity of the matter shows in that, even for this synthetic system, there is a controversy between work suggesting an NEE phase [13–16] and other refuting it [17].

In this Letter, we present a first principles analytic description of NEE states in a deformed version of the Sachdev-Ye-Kitaev (SYK) model [22,23]. The standard SYK model is a system of $2N \gg 1$ Majorana fermions, $[\chi_i, \chi_j]_+ = 2\delta_{ij}$, governed by the interaction Hamiltonian

$$\hat{H}_0 = \frac{1}{4!}\sum_{i,j,k,l=1}^{2N} J_{ijkl}\hat{\chi}_i\hat{\chi}_j\hat{\chi}_k\hat{\chi}_l, \tag{1}$$

where the coupling constants are drawn from a Gaussian distribution, $\langle |J_{ijkl}|^2\rangle = 6J^2/(2N)^3$, and the constant J defines the effective bandwidth of the system as $\gamma = (J/2)(2N)^{1/2}$ [24]. The model (1) is known to be in an ergodic phase with eigenfunctions uniformly distributed in Fock space [24,25]. To make the situation more interesting, we generalize the Hamiltonian to $\hat{H} = \hat{H}_0 + \hat{H}_V$, where

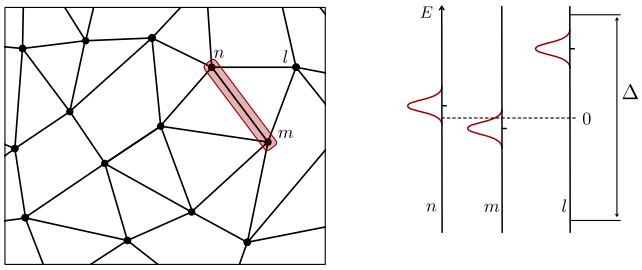

FIG. 1. Left: Cartoon of Fock space sites $n, m, l, \ldots$ (indicated by dots) connected by hopping operator $\mathcal{P}$ (solid lines). For $\Delta \gg 1$ exceeding the bandwidth of the unperturbed model, one may approach the problem perturbatively, i.e., taking the isolated eigenstates of levels v_n, v_m, v_l as a starting point. The hybridization leads to level broadening κ of resonant neighbors (indicated by hatched link) which have both energies v_n, $v_m \lesssim 1$ within the SYK band. Right side: Typical energy distributions of Fock-space neighbors connected by $\mathcal{P}$. The hybridization does, in general, not generate overlap between neighboring sites. For $\Delta < N^2$ wave functions are thus extended ($\rightarrow$ Wigner-Dyson statistics) yet confined to only a fraction $\sim 1/\Delta^2$ of the total Fock space.

$$\hat{H}_V = \gamma \sum_n^D v_n |n\rangle\langle n|, \tag{2}$$

is a sum over projectors onto the occupation number eigenstates $|n\rangle = |n_1, n_2, \ldots, n_N\rangle$, $n_i = 0, 1$, of a system of complex fermions $c_i = \frac{1}{2}(\chi_{2i-1} + i\chi_{2i})$, $i = 1, \ldots, N$ defined via the Majorana operators. The coefficients v_n can be chosen to represent any operator diagonal in the occupation number basis $\{|n\rangle\}$ pertaining to a fixed one-body basis. For example, any one-body operator [26,27] $\hat{H}_0 = \frac{1}{2}\sum_{i,j} J_{ij}\hat{\chi}_i\hat{\chi}_j$ can be diagonalized in the fermion representation and described in this way. However, for our discussion below it will be sufficient to consider realizations of maximal entropy with coefficients v_n drawn from a box distribution of width Δ symmetric around zero. In this way Δ sets the effective strength of the coupling in units of the SYK bandwidth, and in the limit of asymptotically large Δ enforces Fock space localization in states n with energies v_n. The Hamiltonian $\hat{H}_0$ perturbs this "Poisson limit" via transitions $|n\rangle \to |m\rangle$ between states nearby in Fock space. (The two-body $\hat{H}_0$ changes the occupation of a state $|n\rangle$ by at most four, and it preserves the number parity, where we focus on even parity states throughout.) It does so via only an algebraically small number $\sim N^4 \sim \ln(D)$ of independent matrix elements, and thus defines an operator with strong statistical correlation. However, we will see that $\hat{H}_0$ is very efficient in introducing many body chaos, as evidenced by the onset of Wigner-Dyson (WD) spectral statistics, including for values $\Delta \gg 1$, where the diagonal still dominates. Our main objective is to explore the profile of the many body wave functions in this setting.

Qualitative picture.—Before turning to the quantitative analysis of the problem, let us outline an intuitive picture of nonergodic wave function statistics. Let us work in dimensionless units, where the SYK bandwidth $1 \sim JN^{1/2}$ is set to unity, or $J \sim N^{-1/2}$. Consider a situation where the strength of the diagonals $\Delta \sim N^\alpha$, $\alpha > 0$ parametrically exceeds the bandwidth. In this case, we have a situation where the "hopping" in Fock space induced by the SYK Hamiltonian does not effectively hybridize the majority of the $\sim N^4$ states, $m, l, \ldots$, neighboring a given n, cf. Fig. 1. With the characteristic hopping amplitude $t \sim JN^{-3/2} \sim N^{-2}$, a self-consistent golden rule argument may be applied to estimate the residual smearing κ of n as $\kappa \sim |t|^2 [N^4(\kappa/\Delta)](1/\kappa) \sim (1/\Delta) \sim N^{-\alpha}$, where the term in parentheses is the number of neighbors that are in resonance, and $\sim\kappa^{-1}$ is the broadened energy denominator. The effective hybridization of two nearest neighbors requires overlap of their smeared levels, a condition satisfied only by a fraction $(\kappa/\Delta) \sim \Delta^{-2}$ of neighbors. From this argument we infer that typical wave functions occupy only a number $D/\Delta^2 \sim D/N^{2\alpha}$ of the available D sites in Fock space. We also note that for $N^4/\Delta^2 = N^{4-2\alpha} \sim 1$ the number of resonant neighboring levels becomes of $\mathcal{O}(1)$. This is when we expect the wave functions to fragment and a transition to the Poisson regime to take place.

Matrix integral representation.—To obtain a more quantitative picture, we start from a first quantized representation, where the Hamiltonian $\hat{H}$ is considered as a sparse matrix acting in a huge Fock space. This perspective is complementary to that of the more conventional many body $G\Sigma$ formalism [22] probing the physics of collective fluctuations close to the ground state. Formulated in this language, the problem becomes one of random matrix diagonalization and methods such as the powerful supersymmetry technique, originally designed to solve single particle hopping problems, become applicable. Specifically, the occupation number basis $\{|n\rangle\}$ plays a role analogous to the position basis of a fictitious quantum state and $\hat{H}_0$ and $\hat{H}_V$ act as hopping and "on-site potential" Hamiltonians, respectively. Within the first quantized approach, information on the statistics of the many body wave functions $|\psi\rangle$ at the band center, $\epsilon_\psi = 0$ (generalization to generic energies is straightforward but omitted for simplicity), is contained in the matrix elements of the resolvent, $G^{\pm}_{nn'} = \langle n| \pm i\delta - \hat{H})^{-1}|n'\rangle$. Specifically, the qth moment is defined as $I_q \equiv (1/\nu_0)$ $\sum_n \langle |\langle\psi|n\rangle|^{2q}\delta(\epsilon_\psi)\rangle$, where $\langle\ldots\rangle$ denotes averaging over the randomness in the model, and $\nu_0 = \langle\sum_\psi \delta(\epsilon_\psi)\rangle$ is the density of states in the band center. Using the eigenfunction decomposition $G^+_{nn} = \sum_\psi |\langle\psi|n\rangle|^2(i\delta - \epsilon_\psi)^{-1}$, this can be expressed as $I_q = -(1/\pi\nu_0)\lim_{\delta\to 0}(2i\delta)^{q-1}$ $\sum_n \mathrm{Im}G^+_{nn}G^{+(q-1)}_{nn}$ [28], where the last equality relies on the absence of degeneracies $E_\psi \neq E_{\psi'}$, for $\psi \neq \psi'$ in a disordered system. (For completeness, we apply the same setup to compute the eigen*value* statistics and diagnose Wigner-Dyson or Poisson statistics. See Supplemental Material [29] for details.) Our principal workhorse in computing the realization average of these expressions is an exact integral representation $\langle I_q\rangle = \partial_\beta\partial_\alpha^{q-1}\int dY e^{-S(Y,\alpha,\beta)}$. Here, the integration variables $Y = \{Y^{ss',\sigma\sigma'}_{nn'}\}$ are $2\times 2\times D$-dimensional matrices which on top of the Fock space index n contain an index $s, s' = \pm$ labeling advanced and retarded states, and a two-component index $\sigma, \sigma' = \mathrm{b}, \mathrm{f}$ distinguishing between commuting (Y^{bb}, Y^{ff}) and Grassmann valued (Y^{bf}, Y^{fb}) matrix blocks [31]. This "supermatrix structure" [29] is required to cancel unwanted fermion determinants appearing in the computation of purely commuting or anticommuting matrix integrals. (We cannot use replicas to achieve determinant cancellation because the analysis will involve one nonperturbative integration, not defined in the replica formalism.)

Referring for a derivation of the above integral, and the discussion of the source parameters α, β required to generate the wave function moments to the Supplemental Material [29], the action $S(Y) \equiv S(Y, 0, 0)$ of the field integral is given by

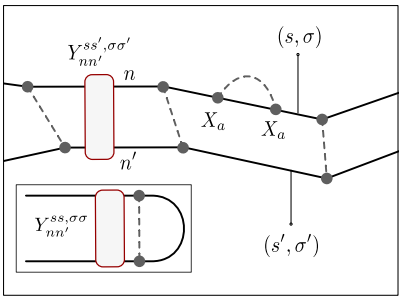

FIG. 2. The scattering of wave function amplitudes in Fock space. Variables $Y^{ss',\sigma\sigma'}_{nn'}$ describe the correlated propagation of resolvents (solid lines) labeled by a conserved index (s,σ). Scattering processes (indicated by dots) can be distinguished into those dressing propagators by "self energies" (dashed lines connecting same resolvent) and vertex contributions (dashed lines connecting different resolvents). Hatched regions summarize repeated, ladder-diagrams of vertex contributions and define the slow modes in the system. Inset: Self consistency equation for self-energy Eq. (4).

$$S(Y) = -\frac{1}{2}\mathrm{STr}(Y\mathcal{P}^{-1}Y) + \mathrm{STr}\ln(i\delta\sigma_3 - \hat{H}_V + i\gamma Y), \qquad (3)$$

where $\mathrm{STr}(X) \equiv \sum_{n,s,\sigma}(-)^{\sigma}X^{ss,\sigma\sigma}_{nn}$ is the canonical trace operation for supermatrices [32]. To understand the structure of the action, notice that the Green functions describe the propagation of wave functions subject to random scattering in Fock space. Contributions surviving the configuration average are correlated as indicated in Fig. 2. The first term in the action describes how the pair amplitudes $Y^{ss',\sigma\sigma'}_{n,n'}$ represent the propagation of two such states, specified by a doublet of indices (n,s,σ) and (n',s',σ'). It is defined by an operator $\mathcal{P}$, which acts as $\mathcal{P}Y \equiv (1/\mathcal{N})\sum_a X_a Y X_a^{\dagger}$, where $\mathcal{N} = \binom{2N}{4}$, i.e., the multiplication of the two states represented by Y by the Majorana product operators contained in the Hamiltonian, where $X_a \equiv \chi_i\chi_j\chi_k\chi_l$, and the shorthand $a = (i,j,k,l)$ is used. The second term couples the Y matrices to the fermion propagator effectively describing the propagation in between SYK-scattering events, where $(\sigma_3)^{ss'} = (-)^s\delta^{ss'}$ does the bookkeeping on causality.

Stationary phase approach.—Our strategy is to evaluate the matrix integral by stationary phase methods backed by excitation gaps present in the limit $\delta \to 0$. The structure of the action suggests looking for solutions of the stationary phase equations $\delta_{\bar{Y}}S(\bar{Y}) = 0$ diagonal in Fock space $Y_{nn'} = Y_n\delta_{nn'}$. Physically, this restriction means that for a fixed realization of the diagonals $v_n \neq 0$ phase coherence of the pair propagation requires $n = n'$ in the representation of Fig. 2. The stationary phase equation then assumes the form

$$Y_n = i\sum_m \Pi_{nm}\frac{1}{i\frac{\delta}{\gamma}\sigma_3 - v_m + iY_m}, \qquad (4)$$

where the projection of the pair-scattering operator $P_d\mathcal{P}P_d \equiv \Pi$ on the space of diagonal matrix configurations acts on diagonal configurations as $(\Pi X)_n = \sum_m \Pi_{nm}X_m = (1/\mathcal{N})\sum_{a,m}|(\hat{X}_a)_{mn}|^2X_m$. The solution of the equation now essentially depends on the structure of this operator. We first note that the operators $\hat{X}_a$ change at most four of the N binary occupation numbers contained in n, implying that Π is a local hopping operator in the space of n states. The permutation symmetry inherent to the sum over all configurations $a = (i,j,k,l)$ further implies that the hopping strengths $\Pi_{nm} = \Pi_{|n-m|}$ depend only on the occupation number difference between Fock space states, where a straightforward counting procedure yields $\Pi_0 = N(N-1)/2\mathcal{N}$, $\Pi_2 = 4(N-2)/\mathcal{N}$, and $\Pi_4 = 16/\mathcal{N}$, and all other matrix elements vanish. Armored with this result, we interpret the right-hand side (r.h.s.) of the mean field equation Eq. (4) as a sum over a large number of terms, which are effectively random due to the presence of the coefficients v_m. In this way, $Y_n(v)$ becomes a random variable depending on the realizations $v = \{v_m\}$.

The structure of the mean field equation, and the transition rates Π_{nm} identifies the components Y^{ss}_n as the self energies dressing the retarded $(s = +)$ and advanced $(s = -)$ Fock space propagators (also cf. inset of Fig. 2.). The solutions Y_n are obtained as sums over large numbers of random contributions, which for small Δ implies a self averaging property $Y_n \simeq \langle Y_n\rangle_v \equiv Y_0$, where the r.h.s. denotes the average over the independent distribution over v_m. Ignoring the imaginary part of Y_n (which does no more than inducing a weak shift $v_n \to v_n + \mathrm{Im}Y_n \simeq v_n$ of the random energies), and averaging v over a box distribution $\langle\ldots\rangle_v = \prod_m\int_{-\Delta/2}^{\Delta/2}(dv_m/\Delta)(\ldots)$, we obtain $Y_0 = \kappa\sigma_3$, where the self energy κ obeys the equation $\kappa = (2/\Delta)\arctan(\Delta/2\kappa)$. The solution smoothly interpolates between $\kappa \simeq 1$ for the weakly perturbed model $\Delta \ll 1$ and $\kappa \simeq \pi/\Delta$ for $\Delta \gg 1$. In accordance with the qualitative discussion above, this decay reflects that for $\Delta \gg 1$ the majority of sites neighboring a fixed n are off resonant and decouple from the self energy. We also note that the averaged density of states $\nu_0 = -\mathrm{Im}\langle\mathrm{tr}(G^+)\rangle = D\kappa/\pi\gamma$ shows the same behavior. Before proceeding, let us ask when the above approximations break down and the stationary solutions become strongly fluctuating in the sense $\mathrm{var}(Y_n) > Y_0^2$. Assuming that $Y_m \simeq Y_0$ on the r.h.s. of Eq. (4), a straightforward calculation leads to $\mathrm{var}(Y_n) \simeq (10\pi/N^4\kappa^2)\mathcal{F}(\Delta/2\kappa)$, where $\mathcal{F}(x)$ is a function monotonically increasing from $\mathcal{F}(0) = 0$ to $\mathcal{F}(x) = \mathcal{O}(1)$ at $x \sim 1$ before decaying as $\mathcal{F}(x) \sim 1/x$ at $x \gg 1$ [33]. A balance $\mathrm{var}(Y_n) \sim Y_0^2$ is reached when $\kappa^2 \sim \Delta^{-2} \sim (1/N^4\kappa^2)(\kappa/\Delta) \sim N^{-4}$, where $\kappa \sim \Delta^{-1}$ was used. This shows that only for disorder strength $\Delta > \Delta_P \sim N^2$ parametrically larger than the bandwidth, the homogeneity of the stationary phase configuration in Fock space gets compromised. This observation is one of the most

important results of this Letter. As we will demonstrate in the following, it provides the basis for the analytical extraction of wave functions and spectra.

Wave function statistics.—In the limit $\delta \to 0$, $Y_0 = \kappa\sigma_3$ is but one element of a manifold of stationary solutions, $Y_0 = \kappa T\sigma_3 T^{-1} \equiv \kappa Q$, where $T = \{T^{ss',\sigma\sigma'}\}$ is a 4×4 rotation matrix in advanced-retarded and super space. The absence of Fock-space indices implies $[\mathcal{P}, Q] = 0$, which in combination with $Q^2 = \mathbb{1}$ means that the first term in Eq. (3) is independent of T. We conclude that the stationary phase action of the matrix integral is given by

$$S[Q] = \mathrm{STr}\,\ln(i\delta\sigma_3 - \hat{H}_V + i\gamma\kappa Q). \tag{5}$$

This action is known to describe [34] the Rosenzweig-Porter (RP) model [35]: a D-dimensional Gaussian random matrix ensemble perturbed by a fixed diagonal, $\hat{H}_V$. We thus conclude that for diagonals with $\Delta < \Delta_P$ the deformed SYK model and this much simpler model are in the same universality class. The first step of the computation of the wave function statistics [34] based on Eq. (5) is the integration over the matrix T. This integration is not innocent, because the 2×2 block T^{bb} defines a noncompact integration manifold [32]. The convergence of the corresponding integral is safeguarded only by the infinitesimal symmetry breaking parameter $i\delta$, and integration over T [29] indeed produces a singular factor δ^{-q+1} canceling the δ dependence in the definition of the wave function moments, and leading to the result

$$I_q = \frac{q!}{\nu_0^q}\sum_n \langle \nu(n)^q\rangle_v, \qquad \nu(n) \equiv \frac{\nu_0}{D(v_n^2+\kappa^2)}. \tag{6}$$

Intuitively, the r.h.s. contains the qth moments of local Green's function matrix elements, with energy denominators broadened by the self energy κ. It is straightforward to average this expression over the box distribution of the individual v_n and obtain

$$I_q = -(-2)^q q D^{1-q}\partial_{y_0^2}^{q-1}(1/y_0\Delta)\arctan(\Delta/2y_0). \tag{7}$$

For $\Delta \ll 1$ smaller than the SYK bandwidth, this asymptotes to the random matrix result $I(q) = q!(D/2)^{1-q}$, demonstrating a uniform state distribution. In the opposite case, $\Delta \gg 1$, $y_0 = \pi/\Delta$ and the moments $I_q = (2\pi^2)^{1-q}q(2q-3)!!\Delta^{2(q-1)}D^{1-q}$, show power law scaling in Δ. Finally, for $\Delta \sim N^\alpha$ the wave functions become nonergodic $I_q \sim [D/N^{2\alpha}]^{1-q}$, and now only occupy a $\sim 1/N^{2\alpha}$ fraction of Hilbert space, in line with the qualitative discussion above. In Fig. 3, these predictions are compared to wave function moments obtained by exact diagonalization for $N = 13$ as a function of the deformation parameter (main panel), or as a function of system size $N = 7, \ldots, 13$ at fixed deformation (lower left panel).

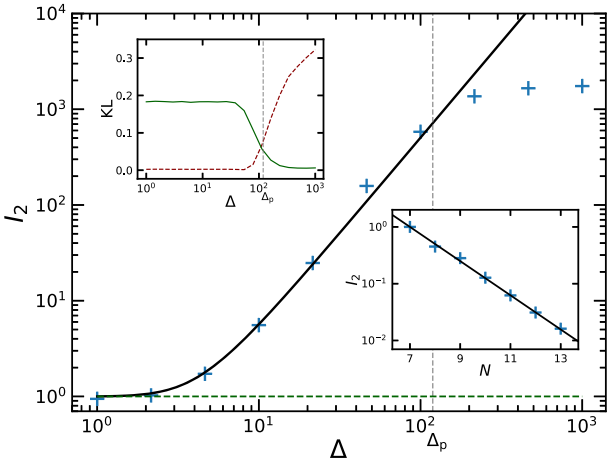

FIG. 3. Inverse participation ratio as a function of Δ, normalized by $I_2(\Delta = 0)$, from exact diagonalization $N = 13$; the analytical prediction Eq. (7) is indicated by the solid line. Left inset: Relative entropy (Kullback-Leibler) between numerical and Wigner Dyson (dashed), respectively, Poisson (solid) distributions. Right inset: Inverse participation ratio as a function of N, normalized by $I_2(N = 7)$, from exact diagonalization at $\Delta = 10$; solid line is the analytical prediction from Eq. (7) [36].

The figure demonstrates excellent, and parameter free agreement with the analytic result.

The figure also confirms the statement that throughout the entire window $\Delta < \Delta_P$, or $0 \le \alpha < 2$, the spectral statistics remains Wigner-Dyson like. This is probed by comparing the relative, or Kullback-Leibler entropies [37] $\mathrm{KL}(p|q) \equiv \sum_k p_k \ln(p_k/q_k)$ between the numerically obtained moments q_k and the Wigner-Dyson, or Poisson distribution p_k, respectively. The upper inset of Fig. 3 shows that the change between the two statistics takes place at the deformation strength analytically predicted as $\Delta \sim \Delta^P \simeq 120$, beyond which both saturation of the wave function moments [36], and the level statistics indicate Poissonian behavior.

Conceptually, the robustness of spectral correlations follows from the equivalence (SYK $\overset{\Delta<\Delta_P}{\sim}$ RP), the latter being a model demonstrating the strong resilience of a single random matrix against perturbations on its diagonal. The domain of the above equivalence is limited by both the deformation strength of SYK $\Delta \lesssim N^2$, and the width of the probed spectrum $\epsilon \lesssim \delta N^2$, where δ is the many body level spacing [38]. Outside this window, for $\Delta \gtrsim N^2$, the theory predicts a fragmentation of the Fock space homogeneous mean field (equivalent to the fluctuations of a single random matrix ensemble) into inhomogeneous stationary configurations, $\kappa \to \kappa_n$. On the background of this inhomogeneous configuration one may construct a lattice field theory that indeed predicts a Fock space localization transition at $\Delta \sim \Delta_P$ [39]. Finally, models of the perturbation different from the identically distributed v_n, lead to similar results. Specifically, a random one-body

term, $\hat{H}_1 \equiv \sum_{j=1}^{N} \eta_{2j-1}\eta_{2j} v_j$ is equivalent to $\hat{H}_V$ with statistically correlated $v_n(\{v_j\})$. Referring to Ref. [39] for details, this leads to similar scaling over a slightly higher tolerance window, $\Delta_P \lesssim N^{9/4}$.

Summary and discussion.—The model considered in this Letter defines the perhaps simplest many body system showing a competition between Fock space localization and ergodicity. We are seeing unambiguous evidence that the passage between the two limits is not governed by a single many body localization transition but contains a parametrically extended intermediate phase characterized by a coexistence of Wigner-Dyson spectral statistics and non-trivial extension of wave functions over Fock space. Methodologically, this phenomenon emerged as the result of a competition: the hopping in Fock space generated by the SYK two-body interaction stabilized a uniform mean field against the "localizing" tendency of the Fock-space diagonal operator $\hat{H}_v$. We have identified an intermediate regime, where the corresponding low energy theory is governed by a homogeneous fluctuation mode T_0, acting on top of a background containing inhomogeneous energy denominators. This mechanism appears to be of a rather general nature and makes one suspect that nonergodic wave function statistics in coexistence with random matrix theory spectral correlations could be a more frequent phenomenon than previously thought.

Discussions with D. Bagrets, A. Kamenev, and H. Wang are gratefully acknowledged. T. M. and F. M. acknowledge financial support by Brazilian agencies CNPq and FAPERJ. Work funded by the Deutsche Forschungsgemeinschaft (DFG, German Research Foundation)—Projektnummer 277101999—TRR 183 (project A03).

[1] D. Basko, I. Aleiner, and B. Altshuler, Ann. Phys. (Amsterdam) **321**, 1126 (2006).
[2] I. V. Gornyi, A. D. Mirlin, and D. G. Polyakov, Phys. Rev. Lett. **95**, 206603 (2005).
[3] V. Oganesyan and D. A. Huse, Phys. Rev. B **75**, 155111 (2007).
[4] I. L. Aleiner, B. L. Altshuler, and G. V. Shlyapnikov, Nat. Phys. **6**, 900 (2010).
[5] M. Pino, L. B. Ioffe, and B. L. Altshuler, Proc. Natl. Acad. Sci. U.S.A. **113**, 536 (2016).
[6] G. Stolz, New J. Phys. **18**, 031002 (2016).
[7] M. Znidaric, T. Prosen, and P. Prelovsek, Phys. Rev. B **77**, 064426 (2008).
[8] A. Pal and D. A. Huse, Phys. Rev. B **82**, 174411 (2010).
[9] A. De Luca and A. Scardicchio, Europhys. Lett. **101**, 37003 (2013).
[10] C. L. Baldwin, C. R. Laumann, A. Pal, and A. Scardicchio, Phys. Rev. B **93**, 024202 (2016).
[11] J. Z. Imbrie, Phys. Rev. Lett. **117**, 027201 (2016); J. Stat. Phys. **163**, 998 (2016).
[12] I. V. Gornyi, A. D. Mirlin, D. G. Polyakov, and A. L. Burin, Ann. Phys. (Berlin) **529**, 1600360 (2017).
[13] A. De Luca, B. L. Altshuler, V. E. Kravtsov, and A. Scardicchio, Phys. Rev. Lett. **113**, 046806 (2014).
[14] V. E. Kravtsov, I. M. Khaymovich, E. Cuevas, and M. Amini, New J. Phys. **17**, 122002 (2015).
[15] B. L. Altshuler, E. Cuevas, L. B. Ioffe, and V. E. Kravtsov, Phys. Rev. Lett. **117**, 156601 (2016).
[16] V. E. Kravtsov, B. L. Altshuler, and L. B. Ioffe, Ann. Phys. (Amsterdam) **389**, 148 (2018).
[17] K. S. Tikhonov and A. D. Mirlin, Phys. Rev. B **99**, 024202 (2019).
[18] L. Faoro, M. Feigel'man, and L. Ioffe, arXiv:1812.06016.
[19] E. J. Torres-Herrera and L. F. Santos, Ann. Phys. (Berlin) **529**, 1600284 (2017).
[20] G. Biroli, A. C. Ribeiro-Teixeira, and M. Tarzia, arXiv:1211.7334.
[21] G. Biroli and M. Tarzia, arXiv:1810.07545.
[22] S. Sachdev and J. Ye, Phys. Rev. Lett. **70**, 3339 (1993).
[23] A. Kitaev, *Proceedings at KITP, 2015*, http://online.kitp.ucsb.edu/online/entangled15/kitaev/, http://online.kitp.ucsb.edu/online/entangled15/kitaev2/.
[24] A. M. García-García and J. J. M. Verbaarschot, Phys. Rev. D **94**, 126010 (2016).
[25] J. S. Cotler, G. Gur-Ari, M. Hanada, J. Polchinski, P. Saad, S. H. Shenker, D. Stanford, A. Streicher, and M. Tezuka, J. High Energy Phys. 05 (2017) 118; H. Gharibyan, M. Hanada, S. H. Shenker, and M. Tezuka, J. High Energy Phys. 07 (2018) 124.
[26] A. M. García-García, B. Loureiro, A. Romero-Bermúdez, and M. Tezuka, Phys. Rev. Lett. **120**, 241603 (2018).
[27] A. R. Kolovsky and D. L. Shepelyansky, Eur. Phys. Lett. **117**, 10003 (2017).
[28] F. Wegner, Z. Phys. B **35**, 207 (1979).
[29] See Supplemental Material at http://link.aps.org/supplemental/10.1103/PhysRevLett.123.125701 where we give details on the derivation of the matrix integral representation, the calculation of wave function and level statistics, and which includes Refs. [30].
[30] A. D. Mirlin, Phys. Rep. **326**, 259 (2000).
[31] We here consider values $2N = 2, 6 \bmod 8$ where the SYK model is in the unitary symmetry class [24]. The description of other cases requires 8-dimensional integration matrices reflecting the symmetry of the orthogonal or symplectic symmetry class, respectively.
[32] K. B. Efetov, *Supersymmetry in Disorder and Chaos* (Cambridge University Press, Cambridge, England, 1999).
[33] The precise definition is $F(x) = [2/\pi(1+x^2)] + (2/\pi x)\arctan(x) - (4/\pi x^2)\arctan^2(x)$, and we used that $\sum_m \Pi_{nm}^{-2} \simeq 42/N^4$.
[34] K. Truong and A. Ossipov, Europhys. Lett. **116**, 37002 (2016).
[35] N. Rosenzweig and C. E. Porter, Phys. Rev. **120**, 1698 (1960).
[36] With $N = 13$, $\kappa \simeq \pi/\Delta$, and the identification $\kappa^2 = (20\pi/N^4\kappa\Delta_P)$ stated above we obtain $\Delta_P \simeq (169\pi/\sqrt{20}) \simeq 119$.
[37] S. Kullback and R. A. Leibler, Ann. Math. Stat. **22**, 79 (1951).
[38] A. Altland and D. Bagrets, Nucl. Phys. **B930**, 45 (2018).
[39] A. Altland and T. Micklitz (in preparation).

Chapter 5

A minimal model of many body localization

The following consists of a reproduction Ref. [2], co-authored with Tobias Micklitz, Masaki Tezuka, and Alexander Altland.

Minimal model of many-body localization

F. Monteiro and T. Micklitz
Centro Brasileiro de Pesquisas Físicas, Rua Xavier Sigaud 150, 22290-180 Rio de Janeiro, Rio de Janeiro, Brazil

Masaki Tezuka
Department of Physics, Kyoto University, Kyoto 606-8502, Japan

Alexander Altland
Institut für Theoretische Physik, Universität zu Köln, Zülpicher Straße 77, 50937 Cologne, Germany

(Received 29 June 2020; accepted 3 December 2020; published 8 January 2021)

We present a fully analytical description of a many-body localization (MBL) transition in a microscopically defined model. Its Hamiltonian is the sum of one- and two-body operators, where both contributions obey a maximum-entropy principle and have no symmetries except Hermiticity (not even particle number conservation). These two criteria paraphrase that our system is a variant of the Sachdev-Ye-Kitaev model. We will demonstrate how this simple zero-dimensional system displays numerous features seen in more complex realizations of MBL. Specifically, it shows a transition between an ergodic and a localized phase, and nontrivial wave-function statistics indicating the presence of nonergodic extended states. We check our analytical description of these phenomena by a parameter-free comparison to high performance numerics for systems of up to $N = 15$ fermions. In this way, our study becomes a test bed for concepts of high-dimensional quantum localization, previously applied to synthetic systems such as Cayley trees or random regular graphs. The minimal model describes a many-body system for which an effective theory is derived and solved from first principles. The hope is that the analytical concepts developed in this study may become a stepping stone for the description of MBL in more complex systems.

DOI: 10.1103/PhysRevResearch.3.013023

I. INTRODUCTION

Quantum wave functions subject to strong static randomness may show nonergodic localized behavior. To date, we distinguish between two broad universality classes of quantum localization: Anderson localization [1] in low-dimensional single-particle systems and many-body localization (MBL) in random many-particle systems [2,3]. In principle, there is no fundamental distinction between these two. They both reflect the lack of ergodicity of wave functions on random lattices due to massive quantum interference. However, the all important difference is that the lattice structure is defined in the former case by a low-dimensional solid and in the latter by the high-dimensional Fock-space lattice formed by the occupation number states of a many-particle system.

Many-body localization is traditionally discussed in the context of spatially extended many-body systems, such as interacting quasi-one-dimensional electron systems [2,3] or random spin chains [4–13]. However, that spatial extension is an added layer of complexity to a problem that manifests itself already in spatially confined geometries: a competition between hopping and randomness on the complex lattice structure defined by an interacting particle problem. In fact, there appears to be a paradigm shift in the field away from studying the quantum critical phenomena of the localization transition in extended systems towards manifestations of MBL in systems of mesoscopic extension, such as interacting quantum dots [14–18], small-size optical lattices [19–21], or small-size superconducting qubit arrays [22,23]. This development is driven in part by pragmatism. The explosion of Fock-space dimensions with increasing system size makes numerical access infamously hard and classical computers may never be powerful enough to probe the scaling regime of the MBL transition with sufficient reliability. Another motivation lies in the fascinating and only partly understood physics of localization in many-body systems of intermediate size.

At this point, even basic aspects of MBL remain enigmatic, including in small-size systems. Among these, one of the most controversial topics concerns the presence or absence of a phase of nonergodic but extended (NEE) states intermediate between the regime of ergodic wave functions at weak and localized wave functions at strong disorder. If existent, such a phase must be born out of the main principles distinguishing MBL from low-dimensional Anderson localization: the high coordination number of Fock space lattices, the strong correlation of their disorder potentials, and the sparsity of the hopping matrix elements in Fock space (see the next section for a more detailed discussion). Reflecting the complexity of the problem, the physics of NEE states is often discussed for

synthetic [24–28] or phenomenological models [29], sidestepping one or several of the above complications. (However, even for these, the existence of NEE phases is discussed controversially.)

Clearly, a numerically and analytically solvable minimal model defined by a microscopic Hamiltonian would provide an important contribution to our understanding of MBL. It would provide a test bed for the validity of analytical approaches by comparison to numerical diagonalization and might turn into a building block in the study of more complex systems. In this paper we report on the definition and solution of such a system. Here the term "solution" refers to the following: (a) the construction of an *effective* theory of the microscopically defined system by parametrically controlled approximation, (b) the computation of observables (many-body wave function and spectral statistics) from that theory, and (c) parameter-free comparison to numerics. In this hierarchy, the perhaps most important element is (a). The effective theory we derive assumes the form of a matrix path integral in Fock space; see Eq. (40) for an impression. From this representation, observables can be extracted by powerful methods developed in the localization theory of high-dimensional lattices. [For a pioneering previous comparison between analytical and numerical results for a concrete model system we refer to Ref. [30]. However, that work was based on scaling theory for a specific class of observables. Lacking element (a), it did not have the scope of the present analysis.]

The model we consider is implicitly defined by the following criteria: Its Hamiltonian $\hat{H} = \hat{H}_2 + \hat{H}_4$ contains the sum of a one-body and a two-body part. Both are maximally entropic and have no symmetries besides Hermiticity (not even particle number conservation). In the noninteracting case $\hat{H}_4 = 0$, the product eigenstates of $\hat{H}_2$ define a basis in which the system is trivially localized. The Hamiltonian $\hat{H}_4$ acts as a hopping operator and at a critical strength will induce a many-body localization transition. In a manner detailed in the next section, the criteria listed above state that $\hat{H}$ is the Majorana Sachdev-Ye-Kitaev (SYK) Hamiltonian.

The maximum-entropy criterion makes the SYK model much simpler than MBL systems with spatial extension. At the same time, it displays a wealth of phenomena characteristic of MBL. Foremost among these is a change from delocalized to localized behavior. For finite N, this is a crossover. However, the exponential dependence of the Fock-space lattice extension on N implies that it rapidly acquires signatures of a transition as N increases. Second, the model supports a regime (not a phase) of NEE states prior to the onset of localization. We will discuss how the diminishing support of these states upon approaching the transition reflects the structure of the system's Fock space and how this differs from phenomenological models. However, the most important point of all is that the spectral and wave-function statistics of the model can be computed analytically and that these results can be numerically tested in a parameter-free comparison. The analytical approach is based on matrix integral techniques imported from the theory of high-dimensional random lattices. We apply these techniques subject to a number of assumptions which should generalize to other many-body systems of small spatial extension and/or a high degree of connectivity. We therefore hope that the approach discussed in this paper may become a stepping stone for the solution of more complex manifestations of MBL.

Plan of the paper. In the next section we introduce our model system, qualitatively discuss its physics, and summarize our main results. The remaining parts of the paper discuss the derivation of these findings, where we try to keep the technical level at a bare minimum. In Sec. III we map the computation of disorder-averaged correlation functions onto that of an equivalent matrix integral. In Sec. IV a stationary-phase approach is applied to reduce the matrix integral to an effective theory describing physics at large timescales. In Secs. V and VI we apply this representation to the discussion of wave-function statistics and the localization transition, respectively. We conclude in Sec. VII with a discussion comparing our results to those obtained for other models and on possible generalizations to other MBL systems. Technical parts of our analysis are relegated to a number of Appendixes.

II. MODEL AND SUMMARY OF RESULTS

In this section we first introduce the SYK model and then discuss its physics of quantum localization in qualitative terms. Much of this outline is formulated in general terms which should carry over to similar models. In the remaining parts of the section we get more concrete and summarize our results in comparison to numerics.

A. The SYK model

The SYK Hamiltonian [31,32]

$$\hat{H}_4 = \frac{1}{4!}\sum_{i,j,k,l=1}^{2N} J_{ijkl}\hat{\chi}_i\hat{\chi}_j\hat{\chi}_k\hat{\chi}_l \tag{1}$$

describes a system of $2N$ Majorana fermions $\{\hat{\chi}_i, \hat{\chi}_j\} = 2\delta_{ij}$, subject to an all-to-all interaction, with matrix elements $\{J_{ijkl}\}$ drawn from a Gaussian distribution of variance $\langle|J_{ijkl}|^2\rangle = 6J^2/(2N)^3$. Defined in this way, it defines an ideal of a massively interacting quantum system lacking any degree of internal structure. Due to the least information principle realized through the stochastic interaction, all single-particle orbitals i stand on equal footing and the absence of a continuous U(1) symmetry prevents the fragmentation of the Fock space into sectors of conserved particle number. Reflecting these features, the physics of the SYK Hamiltonian at large timescales becomes equivalent to that of random matrix theory (RMT), with wave functions homogeneously distributed over the full Hilbert space.

A tendency to Fock-space localization is included by adding to $\hat{H}_4$ a free-particle contribution [33,34]

$$\hat{H}_2 = \frac{1}{2}\sum_{i,j=1}^{2N} J_{ij}\hat{\chi}_i\hat{\chi}_j, \tag{2}$$

with a likewise random antisymmetric matrix $J_{ij} = -J_{ji}$, with matrix elements $\{J_{ij}\}$ drawn from a Gaussian of variance $\langle|J_{ij}|^2\rangle = \delta^2/2N$. Without loss of generality, we may assume $\{J_{ij}\}$ to be diagonalized into a form $\hat{H}_2 = i\sum_i^N v_i\hat{\chi}_{2i-1}\hat{\chi}_{2i}$, where $\pm v_i$ are the eigenvalues of the Hermitian matrix $i\{J_{ij}\}$.

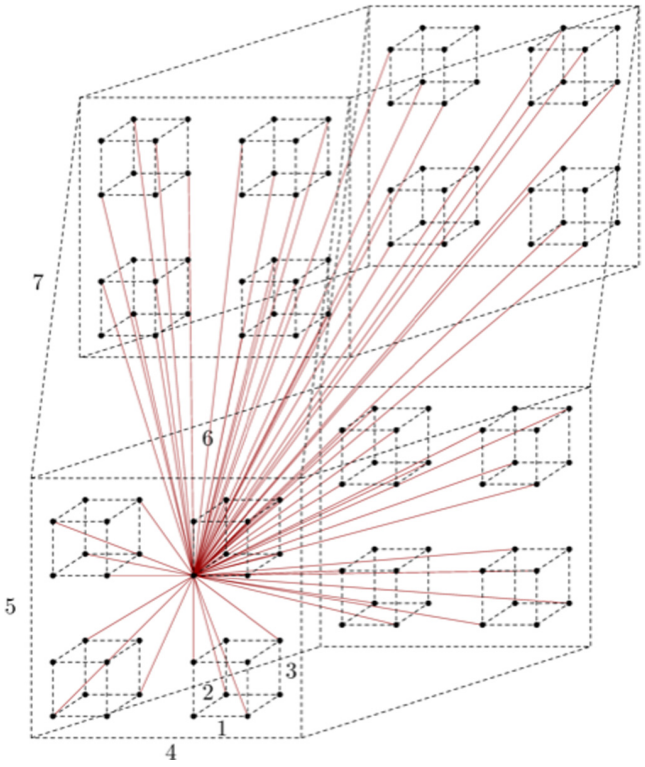

FIG. 1. Hypercubical Fock space of a $2N = 14$ Majorana system. The numbers indicate the bit depth of states in the computational fermion basis and the lines are a qualitative representation of the connectivity of the reference state $|0, 0, 0, 1, 1, 0, 0\rangle$. For large values of N, the pattern of connections becomes sparse. However, there remain exponentially many, proportional to D connections, statistically correlated due to the small number, order of N^4, independent random amplitudes.

For the above distribution of the matrix elements J_{ij} these eigenvalues are random numbers with variance order of δ.

We next translate from the Majorana many-body Hamiltonian formulation to one in terms of a fermion Fock space (lattice). To this end, we define N complex fermion annihilation operators $\hat{c}_i = \frac{1}{2}(\hat{\chi}_{2i-1} + i\hat{\chi}_{2i})$ satisfying $\{\hat{c}_i, \hat{c}_j^\dagger\} = \delta_{ij}$. With the number operators $\hat{n}_i = \hat{c}_i^\dagger \hat{c}_i$, we then have

$$\hat{H}_2 = \sum_{i=1}^{N} v_i(2\hat{n}_i - 1), \quad \text{var}(v_i) = \delta^2. \tag{3}$$

Representing this Hamiltonian in the basis of 2^N occupation number states $|n\rangle = |n_1, n_2, \ldots, n_N\rangle$, $n_i = 0, 1$, it assumes the form of a random potential $v_n = \sum_i v_i(2n_i - 1)$ on the hypercube defined by all sites $n = (\ldots, 0, 0, 1, 0, 0, 1, 0, \ldots)$.[1] In the same basis, the interaction $\hat{H}_4$ assumes the role of a fermion number conserving hopping operator $\hat{H}_4$ connecting sites of bit separation 2 and 4.[2] This hopping introduces a complex connectivity pattern on the two decoupled sublattices of definite (even, say) parity, containing

$$D = 2^{N-1} \tag{4}$$

sites each. Figure 1 illustrates this structure for a Fock space of 14 Majorana fermions. The lines indicate the states connected to the arbitrarily chosen site $|0, 0, 0, 1, 1, 0, 0\rangle$. Notice the high coordination number and the absence of lattice periodicity, symptomatic for this and for other Fock-space lattices. The competition between the localizing random potential $\hat{H}_2$ and the delocalizing hopping $\hat{H}_4$ defines the MBL problem, regardless of their detailed realization.

B. Qualitative discussion

In this section we discuss the physics of the above random system in qualitative terms. Specific topics include the existence of a localization-delocalization transition, its signatures in spectral and wave-function statistics, and a regime of nonergodically extended states. Most parts of this discussion do not make specific reference to the SYK model and should equally apply to other systems.

The single most important system quantity relevant to the understanding of the above observables at a specific energy, say, E, is the local density of states in Fock space

$$\nu_n \equiv -\frac{1}{\pi}\text{Im}\left\langle \langle n| \frac{1}{E^+ - \hat{H}_2 - \hat{H}_4} |n\rangle \right\rangle_J, \tag{5}$$

where $E^+ \equiv E + i\epsilon$ and $\langle \cdots \rangle_J$ indicates that we consider ν_n averaged over realizations of $\hat{H}_4$, but at a single realization of $\hat{H}_2$. (The discussion above shows that the large coordination number of the lattice makes ν_n a largely self-averaging quantity. Averaging over $\hat{H}_4$ is largely a matter of technical convenience.) From the perspective of site n, the large number of nearest neighbors represents an environment and on this basis one expects a Lorentzian profile

$$\nu_n = \frac{1}{\pi}\frac{\kappa_n}{\nu_n^2 + \kappa_n^2}, \tag{6}$$

where we have set $E = 0$ for definiteness and the broadening $\kappa_n = \kappa_n(\Delta_4, \delta, \alpha)$ must be self-consistently determined [cf. Eq. (32) below] in dependence on the following parameters: (a) the many-body band width Δ_4 of the interaction operator ($\Delta_4 = \sqrt{J^2 N/2}$ for the SYK Hamiltonian $\hat{H}_4$),[3] (b) the disorder strength δ or, equivalently, the distribution width Δ_2 of the on-site random potential (3) (for large N, the central-limit theorem implies $\Delta_2 = \delta N^{1/2}$),[4] and (c) the number order of N^α of nearest neighbors m connected to Fock-space

[1] Although the eigenvalues $\{\pm v_i\}$ of J_{ij} are correlated, their sums, i.e., the eigenvalues of $\hat{H}_2$, become uncorrelated for large N.

[2] For two states $|n\rangle$ and $|m\rangle$ we define the Hamming distance $|n - m|$ as the number of bits in which the states differ. Containing four fermion creation/annihilation operators and conserving fermion number parity, the matrix elements of the interaction operator couple states of Hamming distance 0, 2, and 4.

[3] Here we ignore corrections of $O(\frac{1}{N})$. However, for numerically accessible sizes it is important to keep in mind the full expression for the H_4 band width $\Delta_4 = \sqrt{\frac{3J^2}{4N^3}\binom{2N}{4}}$.

[4] In order to compare the analytical predictions with numerical results without any fitting parameters it is important to use the full expression for the H_2 band width $\Delta_2 = \sqrt{\frac{\delta^2}{2N}\binom{2N}{2}}$.

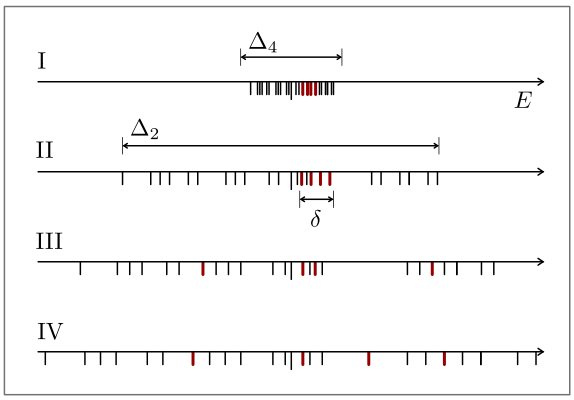

FIG. 2. Four regimes I–IV of increasing disorder strength. The band width Δ_4 of the interaction operator is shown in comparison to the band width of the on-site randomness Δ_2. The distance between neighboring levels is order of $\delta = \Delta_2 N^{-1/2}$ and the relative magnitude of these scales defines the regimes discussed in the text.

sites n by the interaction $\hat{H}_4$ ($\alpha = 4$ for the SYK Hamiltonian). On this basis, we must distinguish between four regimes of qualitatively different level hybridization κ (see Fig. 2).

Regime I: $\delta < \Delta_4 N^{-1/2}$. In this regime, the $\hat{H}_2$ band width $\Delta_2 < \Delta_4$ is below that of $\hat{H}_4$. The on-site randomness is largely irrelevant and states are ergodically spread over the full Fock-space lattice. Hybridization of levels over the full Δ_4 band width implies $\kappa_n = \Delta_4$.

Regime II: $\Delta_4 N^{-1/2} < \delta < \Delta_4$. The $\hat{H}_2$ band width Δ_2 exceeds Δ_4, implying that the majority of sites become inaccessible. States of fixed energy now populate only a fraction of Hilbert-space sites. However, for a given site with energy v_n inside the accessible window Δ_4, the hopping nearest neighbors have accessible energy $v_n \pm O(\delta)$ and thus are also accessible. As a consequence, $\kappa_n = \Delta_4$ for all sites with energy $|v_n| \lesssim \Delta_4$.

Regime III: $\Delta_4 < \delta < \Delta_4 N^{\alpha/2}$. In this regime, the energetic separation even between nearest neighbors $\delta > \Delta_4$ exceeds the interaction band width. In the consequence, the hybridization of levels with energy $v_n \approx 0$ is suppressed down to $\kappa_n \sim \Delta_4 \times (\Delta_4/\delta)$ and the band of accessible sites narrows to this width. For a given site n inside the resonant window, nearest neighbors of energy approximately $O(\delta)$ typically lie outside it. However, a fraction order of $(\Delta_4^2/\delta)/\delta = (\Delta_4/\delta)^2$ of the nearest neighbors does satisfy the resonance condition. With order of N^α neighbors, this gives a number of $N^\alpha(\Delta_4/\delta)^2 > 1$ of hybridizing partner sites, which safeguards the extension of states.

Regime IV: $N^{\alpha/2}\Delta_4 < \delta$. The number of nearest neighbors satisfying the resonance condition becomes lesser than unity, which implies strong localization of states in Fock space.

Regimes I–IV cover the entire spectrum from fully extended states I over NEE states II and III to localization IV. (In regimes II and III states cover only a fraction of the Fock-space sites. In this paper we are following the convention to call such nonuniformly distributed states nonergodic. This is a misnomer in that the states do remain uniformly distributed over an energy shell of resonant sites.) The level broadening characterizing the local spectral density in the respective regimes is described by the universal formula

$$\kappa_n \approx \kappa e^{-v_n^2/\kappa^2}, \tag{7}$$

where the value of the hybridization parameter and the corresponding disorder strengths are summarized in Table I.

Before leaving this section, it is worthwhile to comment on various phenomenological approaches to MBL. We distinguish between three categories of phenomenological formulations. The most phenomenological class models Fock space by a random matrix. For example, the Rosenzweig-Porter model contains a Gaussian distributed random matrix (as a proxy of the interaction operator $\hat{H}_4$) perturbed by a likewise random diagonal representing $\hat{H}_2$ [29,35]. The second class replaces Fock space by a high-dimensional synthetic lattice, such as the Bethe lattice [24,25,36], or a random regular graph [26,27,37,38]. Finally, there is the random energy model, which retains the microscopic structure of Fock space but replaces the amplitudes v_n by 2^N uncorrelated random variables (see our previous publication [39] for an application of this idea to the SYK Hamiltonian). These models are designed to mimic specific aspects of localization and wave-function statistics in high-dimensional environments. However, they fall short of describing the characteristic correlations between site energies and high lattice coordination number essential to the distinction of regimes I–IV and their statistical properties reviewed in the next section.

One of the main messages of this paper is that the analytical theory for real systems need not be more difficult than that for synthetic models. What at first sight looks like a complication,i.e., the combination of high coordination numbers and correlations in the microscopic Fock space, actually is a resource and leads to self-averaging (a source of simplicity) at several stages of our computations below.

On this basis, we now discuss quantitative results obtained for the description of regimes I–IV. For notational simplicity, we work in units where the variance of the $\hat{H}_4$ matrix elements equals $J = (2/N)^{1/2}$. At this value, the band width of the interaction operator $\Delta_4 \equiv \sqrt{J^2 N/2} = 1$.

C. Spectral statistics

We describe the statistics of the system's many-body spectrum in terms of the spectral two-point correlation function at the band center

$$K(\omega) \equiv \frac{1}{\nu^2}\left\langle \nu\left(\frac{\omega}{2}\right)\nu\left(-\frac{\omega}{2}\right)\right\rangle_c, \tag{8}$$

where $\nu = \nu(E = 0)$, with $\nu(E) = \sum_\psi \langle \delta(E - \epsilon_\psi)\rangle_J$ the $\hat{H}_4$ averaged many-body density of states at zero energy $E \simeq 0$, and the subscript c stands for the cumulative average $\langle AB\rangle_c = \langle AB\rangle_J - \langle A\rangle_J \langle B\rangle_J$.

1. Regimes I–III

In these regimes, wave functions are extended and their eigenenergies are correlated and described by Wigner-Dyson statistics. Assuming an odd number N of complex fermions (for which the SYK model is in the unitary symmetry class A), this reflects in the spectral statistics of the Gaussian unitary

TABLE I. Different regimes of disorder strength, the associated level hybridization, spectral statistics, and eigenfunction support in Fock space.

	Regime	Disorder δ	Level broadening κ	Spectral statistics	State extension
I	RMT	$\delta N^{1/2} = \Delta_2 < \Delta_4$	$\kappa \sim \Delta_4$	Wigner-Dyson	D
II	NEE_1	$\Delta_4 N^{-1/2} < \delta < \Delta_4$	$\kappa \sim \Delta_4$	Wigner-Dyson	$D\Delta_4/\sqrt{N\delta}$
III	NEE_2	$\Delta_4 < \delta < \Delta_4 N^{\alpha/2}$	$\kappa \sim \Delta_4^2/\delta$	Wigner-Dyson	$D\Delta_4^2/\sqrt{N\delta^2}$
IV	localization	$\Delta_4 N^{\alpha/2} < \delta$	$\kappa = 0$	Poisson	$O(1)$

ensemble (GUE),

$$K(s) = 1 - \frac{\sin^2 s}{s^2} + \delta\Big(\frac{s}{\pi}\Big), \quad s = \pi\omega\nu, \tag{9}$$

where $\nu = \sum_n \nu_n$ is the average density of states. With the local densities given by Eq. (6) and the ν_n distributed over a range $N^{1/2}\delta$, we find

$$\nu \equiv \sum_n \nu_n = cD \times \begin{cases} 1 & \text{in regime I} \\ \frac{1}{\sqrt{N\delta}} & \text{in regimes II and III.} \end{cases} \tag{10}$$

Here and throughout, $c = O(1)$ represents numerical constants. The second line of Eq. (10) states that in the regimes of intermediate disorder strength, only a fraction $D/\sqrt{N\delta}$ of active sites contributes to the spectral support of wave functions.

2. Regime IV

In the regime of strongly localized states, eigenenergies become uncorrelated and we expect Poisson statistics. In this paper we use the change from Wigner-Dyson to Poisson statistics as one of two indicators for the Anderson transition at the boundary between regimes III and IV. Referring for a more detailed discussion of the localization transition to Sec. II E below, we note that in the literature [5], the difference between the two types of statistics is often monitored by analysis of r ratios [40], i.e., numerical comparison of the ratios $r_k \equiv \frac{\epsilon_{k+1}-\epsilon_k}{\epsilon_k-\epsilon_{k-1}}$ between nearest-neighbor many-body energy levels ϵ_k with the expected ratios for Poisson and Wigner-Dyson statistics. However, we have observed that naked eye comparisons can easily trick one into premature and qualitatively wrong conclusions. Instead, we adopt a more sophisticated entropic procedure detailed in Sec. V C and compute Kullback-Leibler divergences, where the latter are defined as relative entropies of the numerically observed distribution to the Poisson and Wigner-Dyson distribution, respectively. Figure 3(b) shows how this entropic measure changes abruptly at the localization transition.

D. Wave-function statistics

The second class of observables considered in this paper is the moments of wave functions $|\psi\rangle$ of zero energy $\epsilon_\psi = 0$,

$$I_q \equiv \frac{1}{\nu}\sum_n \langle |\langle\psi|n\rangle|^{2q}\delta(\epsilon_\psi)\rangle_J. \tag{11}$$

The statistics of these moments not only indicate the localization transition but, unlike spectral statistics, also differentiate between the three weak-disorder regimes I–III.

1. Regime I

Wave functions are ergodically distributed over the full Fock space, with moments given by those of the

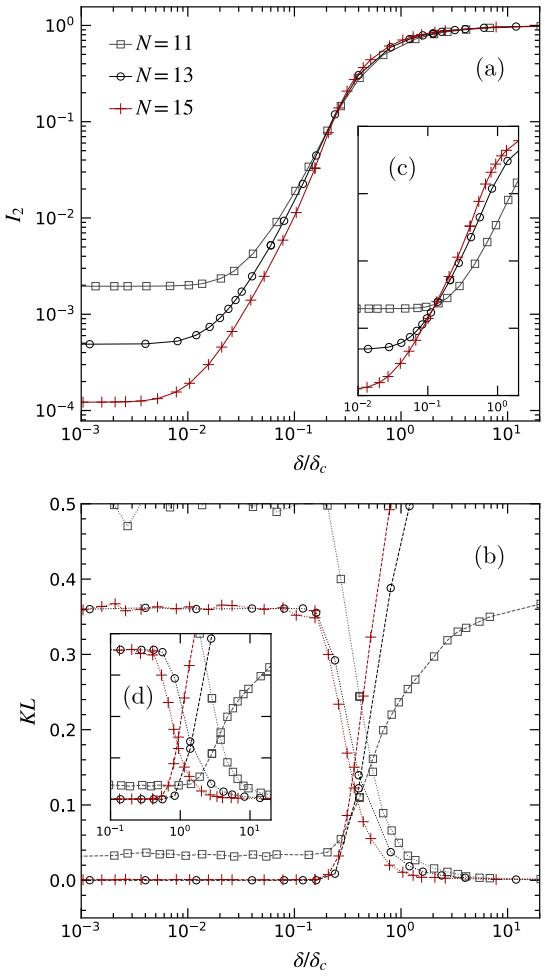

FIG. 3. (a) Scaling of the inverse participation ratio I_2 for system sizes $N = 11, 13, 15$ as a function of the dimensionless disorder strength δ/δ_c, where δ_c is the critical strength obtained by analytical solution of the model in Eq. (F3). (b) Plot of the relative Kullback-Leibler entropies KL between the numerical spectral statistics and the Wigner-Dyson (dashed lines) and Poisson distributions (dotted lines), respectively, for the same set of system sizes. In either case, the analytically obtained δ_c overestimates the critical strength by an N-independent factor of $O(1)$. (c) and (d) Scaling of I_2 and KL, respectively, as a function of δ/δ_c, employing Eq. (16) with two adjusted numerical parameters (see the discussion in the text).

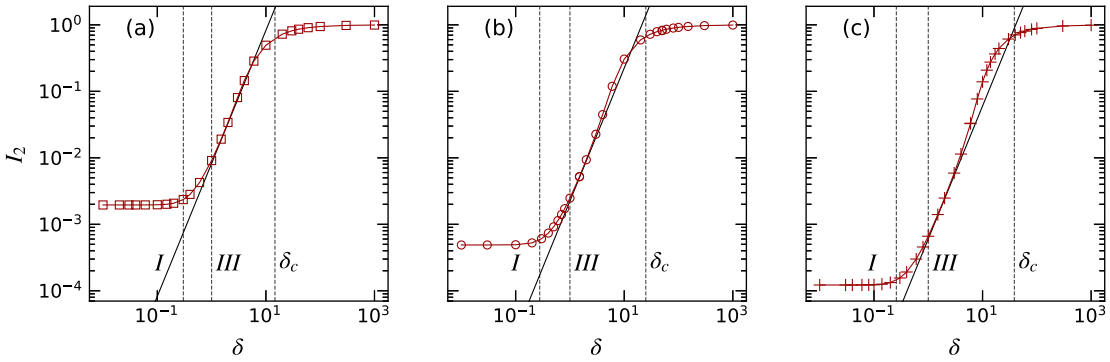

FIG. 4. Comparison of the numerical computation of the inverse participation ratio I_2 as a function of the disorder strength δ for system sizes (a) $N = 11$, (b) $N = 13$, and (c) $N = 15$ with the analytical prediction $I_2 = 8\sqrt{N}\delta^2/\pi D$ [see Eq. (E8)]. Vertical dashed lines mark the end of region I, the beginning of region III, and the scale δ_c at which Fock-space localization sets in [estimated from Eq. (F3)]. (Notice that the inverse participation ratio here has not been normalized by its value at $\delta = 0$, as in our previous publication [39].)

Porter-Thomas distribution

$$I_q = q!D^{1-q} \quad \text{in regime I,} \tag{12}$$

otherwise found for the wave functions of random matrix Hamiltonians. The result states that the complex amplitudes $\langle n|\psi\rangle$ are independently distributed Gaussian random variables.

2. *Regimes II and III*

The wave functions no longer ergodically occupy the full Fock space. The bulk of their support is concentrated on the subset of resonant sites $v_n \sim \kappa_n$. This behavior reflects in the moments

$$I_q = c^q \left(\frac{D}{\sqrt{N}\delta}\right)^{1-q} \frac{2q(2q-3)!!}{\kappa^{q-1}} \quad \text{in regimes II and III,} \tag{13}$$

where $c = O(1)$. To make the connection of this expression to Eq. (12) more transparent, consider the case of large q, where

$$I_q = cq!D_{\text{res}}^{1-q}, \quad q \gg 1,$$
$$D_{\text{res}} = D \times \begin{cases} \frac{1}{\sqrt{N}\delta} & \text{in regime II} \\ \frac{1}{\sqrt{N}\delta^2} & \text{in regime III.} \end{cases} \tag{14}$$

These moments again coincide with those of a Gaussian distribution, now defined on the diminished number D_{res} of resonant sites in Fock space, over which the wave functions are uniformly spread.

Noting that $\delta \sim N^\eta$, $\eta < 2$, the dependence of D_{res} on D is approximated as

$$D_{\text{res}} = D/\ln D^\beta, \quad \beta = \begin{cases} \eta + \frac{1}{2} & \text{in regime II} \\ 2\eta + \frac{1}{2} & \text{in regime III.} \end{cases} \tag{15}$$

This suggests an interpretation in terms of a fractal whose dimension differs from the naive dimension by a factor $D/\ln D^\beta \sim D/D^0$, rather than the more usual D/D^γ with some $\gamma > 0$. Alternatively, we may interpret the wave functions as ergodically or thermally extended over an energy shell of sites defined by the condition $v_n \approx \kappa_n$.

Figures 4 and 5 show a comparison of our analytical predictions for the wave-function moments dependence on δ (Fig. 4) and on q and N (Fig. 5) to numerical simulations for $2N = 22, 26, 30$ Majorana fermions. Vertical dashed lines

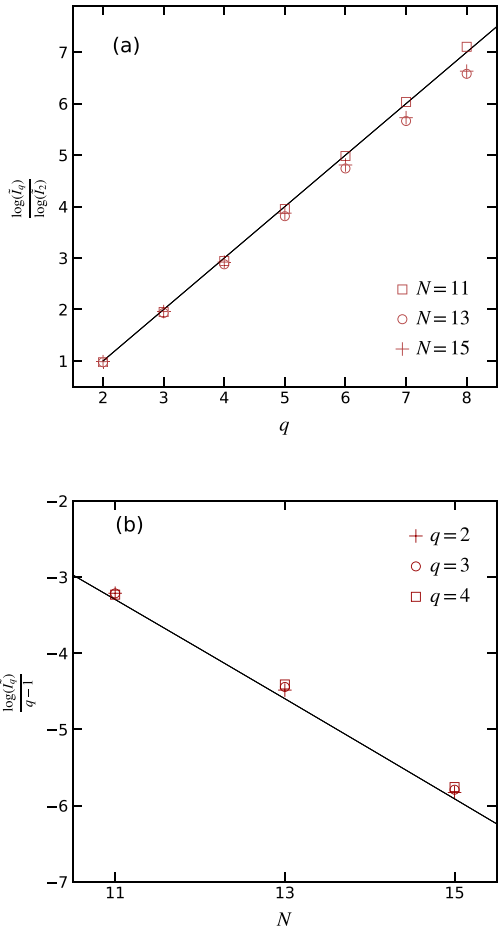

FIG. 5. Verification of the scaling of our analytical prediction (13) in q and N, respectively. In both panels we consider $\delta = 3$ deep in regime III and $\tilde{I}_q \equiv I_q/q(2q-3)!! = (4\sqrt{N}\delta^2/\pi D)^{q-1}$, where the constants are taken from the accurate result for I_q in regime III [Eq. (E8)].

in Fig. 4 mark the boundaries between different regimes and δ_c is the scale at which Fock-space localization sets in [see Eq. (16) and the refined expression (F3) accounting for $1/N$ corrections]. For the numerically accessible N values, regime II, $N^{-1/2} \ll \delta \ll 1$, lacks the width required for the comparison with power laws and we concentrate on regime III. Given that there is no fitting of numerical parameters and numerical error bars are smaller than symbol size, the comparison is good. We notice a slight deviation in the q scaling, increasing for large moments q. However, this mismatch does not show consistent system size dependence and we cannot attribute a clear trend to it. Starting from $N = 13$, we also see deviations of the predicted δ scaling at large values, which is a first indication of the proximity of the Anderson transition. At first sight, it may seem paradoxical that these signatures are first seen for larger N, where the parametric dependence of the localization threshold $\delta \gtrsim N^2$ increases in N. However, the situation becomes clearer when we represent the inverse participation data as a function of a scaled parameter, as we will discuss next.

E. Strong localization

The wave functions describing random hopping on a lattice are localized on small-size clusters if statistically the nearest-neighbor hopping matrix elements become smaller than the variations of the local site energies. In this work we numerically and analytically compute the threshold strength of the disorder where this happens.

1. Analytical approach

Above we reasoned that the problem of MBL is defined by a competition of localizing on-site disorder and delocalizing hopping in a complex high-dimensional lattice. Unlike in previous work on Anderson localization in high dimensions, which is formulated on simplified synthetic lattice structures such as the Bethe lattices [41,42] or random regular graphs [24,41,43,44], here we directly work in Fock space. What helps to keep this more complicated problem under control is the huge effective lattice coordination number of $O(N^4)$ and a simplification known as the effective-medium approximation [45]. This approximation is commonly applied in the discussion of Anderson localization on high-dimensional lattices and backed by their large coordination numbers. It describes transport as a process avoiding local loops (see Fig. 6), while multiple link traversals [Fig. 6(a)] are included. The rationale behind this simplification is that at any given order in hopping perturbation theory, amplitudes with the lowest number of statistically independent energy denominators contribute the strongest. Its application to the SYK lattice, detailed in Sec. VI, sums these processes via recursion relations [such as Eq. (44)] whose solution leads to prediction (F3) for the critical disorder strength. For large $N \gg 1$ this formula simplifies to

$$\delta_c \simeq \frac{N^2}{4\sqrt{3}} \ln N, \quad N \gg 1. \tag{16}$$

The characteristic $\delta_c \sim N^2 \ln N$ scaling was first predicted in Ref. [14], where the logarithmic correction relative to the naive estimate $\delta_c \sim N^2$ mentioned in the Introduction accounts for resonant hybridization with sites beyond nearest neighbors.

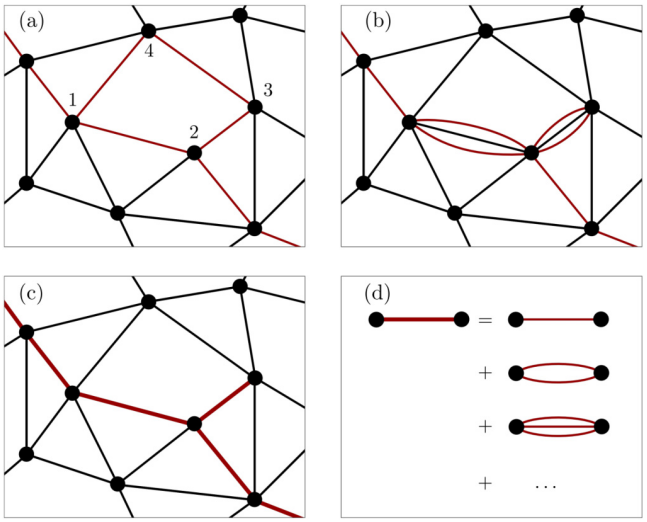

FIG. 6. (a) Cartoon representation of a subset of sites in Fock space connected by a hopping amplitude containing a loop insertion. The four hopping amplitudes constituting the loop come with four independent energy denominators. (b) This fourth-order hopping amplitude with site revisits has only two independent energy denominators and contributes parametrically stronger. (c) Hopping amplitudes resumed according to the procedure shown in (d).

However, our aim here is to compare to the real world of small-size systems $N = O(10)$ where things get more complicated. For one, the difference between the asymptotic result and the more precise expression (F3) becomes noticeable. Second, various approximations in the execution of the effective-medium program rely on the largeness of N and again may lead to errors in terms subleading in N. These uncertainties must be kept in mind when we compare to the numerical computation of the threshold.

2. Numerical approach

As indicated above, we detect the onset of localization via two indicators. The first is the wave-function statistics, where I_2 serves as a transition order parameter jumping between the values $I_2 \sim D^{-1}$ in the ergodic weak-disorder regime to $I_2 \sim 1$ in the localized phase. Here the first value must be taken with a grain of salt, again due to finite system size. Our discussion in the preceding section shows that before reaching the transition, in regimes II and III, we have deviations away from the ergodic limit $I_2 \sim 1/D$. In the thermodynamic limit, these are inessential [because D is exponential in N while the corrections of Eq. (14) are in powers of N]. However, for system sizes in numerical reach, we cannot expect an actual jump in the order parameter. The best one can hope for is gradual steepening of the curve $I_2(\delta)$ for $\delta \to \delta_c$ upon increasing system size.

The second diagnostic is spectral statistics, where we monitor the proximity to a Wigner-Dyson or Poisson distribution via the Kullback-Leibler entropy as discussed in Sec. V A.

Ideally, one would hope that both signatures, inverse participation ratio and spectral statistics, reveal a phase transition via a crossing point when subjected to appropriate finite-size scaling and that these crossing points sit at the same value. In reality, we almost, but not fully, observe this behavior. In Fig. 3 we show the inverse participation ratio I_2 and the Kullback-Leibler entropy as a function of the scaled variable δ/δ_c, where δ_c is given by the analytical prediction (F3) in terms of the Lambert W function. We observe that (i) both observables show reasonably well defined crossings with a tendency of sharpening behavior for increasing system size, however, (ii) these crossings deviate from the analytically predicted value $\delta/\delta_c = 1$ by a numerical factor of $O(1)$ and by a factor of similar magnitude among themselves. Turning to different scaling variables, one may sharpen the finite-size scaling of either one of the two observables. For example, Fig. 3(c) shows I_2 as a function of δ/δ_c, with δ_c from Eq. (16) with two numerical parameters outside and inside the logarithm adjusted to improve visibility of the crossing point.[5] However, this comes at the expense of a more diffuse scaling of the entropy, as shown in Fig. 3(d). We observe that the numerically obtained scaling for small systems responds sensitively to the finite-N corrections [Eq. (F3) vs Eq. (16)].

All in all, we consider the agreement with the numerics quite favorable. We see clear evidence of critical behavior in two observables and the position of the transition is obtained without free fit parameters from the analytical solution of an effective lattice model. This is a genuine Fock-space localization problem where a first-principles solution of this kind is possible.

In the following sections we discuss the derivation of the analytical results mentioned above. Hoping that elements of this computation might become blueprints for the analysis of other models of MBL, we try to be as pedagogical as we can. Various technical details are relegated to the Appendixes.

III. MATRIX MODEL

We start the derivation of the results summarized above by constructing an exact matrix integral representation of the correlation functions introduced above to describe many-body wave functions and spectra. The unconventional perspective of this approach is that there will be no second quantized representation of Fock space: We think of the SYK Hamiltonian as a big matrix and treat it like that. In this section we discuss the construction of a matrix integral representing the theory averaged over $\hat{H}_4$ disorder. The physics behind this formulation and that of a subsequent stationary-phase analysis of the theory will be discussed in the next section.

All information on spectra and wave functions of the system is contained in the Fock-space matrix elements of resolvent operators

$$G^{\pm}_{nm} = \langle n|(z_\pm - \hat{H})^{-1}|m\rangle, \tag{17}$$

where $z_\pm = \pm(\frac{\omega}{2} + i\eta)$ and, here and throughout, η is infinitesimal (with a limit $\eta \searrow 0$ to be taken in the final step of all calculations). Specifically, the correlation functions above are obtained as

$$I_q = \frac{(2i\eta)^{q-1}}{2i\pi\nu}\sum_n \langle G^{+(q-1)}_{nn} G^{-}_{nn}\rangle_J,$$
$$K(\omega) = \frac{1}{2\pi^2\nu^2}\sum_{nm}\mathrm{Re}\langle G^{+}_{nn} G^{-}_{mm}\rangle_J, \tag{18}$$

where I_q is computed at $\omega = 0$ and $\langle\cdots\rangle_J$ denotes the average over coupling constants $\{J_{ijkl}\}$ of $\hat{H}_4$.

A. Construction of the matrix integral

Following standard protocols, we raise the Green's functions to an exponential representation before performing the Gaussian average. The basic auxiliary formula in this context is $M^{-1}_{nm} = \int D(\bar\psi,\psi) e^{-\bar\psi M\psi}\psi^\sigma_m\bar\psi^\sigma_n$, where M is a general $L\times L$ matrix and the $2L$-dimensional graded vector $\psi = (\psi^{\mathrm{b}}, \psi^{\mathrm{f}})^T$ contains L-commuting components ψ^{b}_n and an equal number of Grassmann components ψ^{f}_n. The double integral over these variables cancels unwanted determinants $\det(M)$, while the preexponential factors, either commuting or anticommuting, $\sigma = \mathrm{b},\mathrm{f}$, isolate the inverse matrix element. With the identification $M = \mathrm{diag}(-i[G^+]^{-1}, i[G^-]^{-1}) = -i\sigma_3(E + z - \hat{H})$, we are led to consider the generating function

$$\mathcal{Z}[j] = \int D(\bar\psi,\psi)\langle e^{-\bar\psi(E+z-\hat{H}-j)\psi}\rangle_J. \tag{19}$$

Here $z \equiv (\frac{\omega}{2} + i\eta)\sigma_3$ contains the energy arguments of the Green's functions and σ_3 is a Pauli matrix distinguishing between advanced and retarded components. The matrix j acts as a source for the generation of the required moments of Green's-function matrix elements. Specifically, we define

$$j_K(\alpha,\beta) = \alpha\pi^{\mathrm{b}}\otimes\pi^+ + \beta\pi^{\mathrm{f}}\otimes\pi^-, \tag{20}$$

$$j_{I,n}(\alpha,\beta) = j_K(\alpha,\beta)\otimes|n\rangle\langle n|, \tag{21}$$

where $\pi^{\mathrm{b,f}}$ is a projector onto commuting and anticommuting variables, respectively, $\bar\psi\pi^\sigma\psi = \bar\psi^\sigma\psi^\sigma$, and $\pi^\pm$ projects in causal space $\bar\psi\pi^s\psi = \bar\psi^s\psi^s$, $s = \pm$. With these definitions, an elementary computation shows that

$$K(\omega) = \frac{1}{2\pi^2\nu^2}\mathrm{Re}\partial^2_{\beta\alpha}\mathcal{Z}[j_K]|_{\alpha,\beta=0}, \tag{22}$$

$$I_q = c_q(2i\eta)^{q-1}\sum_n \partial_\beta\partial^{q-1}_\alpha\mathcal{Z}[j_{I,n}]|_{\alpha,\beta=0}, \tag{23}$$

with $c_q \equiv 1/2i\pi\nu(q-1)!$. In the following, we consider the sources absorbed in a redefined energy matrix $z \to z - j$ and recall their presence only when needed.

At this point, the averaging over $\hat{H}_4$ can be performed and it generates a quartic term

$$\mathcal{Z} = \int D(\bar\psi,\psi)\exp\left(-\bar\psi\hat{G}^{-1}\psi + \frac{w^2}{2}\sum_a(\bar\psi\hat{X}_a\psi)^2\right), \tag{24}$$

where we defined $w^2 = 6J^2/(2N)^3 \equiv \frac{3}{2}N^{-4}$ for the scaled variance of the SYK Hamiltonian $\hat{H}_4$, $\hat{G} \equiv (E + z - \hat{H}_2)^{-1}$,

$$\hat{X}_a \equiv \hat\chi_i\hat\chi_j\hat\chi_k\hat\chi_l, \tag{25}$$

[5] More specifically, we used $\delta_c = \frac{\sqrt{\pi}Z}{2\sqrt{\rho}}\ln(\frac{\sqrt{\pi}Z}{32\pi^2})$.

and $a = (i, j, k, l)$ with $i < j < k < l$. We next perform an innocuous but physically meaningful (see the next section) rearrangement $(\bar{\psi}\hat{X}_a\psi)^2 = \mathrm{STr}[(\psi\bar{\psi}\hat{X}_a)^2]$, where the supertrace [45] $\mathrm{STr}(X) \equiv \mathrm{tr}(X^{\mathrm{bb}}) - \mathrm{tr}(X^{\mathrm{ff}})$ accounts for the minus sign caught when exchanging anticommuting variables. The next step is a Hubbard-Stratonovich transformation decoupling the matrices $\psi\bar{\psi}\hat{X}_a \sim A_a$ in terms of $(2N)^4/4!$ auxiliary matrix fields A_a. Referring for details of the procedure to Appendix A, we note that after the decoupling the integral over ψ variables has become Gaussian and can be carried out. A more interesting statement is that of the $\rho \equiv \binom{2N}{4}$ Hubbard-Stratonovich fields A_a, all but one can be removed too by straightforward Gaussian integration. Upon restricting to $E = 0$ this leaves us with a single integration

$$\mathcal{Z} = \int \mathcal{D}Y e^{-S[Y]},$$

$$S[Y] = -\frac{1}{2}\mathrm{STr}(Y\mathcal{P}Y) + \mathrm{STr}\ln(z - \hat{H}_2 + i\mathcal{P}Y), \qquad (26)$$

over a $(2 \times 2 \times D)$-dimensional matrix $Y = \{Y_{nn'}^{\sigma\sigma',ss'}\}$ carrying indices in causal space, superspace, and Fock space. The information on the SYK system now sits in the site-diagonal one-body term $\hat{H}_2$ and the hopping operator $\mathcal{P}$, which represents the interaction and acts on matrices $Z = \{Z_{nm}\}$ in Fock space as

$$\mathcal{P}Z \equiv \frac{1}{\rho}\sum_a \hat{X}_a Z \hat{X}_a^\dagger. \qquad (27)$$

Finally, $\gamma = w\rho^{1/2} = 1$ represents the $\hat{H}_4$ band width, which we have set to unity. To simplify formulas, we will consider energies $\hat{H}_2 \to \gamma\hat{H}_2$ and $\omega \to \gamma\omega$ scaled by this parameter and suppress it throughout.

B. Discussion of the matrix integral

This is now a good point to discuss the meaning of the above Hubbard-Stratonovich transformation and of the matrix representation. The two-fermion vertices $\bar{\psi}\hat{X}_a\psi$ entering the theory after disorder averaging describe the scattering of Fock-space states off the four Majorana operators contained in the Hamiltonian and in this way introduce the lattice connectivity indicated in Fig. 1. While a direct analysis of individual Fock-space amplitudes seems hopeless, progress can be made if the propagators are paired to two-amplitude composites as indicated in Fig. 7. For two reasons, the pair amplitudes $Y_{nn'}^{ss',\sigma\sigma'} = \psi_n^{s\sigma}\bar{\psi}_{n'}^{s'\sigma'}$ are more convenient degrees of freedom. First, the pair action $Y \to \sum_a \hat{X}_a Y \hat{X}_a = \rho\mathcal{P}Y$ governing scattering in the two-state channel [cf. the structure of the action (26)] is relatively easy to describe (discussed below). Second, the advanced/retarded combinations $Y_{nn}^{-+,\sigma\sigma'} = \psi_n^{-\sigma}\bar{\psi}_n^{+\sigma'}$ appear as terminal vertices in the computation of Green's functions $G_n^+G_n^-$, where the dots stand for the unspecified final points of the correlation function. With the exact identity $(G^+)^{-1} - (G^-)^{-1} = \omega^+ \equiv \omega + 2i0$, we have $\langle G_{mn}^+G_{nm}^-\rangle_J = \langle \mathrm{tr}(G^+G^-)\rangle_J = \frac{1}{\omega^+}\langle \mathrm{tr}(G^+)[(G^+)^{-1} - (G^-)^{-1}]G^-\rangle_J = \frac{1}{\omega^+}\langle \mathrm{tr}(G^- - G^+)\rangle_J \simeq \frac{2\pi i}{\omega^+}\nu$, where ν is the density of states at the band center. The way to read this (Ward) identity is that the product of Green's functions contains a singularity, *provided* $\mathrm{tr}(G^- - G^+) \sim \nu$ is a structureless quantity. (The latter condition does not hold in systems with localization, where the isolated eigenstates support a point spectrum with poles rather than a uniform cut.) This argument indicates that the soft mode $G^+G^- \sim \omega^{-1}$ is key to the understanding of observables probing the spectrum and eigenfunctions of the system.

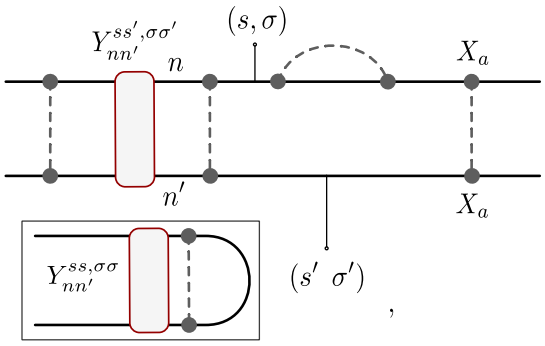

FIG. 7. Composite matrix degree of freedom $Y_{nn'}^{ss',\sigma\sigma'}$ representing the pair propagation of Fock-space scattering amplitudes. See the text for discussion.

In the matrix integral framework, the above singularity shows in the presence of a soft mode in the integration over the variables $Y_{nn}^{-+,\sigma\sigma'}$. To isolate this mode, we note that Eq. (26) has an approximate symmetry

$$Y \to TYT^{-1}, \quad T = \{T^{ss',\sigma\sigma'}\} \qquad (28)$$

under rotations homogeneous in Fock space. The set of these transformations defines GL(2|2), i.e., the group of invertible 4×4 matrices with anticommuting entries. Invariance under this symmetry is weakly broken only by the frequency/source matrix z, which, ignoring the infinitesimal sources, transforms as $\frac{\omega}{2}\sigma_3 \to \frac{\omega}{2}T^{-1}\sigma_3 T$. This reduces the symmetry down to the transformations diagonal in advanced-retarded (s-index) space GL(1|1) × GL(1|1).

The essential question now is whether the above weak explicit symmetry breaking is *spontaneously broken* in the matrix integral (much as a weak explicit symmetry breaking by a finite magnetic field gets upgraded to spontaneous symmetry breaking in a ferromagnetic phase). In the latter case, we expect a soft Goldstone mode whose mass is set by the symmetry-breaking parameter ω and ω^{-1} singularities in line with the observation above. To investigate this question and the consequences in the observables $K(\omega)$ and I_q, we next subject the theory to a stationary-phase analysis.

IV. EFFECTIVE THEORY

In this section we map the exact theory (26) to an approximate but more manageable effective theory. The conceptual steps are standard and consist of a saddle-point analysis, followed by a Ginzburg-Landau-style expansion (see Sec. VI) of the exact action in fluctuations around a homogeneous saddle point.

We have already established the presence of an exact (in the limit $\omega \to 0$) rotational soft mode isotropic in Fock space. Since much of the analysis below will focus on strong $\hat{H}_2$ with eigenvalues v_n of $\hat{H}_2$ comparable to or exceeding the $\hat{H}_4$,

we anticipate that fluctuations of lowest action cost will be commutative in the sense $[\hat{H}_2, Y] = 0$. We thus start from an ansatz $\langle n|Y|m\rangle = Y_n\delta_{nm}$ where fluctuations are diagonal in the occupation basis. In view of the fermion parity conservation of both $\hat{H}_{2,4}$, we focus on a sector of definite parity, chosen to be even. The locality of $\hat{H}_2$ in the occupation number basis is in competition with the hopping described by $\mathcal{P}$. However, what works to our advantage is that the action of $\mathcal{P}$ on the states Y is remarkably simple: Thinking of Y_{nm} as the matrix elements of a density matrix Y_n represents a state without off-diagonal matrix elements. It is a nontrivial feature of $\mathcal{P}$ that it preserves this structure, $(\mathcal{P}Y)_m = \sum_n \mathcal{P}_{|n-m|}Y_m$, i.e., the adjoint action $\hat{X}_a Y \hat{X}_a$ on Fock-space diagonal matrices Y does not generate superpositions of off-diagonal states. A straightforward combinatorial exercise shows that (see Appendix B for details)

$$\mathcal{P}_0 = \frac{N(N-1)}{2\rho}, \quad \mathcal{P}_2 = \frac{4(N-2)}{\rho}, \quad \mathcal{P}_4 = \frac{16}{\rho}, \tag{29}$$

with all other matrix elements vanishing, and normalization $\sum_m \mathcal{P}_{m,n} = 1$. Notice that for a given n, we have $\binom{N}{4}$ neighbors with hamming distance 4, connected to n by $\binom{N}{4}\mathcal{P}_4 \overset{N\gg 1}{\sim} 1$. This shows that distance 4 hopping is the most important by phase volume.

With these structures in place, a variation of action (26) leads to

$$-iY = \frac{1}{z - \hat{H}_2 + i\mathcal{P}Y}. \tag{30}$$

Notice that Y resembles $-i$ times the local propagator (see the inset of Fig. 7) of site n, dressed with a self-energy $i\mathcal{P}Y$ due to hopping via $\mathcal{P}$ to neighboring sites. It is this term which makes the stationary-phase equation nontrivial. In a first step towards the solution, we neglect imaginary contributions to Y and focus on the local spectral density $\mathrm{Re}(Y)$ instead. (In the effective action, the imaginary part of Y describes an energy shift $\nu_n \to \nu_n + \mathrm{Im}Y_n$, which is inessential to our problem.) Causality requires $\mathrm{sgn}Y = \mathrm{sgn}\,\mathrm{Im}z$, i.e., the sign of the self-energy is dictated by that of the imaginary part contained in the energy arguments. Otherwise the saddle-point equation is rotationally invariant in the internal indices of the theory. This motivates an ansatz

$$\mathrm{Re}Y = \sum_n (\mathrm{Re}Y)_n |n\rangle\langle n| \equiv \sum_n \pi\nu_n |n\rangle\langle n| \otimes \sigma_3 \otimes \mathbb{1}_{\mathrm{bf}} \tag{31}$$

with real coefficients ν_n. Inspection of Eq. (30) shows that these coefficients afford an interpretation as a mean-field local density of states.

Substituting this expression into the equation and temporarily ignoring the small energy argument z as small compared to both $\hat{H}_2$ and Y, we obtain the variational equation

$$\nu_n = \frac{1}{\pi}\mathrm{Im}\frac{1}{\nu_n - i\kappa_n},$$
$$\kappa_n \equiv \pi(\mathcal{P}\hat{\nu})_n \equiv \pi\sum_m \mathcal{P}_{|n-m|}\nu_m, \tag{32}$$

where $\hat{\nu}$ denotes the matrix diagonal in the occupation basis, with elements ν_n, and where we introduce the variational level hybridization κ_n. The structure of this equation contains the key to its solution: For $\nu_n = 0$, the normalization $\sum_m \mathcal{P}_{|n-m|} = 1$ implies that it is solved by $\kappa_n = 1$. In the chosen units, this is π times the density of states at the SYK band center. For finite ν_n, the summation over m implements an effective average over the connected states, which now carry random energy. In Appendix C we show that the average stabilizes the solution (33),

$$\kappa_n \simeq \kappa\Theta(C - |\nu_n|),$$
$$(\kappa, C) = \begin{cases} (1,1), & \delta < 1 \text{ (regimes I and II)} \\ (\delta^{-1}, \delta), & \delta > 1 \text{ (regimes III and IV)}, \end{cases} \tag{33}$$

where $\simeq$ stands for equality up to corrections exponentially small in $\exp[-(\nu_n/\delta)^2]$. We interpret this result as the spectral density of sites with energy ν_n and decay rate κ_n into neighboring sites. The latter is finite for states below a threshold $|\nu_n| < C$. For $\delta > 1$, the rate is given by the energy denominator $\kappa \sim \delta^{-1}$ of neighboring sites. In the opposite regime $\delta < 1$, the energy denominators of states $\nu_n \sim 1$ in resonance with the SYK band width are of $O(1)$, leading to the second line in Eq. (33).

The saddle-point solutions discussed thus far are distinguished for their diagonality in all matrix indices. However, we now recall that the $z = 0$ action is invariant under Fock-space uniform rotations (28), implying that uniformly rotated saddle-point configurations $Y_n \to TY_nT^{-1}$ are solutions too. (Technically, this follows from the cyclic invariance of the trace.) Next to this uniform Goldstone mode, configurations $Y_n \to T_nY_nT_n^{-1}$ with site-diagonal rotations commutative with $\hat{H}_2$ are expected to cost the least amount of action. With $Y_n = \pi\nu_n\sigma_3$, this makes $Y_n \to \pi\nu_nQ_n$, $Q_n = T_n\sigma_3T_n^{-1}$, the effective degrees of freedom of the theory, and substitution into Eq. (26) defines the Goldstone mode integral

$$\mathcal{Z} = \int \mathcal{D}Q\, e^{-S[Q]},$$
$$S = -\frac{\pi^2}{2}\mathrm{STr}[(\hat{\nu}\hat{Q})\mathcal{P}(\hat{\nu}\hat{Q})] + \mathrm{STr}\ln[z - \hat{H}_2 + i\pi\mathcal{P}(\hat{\nu}\hat{Q})], \tag{34}$$

where $\hat{Q}$ again denotes the matrix diagonal in the occupation basis, with elements Q_n. In the next two sections, we investigate what this integral indicates about wave-function statistics and Fock-space localization, respectively.

V. SPECTRAL AND WAVE-FUNCTION STATISTICS

In this section we explore the spectral and wave-function statistics in regimes I–III. The presumption is that wave functions are not yet localized and correlated with each other. This should lead to Wigner-Dyson spectral statistics and wave-function moments reflecting the extended nature on the subsets of Fock space corresponding to active or resonant sites.

To test these hypotheses it is sufficient to consider the integral (34) in the presence of effectively infinitesimal explicit symmetry breaking z: Besides the sources j, this parameter contains a frequency argument $\omega \sim D^{-1}$ of the order of the exponentially small inverse many-body level spacing in the case of spectral statistics, Eq. (22), or the infinitesimal parameter η in the case of wave-function statistics, Eq. (23). On general

grounds, we expect the smallness in the explicit symmetry breaking in a Goldstone mode integral to lead to singular contributions order of z^{-n} proportional to the inverse of that parameter after integration. (Inspection of the prefactors η^{q-1} in the definition of the wave-function statistics shows that such singularities are actually required to obtain nonvanishing results.) These most singular contributions to the integral must come from the Goldstone mode fluctuations of least action, which are fluctuations homogeneous in Fock space,

$$Q_n = T_n \sigma_3 T_n \to T\sigma_3 T^{-1} \equiv Q. \tag{35}$$

With $[T, \mathcal{P}] = 0$, the substitution $\hat{\nu}\hat{Q} \to \hat{\nu}Q$ into the action (34) leads to

$$S_0[Q, j] = \mathrm{STr}\ln(z - j - \hat{H}_2 + i\hat{\kappa}Q), \tag{36}$$

where we made the dependence $z \to z - j$ of the action on the sources $j \equiv j_{I,n}$ required to calculate moments via Eq. (21) explicit again and we used that $\pi\mathcal{P}\hat{\nu} = \hat{\kappa}$.

Before proceeding, we note that the structure of this action is identical to that describing the Rosenzweig-Porter model, a single random matrix of dimension D containing Gaussian distributed disorder on the matrix diagonal [46]. An important difference is however that the diagonal disorder in the latter is uncorrelated, while the Fock-space diagonal disorder induced by $\hat{H}_2$ is highly correlated. As a consequence, the effective action for the Rosenzweig-Porter model only allows for homogeneous saddle-point solutions [39,46], while here we encounter solutions that become inhomogeneous in Fock space once on-site disorder exceeds the $\hat{H}_4$ band width. The inhomogeneity accounts for a site-dependent broadening κ_n, induced by correlations in the disorder amplitudes and also manifests in a separation into regimes II/III of the regime of nonergodic extended states. In the following, we discuss what this reduction of the model reveals about spectral and wave-function statistics.

A. Spectral statistics

To obtain a prediction for spectral correlations based on the representation (34) with Fock-space zero mode, we consider the correlation function (8), represented through matrix integral Green's functions as in Eqs. (18) and (22). To compute these quantities from the effective theory, we need to expand the action (36) to lowest order in the parameter $\omega/\kappa \sim 1/D$ and to second order in the sources (20). The straightforward ω expansion yields [cf. Eq. (D3)]

$$S_\omega[Q] \equiv -i\frac{\pi\nu(\omega + i\eta)}{2}\mathrm{STr}(Q\sigma_3), \tag{37}$$

where ν is the zero-energy density of states (10). What remains is the source differentiation and the integration over the matrix Q. To get some intuition for the integral, note that the nonlinear degree of freedom $Q = T\sigma_3 T^{-1}$ affords a representation $Q = UQ_0U^{-1}$, where U contains various compact angular variables (cf. Appendix E) and

$$Q_0 = \begin{pmatrix} \cos\hat{\theta} & i\sin\hat{\theta} \\ -i\sin\hat{\theta} & -\cos\hat{\theta} \end{pmatrix}, \tag{38}$$

a rotation matrix in causal space. Diagonal in superspace, this matrix is parametrized in terms of the two Bogoliubov angles $\hat{\theta} = (i\theta_\mathrm{b}, \theta_\mathrm{f})^T$, where $\theta_\mathrm{f} \in [0, \pi]$ is a compact rotation variable and $\theta_\mathrm{b} \in \mathbb{R}^+$ a noncompact real variable. This representation reveals the geometry of the integration manifold as the product of a sphere θ_f and a hyperboloid θ_f (coupled by variables contained in U). Where the physics of nonperturbative structures in spectral and wave-function statistics and localization is concerned, the most important player is the noncompact variable θ_b as only this one has the capacity to produce singular results. Heuristically, one may think of the model reduced to its dependence on this variable as a noncompact version of a Heisenberg model, containing hyperboloidal rather than compact spins as degrees of freedom.

Referring for details of the source differentiation and the subsequent integration over the matrix Q [45] to Appendix E, the above reduction of the model yields the GUE spectral correlation function (9) for the spectral statistics on scales of the many-body level spacing in regimes I–III. With increasing energies, the assumption of homogeneity of fluctuations in Fock space breaks down (cf. the next section) beyond a Thouless energy whose value depends on the specific observable under consideration.[6] However, the detailed investigation of Thouless thresholds for the present model is beyond the scope of the paper.

B. Wave-function statistics

In the same manner, we may consider the local moments of wave functions (11), represented via Green's functions (18) and obtained from the matrix integral through Eq. (23). A key feature of this expression is that it contains a limit $\lim_{\eta\to 0}\eta^{q-1}(\cdots)$; the factor η^{q-1} must thus be compensated for by an equally strong singularity η^{1-q} from the integral, where η couples through $z = i\eta\sigma_3$. Setting $\omega = 0$ in Eq. (37) and integrating over the functional differentiated in sources (a calculation detailed in Appendix E) then yields the moments (12)–(14).

The support of wave functions in regimes II and III is different [as indicated by the different value of D_res in Eqs. (14)], while the density of states (DOS) (10) assumes the same value. The reason for this is that, in regime II, there is no distinction between active and resonant sites: There are order of $D/\sqrt{N}\delta$ active sites contributing with unit weight to the DOS. By contrast, in regime III, the dominant contribution to the DOS comes from the smaller number of $D_\mathrm{res} \sim D/\sqrt{N}\delta^2$ resonant sites, with sharply peaked spectral weight order of δ, $\nu \sim D_\mathrm{res}\delta \sim D/\sqrt{N}\delta$.

C. Comparison to numerics

To numerically check the predictions for the statistics of many-body wave functions and spectra, we calculated eigenfunctions and spectrum from exact diagonalization of

[6] Unlike with low-dimensional single-particle problems, the effectively high dimension of Fock space implies nonuniversality of the Thouless energy. For example, nonzero-mode corrections to the spectral form factor (the Fourier transform of the two-point correlation function in energy) and the two-point function itself, respectively, become visible at different energy scales.

the Hamiltonian $\hat{H} = \hat{H}_4 + \hat{H}_2$ [see (1) and (3)] for $\{v_i\}$ obtained by diagonalizing (2) as a one-body problem, for $2N = 22, 26, 30$ Majorana fermions and varying values of δ. We kept $\frac{1}{7}$ of the total spectrum and verified both a nearly constant density of states and that results remain unchanged when we restrict to a smaller energy window. From the selected eigenfunctions in the center of the band, we calculated the statistics of the moments of the wave function according to Eq. (11). The eigenfunctions are normalized in each definite parity subspace. For the spectrum we compared the numerical statistical distribution with both Wigner-Dyson and Poisson distributions by calculating the Kullback-Leibler divergence $\mathrm{KL} \equiv D(P||Q) = \sum_k p_k \ln(\frac{p_k}{q_k})$, where p_k is the spectral statistics from numerical data and q_k the respective distribution. In order to avoid level unfolding, we followed Ref. [40] and studied the statistics of ratios of energy spacings $r_j = \min(\frac{s_j}{s_{j-1}}, \frac{s_{j-1}}{s_j})$, where $s_j = \epsilon_{j+1} - \epsilon_j$ is the nearest-neighbor spacing of the eigenenergies $\{\epsilon_j\}$. The q_k are then given by numerically integrating either the Wigner-Dyson or the Poisson distribution for the variable r over each bin centered at r_k, given by Ref. [47],

$$P(r) = \begin{cases} \frac{81\sqrt{3}}{2\pi} \frac{(r+r^2)^2}{(1+r+r^2)^4} + \delta P(r) & \text{[Wigner-Dyson (GUE)]} \\ \frac{2}{(1+r)^2} & \text{(Poisson)}, \end{cases} \tag{39}$$

where δP is a numerical correction given by $\delta P = \frac{2C}{(1+r)^2}[(r + 1/r)^{-2} - c_2(r + 1/r)^{-3}]$, with $c_2 = 4(4-\pi)/(3\pi - 8)$ and $C = 0.578\,846$ is obtained from fitting numerical results in the GUE [47].

In all figures the numerical values result from averaging over eigenvectors and the spectrum, taken from the band center and from both parity sectors, of at least 1000 independent realizations of the model. In computing the Kullback-Leibler divergence, the numerical distribution for r_j is obtained by splitting the interval [0, 1] into 50 bins of equal widths.

VI. EXTENDED-TO-LOCALIZED TRANSITION

In regimes II and III, the dominant contribution to the matrix integral at the lowest energies comes from homogeneous contributions Q. Upon approaching the localization threshold III/IV, inhomogeneous fluctuations $Q \to \hat{Q} = \{Q_n\}$ gain in importance and eventually destabilize the mean-field theory. To describe this physics, we need an effective action generalized for inhomogeneous fluctuations and more manageable than Eq. (34). We derive it in Appendix D under the assumption that the sum over a large number of fluctuating terms represented by the term $\mathcal{P}(\hat{v}\hat{Q})$ is largely self-averaging. An expansion to lowest order in fluctuations around the homogeneous average then leads to the effective hopping action

$$S[Q] = S_{\mathcal{P}}[Q] + S_\omega[Q],$$

$$S_{\mathcal{P}}[Q] = \frac{\pi^2}{2} \sum_{n,m} \nu_n \nu_m \mathcal{P}_{n,m} \mathrm{Str}(Q_n Q_m), \tag{40}$$

$$S_\omega[Q] = -i\pi \sum_n \nu_n \mathrm{Str}(z Q_n), \tag{41}$$

where $Q_n = T_n^{-1}\sigma_3 T_n$ and Str traces only over internal degrees of freedom. Equations (40) and (41) are the main result of this section. Depending on the value of κ_n [Eq. (33)], this action describes the entire range from vanishing to large deformations $\hat{H}_2$. We next discuss what this action reveals about the ergodic-to-localization transition.

The key element in this problem is the hopping term (40), where Q matrices at $\hat{H}_4$-neighboring sites are coupled, subject to a weight which contains the local spectral densities. In analytic approaches to localization on high-dimensional lattices, it is common to set these weights to unity. However, in view of the massive site-to-site fluctuations of ν_n, we prefer not to make this assumption and work with a given realization $\{\nu_n\}$ for as long as possible. Approaching the transition from the localized side where the integration over Q's is subject to only small damping ν_n, the essential degrees of freedom are once again the noncompact variables θ_b contained in Q_0 [Eq. (38)].

To better understand the significance of this structure, we write $Q_n Q_m = (Q_n - \sigma_3)(Q_m - \sigma_3) + \sigma_3 Q_n + \sigma_3 Q_m - \mathbb{1}$ to represent the hopping part of the action as

$$S_{\mathcal{P}}[Q] = \pi \sum_n \Gamma_n \mathrm{Str}(Q_n \sigma_3) + \frac{\pi^2}{2} \sum_{n,m} \nu_n \nu_m \mathcal{P}_{n,m} \mathrm{Str}[(Q_n - \sigma_3)(Q_m - \sigma_3)],$$

where $\Gamma_n \equiv \nu_n \sum_m \mathcal{P}_{n,m} \nu_m$. Consider a situation where the accumulate hopping weights Γ_n out of site n are small. In this case, large fluctuations of the noncompact angles $\lambda_{\mathrm{b},n} \equiv \cosh(\theta_{\mathrm{b},n})$ dominate the functional integral. To understand the consequences, we note that the measure of the Q integration in the angular representation is given by [45]

$$\int dQ = \int dU \int_{-1}^{1} d\lambda_\mathrm{f} \int_1^\infty d\lambda_\mathrm{b} \frac{1}{(\lambda_\mathrm{b} - \lambda_\mathrm{f})^2},$$

where $\lambda_\mathrm{f} = \cos(\theta_\mathrm{f})$. For small typical values $\Gamma \sim \Gamma_n \ll 1$, the exponential weights effectively cut off the integration over λ_b at $\sim \Gamma^{-1} \gg 1$. Individual terms in the second line of the above representation of $S_{\mathcal{P}}$ are smaller than the accumulated weights in the first line, and so the integral can be approached by perturbative expansion in the hopping terms. As an example, consider the sixth-order expansion indicated via the highlighted links in Fig. 6. Retaining only the information on the noncompact integrations $\lambda \equiv \lambda_\mathrm{b}$, the contribution with a loop (left) and that with doubly occurring links evaluate to

$$\int_1^{\Gamma^{-1}} \frac{d\lambda_1}{\lambda_1^2} \frac{d\lambda_2}{\lambda_2^2} \frac{d\lambda_3}{\lambda_3^2} \frac{d\lambda_4}{\lambda_4^2} \lambda_1^3 \lambda_2^3 \lambda_3^2 \lambda_4^2 \sim \Gamma^{-6} \quad \text{(loop)},$$

$$\int_1^{\Gamma^{-1}} \frac{d\lambda_1}{\lambda_1^2} \frac{d\lambda_2}{\lambda_2^2} \frac{d\lambda_3}{\lambda_3^2} \lambda_1^3 \lambda_2^5 \lambda_3^2 \sim \Gamma^{-7} \quad \text{(no loop)}, \tag{42}$$

where the indices refer to the participating Q matrices $Q_{1,\ldots,4}$. This estimate shows that the contribution of loops in the perturbation expansion is suppressed. At the same time, the largeness of the individual contributions signals that infinite-order summations are required. The effective-medium approximation achieves this summation, loops excluded. The approximation is called an effective medium because from the perspective of individual sites in Fock space the contribution

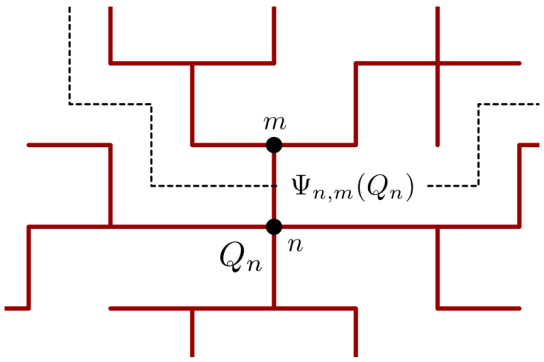

FIG. 8. Idea of the effective-medium approximation. Sites n are connected to the stems of coral-like structures, each labeled by a connected neighbor m, which represent the summation over all hopping terms excluding loops. The recursive nature of the structure allows for a self-consistent resummation.

of all hopping processes terminating at that site adds up to the influence of an effectively homogeneous background medium, transmissive or not depending on the strength of the couplings.

To see how this comes about, consider a site n with local configuration Q_n and let $\Psi_{n,m}(Q_n) = \int_{\text{coral}\,m,Q} DQ\, e^{-S[Q]}$ be the contribution to the functional integrated over all links connected to n via the neighbor m, through the loopless coral-like structure indicated in Fig. 8. The essence of the approximation is the recursion relation

$$\Psi_{nm}(Q) = \int dQ' N_{w_{nm}}(Q,Q') e^{-S_0(Q')} \prod_o \Psi_{mo}(Q'),$$

$$N_w(Q,Q') = e^{w\,\mathrm{Str}(QQ')},$$

where the product extends over all sites o connected to m by hopping, $S_0(Q) \equiv S_{\omega\to i\delta}(Q)$ acts as a convergence generating factor, and we defined

$$w_{nm} \equiv \frac{\pi^2}{2} \nu_n \nu_m \mathcal{P}_{n,m} \tag{43}$$

for the coupling constants weighting the hopping kernel. If we now take the product $\Psi_n(Q) \equiv \prod_m \Psi_{n,m}(Q)$ [assuming self-averaging in the sense that the fully integrated amplitude Ψ_n depends on the terminal site n but not on the detailed values of the $O(N^4)$ neighbor amplitudes], the equation assumes the form

$$\Psi_n(Q) = \prod_m \int dQ' N_{w_{n,m}}(Q,Q') \Psi_m(Q'),$$

where the presence of the convergence generator $\exp(-S_0)$ is left implicit. In the deeply localized regime $N_{w_{n,m}} \approx 1$, the integral decouple and $\Psi_n = 1$ is a solution by supersymmetry (i.e., the unit normalization of all sourceless integrals in the present formalism). This suggests [45] a linearization $\Psi_n(Q) = 1 - \Phi_n(Q)$, where the emergence of a nontrivial solution Φ_n is taken as a criterion for the localization transition. Substituting this ansatz into the equation and again using supersymmetry $\prod_m \int dQ' N_w(Q,Q') = 1$, we obtain

$$\Phi_n(Q) = \sum_m \int dQ' N_{w_{nm}}(Q,Q') \Phi_m(Q'). \tag{44}$$

This is a linear integral equation governed by a random lattice structure in Fock space via the couplings w_{nm} and an internal structure encoding the randomness of the $\hat{H}_4$ system via the Q' integrals. Although the integral equation may look helplessly complicated, progress is possible recalling our previous observation: We again have a situation where the Q integrations extend over wide parameter intervals such that the leading noncompact variable is the key player. Assuming that the solutions depend on the noncompact variable as $\Phi(Q) \to \Phi(t)$, $t \equiv \ln(\lambda_1/\delta)$, and referring to Ref. [48] for details of the integration over remaining variables, the reduction of Eq. (44) to the regime of interest $t \ll 0$ and $w_{mn} \ll 1$ reads

$$\Phi_n(t) = \sum_m \int dt' L_{w_{mn}}(t-t') \Phi_m(t'),$$

$$L_w(t) = \left(\frac{w}{2\pi}\right)^{1/2} e^{-w\cosh(t)+t/2} \left(w\cosh t + \frac{1}{2}\right). \tag{45}$$

Reference [48] contains a pedagogical discussion of the solution of the homogeneous variant $w_{mn} = \text{const}$ of this equation, including the somewhat subtle issue of boundary conditions. It turns out that the key to the stability of the localized solution $\Psi = 1$ lies in the spectrum of the linear kernel $\{L_{w_{mn}}(t-t')\}$: A spectrum with lower bound $\epsilon > 1$ means that perturbations $\delta\psi$ will grow under the application of the linearized kernel, signifying destabilization of the null solution $\Psi = 1$. We thus declare the existence of a minimal eigenvalue $\epsilon = 1$ as a delocalization criterion. Due to translational invariance in $t - t'$ eigenstates are of the form $e^{\theta(t-t')}\Phi_n$, where the coefficients are determined by the reduced equation $\Phi_n = \sum_m L_{\theta,nm}\Phi_m$, with

$$L_{\theta,nm} = \int_{-\infty}^{\infty} dt L_{w_{mn}}(t) e^{-\theta t}.$$

Substitution of the kernel in Eq. (45) followed by differentiation in θ shows that the positive matrix $L_{\theta,nm}$ assumes its smallest values at $\theta = 1/2$ and the straightforward integration at that value defines the matrix

$$\begin{aligned} L_{nm} &\equiv L_{1/2,nm} \\ &= \left(\frac{w_{nm}}{2\pi}\right)^{1/2} \int dt\, e^{-w_{nm}\cosh t} \left(w_{nm}\cosh t + \frac{1}{2}\right) \\ &\simeq \left(\frac{w_{nm}}{2\pi}\right)^{1/2} \ln\left(\frac{2}{w_{mn}}\right). \end{aligned}$$

We thus arrive at the eigenequation

$$\Phi_n = \frac{2\sqrt{\pi}}{\sqrt{\rho}} \sum_{|n-m|=4} a_{nm}\Phi_m,$$

$$a_{nm} = \sqrt{\nu_n\nu_m} \ln\left(\frac{\rho}{(2\pi)^2\nu_n\nu_m}\right), \tag{46}$$

where the sum extends over $Z \equiv \binom{N}{4}$ sites in Hamming distance 4 to the reference site[7] n and we recall that $\rho \equiv \binom{2N}{4}$. We

[7]We here neglect the parametrically smaller number of sites with $|n-m| = 2$ connected to n by matrix elements changing the occupation of just two fermion orbitals.

read Eq. (46) as an equation for the existence of a unit eigenvalue whose solvability depends on the value of δ determining the local density of states ν_n. In Appendix F we show that the summation in this equation is dominated by resonant sites and how this simplifies its logarithmic dependence. Once again using the self-averaging feature to replace the sum by an average over the distribution of ν_m, we find that Eq. (46) has a solution for $\delta = \delta_c$ determined by the criterion (F3). In the limit $N \gg 1$ the latter simplifies to Eq. (16). However, as discussed in Sec. II E, the numerical data for small values $N = 10^1$ responds sensitively to such approximations and improved agreement is obtained by working with the solution (F3).

VII. DISCUSSION

In this paper we have presented a first-principles analysis of Fock-space localization in the Majorana SYK_{4+2} model, describing a competition of the two-body interaction and one-body potential. Within this setting, we provided a complete description from an ergodic regime, over an intermediary regime of nonergodic extended states to the localized phase, all formulated in the eigenbasis of the one-body Hamiltonian. Our main results are the identification of the MBL transition point and the quantitative characterization of wave functions, particularly in regimes where they are neither localized nor trivially extended.

We compared the analytical results to numerical data for systems of size $N = 11$–15 without fitting parameters. For systems of this size, the intermediate regime II is too narrow for a reliable comparison. However, in the ergodic regimes I and the strongly nonergodic regime III we obtained good agreement between analytical and numerical results. The finite-size scaling of both wave-function and spectral statistics revealed an Anderson transition at a critical point which agreed with the theoretically predicted value up to a size-independent numerical constant of $O(1)$. In view of the numerous large-N approximations involved in the construction of the theory, we consider this a reassuring test for the applicability of localization theory on high-dimensional lattices to realistic systems.

Conceptually, the main contribution of the present work is an analytical description which actually is not more complex than theories for phenomenological models of MBL. The high coordination number of the microscopic Fock space gave the system self-averaging properties facilitating its analytic description. The resulting theory was tested for small-size systems $N = O(10)$. However, it is expected to work better the larger N is, while the situation with computers is the other way around. On this basis, one may be cautiously optimistic that the concepts discussed here may become building blocks for the description of more complex MBL problems, including those with spatial structure.

ACKNOWLEDGMENTS

Discussions with A. D. Mirlin, K. Tikhonov, D. A. Huse, A. Kamenev, and H. Wang are gratefully acknowledged. F.M. and T.M. acknowledge financial support from the Brazilian agencies CNPq and FAPERJ. The work of M.T. was partially supported by JSPS KAKENHI Grants No. JP17K17822, No. JP20K03787, and No. JP20H05270. This work was funded by the Deutsche Forschungsgemeinschaft (German Research Foundation), Project No. 277101999, TRR 183 (Project A03). Part of the numerical computation in this work was carried out at the Supercomputer Center, ISSP, University of Tokyo.

APPENDIX A: DERIVATION OF THE ACTION (26)

We here derive the action (26) from the averaged functional (24). We start by rewriting the quartic term as $(\bar\psi\hat X_a\psi)^2 = \mathrm{STr}[(\psi\bar\psi\hat X_a)^2]$. To decouple this nonlinearity, we multiply the functional with the unit normalized Gaussian integral $1 = \int DA\, \exp[-\frac{1}{2}\sum_a \mathrm{STr}(A_a\hat X_a)^2]$, where $DA \equiv \prod_a dA_a$ and $A_a = \{A_{nn'}^{ss',\sigma\sigma'}\}$ are $4D$-dimensional matrices. A shift $A_a \to A_a + w\psi\bar\psi$ then removes the quartic term and the subsequent integration over ψ leads to

$$\mathcal{Z}[j] = \int DA \exp\Bigg[-\frac{1}{2}\sum_a \mathrm{STr}(A_a\hat X_a)^2 - \mathrm{STr}\ln\Bigg(\hat G^{-1} + w\sum_a A_a\Bigg)\Bigg],$$

where $\hat G^{-1} = z - \hat H_2$ and we changed $A_a \mapsto \hat X_a A_a \hat X_a$. We now observe that the nonlinear part of the action couples only to the combination $\sum_a A_a$. This motivates the definition $A_a = \frac{i}{\rho}(Y + Y_a)$, where the factor of i is included for later convenience and $\sum_a Y_a = 0$. Adding a Lagrange multiplier $\frac{i}{\rho}\sum_a \mathrm{STr}(Y_a\Lambda)$ to enforce the constraint, we are led to consider the functional $\mathcal{Z}[j] = \int DY D\Lambda \exp(-S[Y,\Lambda])$, with action

$$S[Y,\Lambda] = -\frac{1}{2\rho^2}\sum_a \mathrm{STr}[(Y+Y_a)P_a(Y+Y_a)] + \frac{i}{\rho}\sum_a \mathrm{STr}(\Lambda Y_a) + \mathrm{STr}\ln(\hat G^{-1} + iwY),$$

where $\rho = \binom{2N}{4}$ and we defined the operator $\hat P_a B = \hat X_a B \hat X_a$. Note that $\hat P_a$ is self-inverse, $\hat P_a^2 B = \hat X_a^2 B \hat X_a^2 = B$, and Hermitian in the sense that $\mathrm{STr}(C\hat P_a B) = \mathrm{STr}(\hat P_a C B)$. We now do the Gaussian integrals over Y_a to obtain

$$S[Y,\Lambda] = -\mathrm{STr}\Big(\frac{\rho}{2}\Lambda\mathcal{P}\Lambda + i\Lambda Y\Big) + \mathrm{STr}\ln(\hat G^{-1} + iwY),$$

where $\mathcal{P} = \frac{1}{\rho}\sum_a \hat P_a$. The Gaussian integration over Λ may now be performed and after rescaling $Y \to \rho^{1/2}Y$ and defining $\gamma = w\rho^{1/2} = \frac{J}{2}(2N)^{1/2}$ we obtain the action $S[Y] = -\frac{1}{2}\mathrm{STr}(Y\mathcal{P}^{-1}Y) + \mathrm{STr}\ln(z - \hat H_2 + i\gamma Y)$. In a final step, we perform a linear transformation $\mathcal{P}^{-1}Y \to Y$ and recall that in our units $J^2 = 2/N$ and $\gamma = 1$ to arrive at Eq. (26).

APPENDIX B: OPERATOR $\mathcal{P}$

In this Appendix we discuss the action of the operator $\mathcal{P}$ states $|n\rangle\langle n|$ diagonal in the occupation number basis. To this end, note that for a state $|n\rangle = |n_1,\ldots,n_i,\ldots,n_N\rangle$, the action of the Majorana operator $\hat\chi_{2i} = c_i + c_i^\dagger$ produces the state $|n_i\rangle \equiv \hat\chi_{2i}|n\rangle = |n_1,\ldots,\bar n_i,\ldots,n_N\rangle$, where $\bar n$ is 0 for $n = 1$ and vice versa. Similarly, $\hat\chi_{2i-1}|n\rangle = i(-)^{n_i}|n_i\rangle$. Except

for n_i all other occupation numbers remain unchanged and no superpositions of states are generated. The adjoint action thus generates $\hat{\chi}_{2i}|n\rangle\langle n|\hat{\chi}_{2i} = \hat{\chi}_{2i-1}|n\rangle\langle n|\hat{\chi}_{2i-1} = |n_i\rangle\langle n_i|$, which we interpret as nearest-neighbor hopping in Fock space. Notice that $(\hat{\chi}_{2i}\hat{\chi}_{2i-1})|n\rangle\langle n|(\hat{\chi}_{2i-1}\hat{\chi}_{2i}) = |n\rangle\langle n|$ leaves the state unchanged.

With these structures in place, it is straightforward to describe the action of $\mathcal{P}|n\rangle\langle n| = \frac{1}{\rho}\sum_a \hat{X}_a|n\rangle\langle n|\hat{X}_a$. The summation contains contributions changing the particle number $|n|$ by 0, 2, and 4. With $\mathcal{P}_{n,m} = \langle m|(\mathcal{P}|n\rangle\langle n|)|m\rangle$, the diagonal contribution $\mathcal{P}_0$ is obtained from the $\binom{N}{2}$ terms of the structure $\hat{\chi}_{2i}\hat{\chi}_{2i+1}\hat{\chi}_{2\beta}\hat{\chi}_{2\beta+1}$. Similar counting for the contributions changing $|n|$ by 2 and 4 gives the matrix elements in (29) and it is verified that

$$\sum_m \mathcal{P}_{m,n} = \binom{N}{0}\frac{N(N-1)}{2\rho} + \binom{N}{2}\frac{4(N-2)}{\rho} + \binom{N}{4}\frac{16}{\rho} = 1. \tag{B1}$$

APPENDIX C: SADDLE-POINT EQUATIONS

In this Appendix we address the solution of the saddle-point equation (32). The nontrivial element in this equation is the quantity $\kappa_n \equiv \pi(\mathcal{P}\hat{\nu})_n$ in the denominator. In terms of this quantity, Eq. (32) becomes the simple algebraic equation (33). A closed yet site nonlocal equation for κ is obtained by acting on Eq. (32) with the operator $\mathcal{P}$,

$$\kappa_n = \sum_m \mathcal{P}_{|n-m|}\mathrm{Im}\frac{1}{v_m - i\kappa_m} = \sum_m \mathcal{P}_{|n-m|}\mathrm{Re}\int_0^\infty dt\, e^{iv_m t - \kappa_m t},$$

where in the second line we switch to a temporal Fourier representation to facilitate the treatment of the argument v_m. The solution of this equation relies on two conceptual elements, first the ansatz (33) and second a replacement of the sum over the ρ neighboring sites m by a Gaussian average over energies v_m. Specifically, we note that up to corrections small in N^{-1}, the neighbor sites m are separated by Hamming distance 4 from n and each change in n_i changes $v_n \mapsto v_n \pm 2v_i$. This means that $v_m = v_n + v$, where we assume v to be Gaussian distributed with width $\sqrt{4}2\delta = 4\delta$. Substituting the ansatz $\kappa_m = \kappa\Theta(C - |v_m|)$ into the equation and splitting the integral over v into regions with $C - |v_m| = C - |v_n + v|$ smaller and larger than zero, respectively, we obtain, after shifting $v \mapsto v - v_n$,

$$\kappa_n = \frac{1}{\sqrt{32\pi}\delta}\mathrm{Re}\int_0^\infty dt\left(\int dv\, e^{-(v-v_n)^2/32\delta^2} + \int_{-C}^{C} dv\, e^{-(v-v_n)^2/32\delta^2}(e^{-\kappa t} - 1)\right)e^{ivt}.$$

With $\mathrm{Re}\int_0^\infty dt\, e^{ivt} = \pi\delta(v)$, the first and the third term in the second line cancel out, and the t integration of the second term gives

$$\kappa_n = \frac{\sqrt{\pi}}{\sqrt{32}\delta}\int_{-C}^{C} dv\, e^{-(v-v_n)^2/32\delta^2}\frac{\kappa}{\pi(v^2+\kappa^2)}, \tag{C1}$$

where the notation emphasizes that the κ-dependent term effectively represents a δ function $\delta_\kappa(v) = \frac{\kappa}{\pi(v^2+\kappa^2)}$ in v, smeared over scales order of κ. This expression defines the mean-field amplitude κ_n at site n, in dependence on the tolerance window C for the energy v_n, and κ itself. We now explore for which configurations (C, κ) it represents a self-consistent solution.

The details of this analysis depend on whether we work with weakly (I and II) or strongly (III and IV) distributed on-site energies.

Strong on-site disorder regimes III and IV. Anticipating that all solutions satisfy $\kappa \ll 1$, the width of $\delta_\kappa(v)$ is much smaller than that of the Gaussian weight δ. The function δ_κ thus collapses the integral and we obtain

$$\kappa_n = \frac{\sqrt{\pi}}{\sqrt{32}\delta}e^{-v_n^2/32\delta^2}. \tag{C2}$$

This is consistent with our ansatz with $C = 2\delta$ and $\kappa \sim \delta^{-1}$.

Narrow on-site disorder regimes I and II. In these regimes, we test for the validity of the ansatz with $C = 1$ and $\kappa = 1$. First assume $|v_n| > 1 = C \gg \delta$. In this case, the ansatz requires exponentially suppressed κ, the δ_v function again becomes effective, and the integral collapses to $\kappa_n = \frac{\sqrt{\pi}}{\sqrt{32}\delta}\exp(-\frac{v_n^2}{32\delta^2})$, consistent with the assumed smallness of κ. Conversely, for $|v_n| < 1 = C$, the ansatz requires $\kappa = 1$. The function $\delta_\kappa = \delta_1$ is now much wider than the width of the Gaussian, order of δ, and the integration boundaries can be extended to infinity. Doing the integral, we obtain $\kappa_n \equiv \kappa = 1/\kappa$, or $\kappa = 1$, consistent with Eq. (33).

APPENDIX D: EFFECTIVE MATRIX THEORY

In this Appendix we discuss the derivation of Eqs. (40) and (41) from Eq. (26). In Eq. (26) we substitute $Y \to \pi\hat{\nu}\hat{Q}$ with $Q_n = T_n\sigma_3 T_n^{-1}$. The expansion of the action in fluctuations then comprises three parts: the Gaussian weight, the expansion of the Str ln in site-to-site fluctuations, and the expansion of the Str ln in small frequency arguments z (reflecting the noncommutativity $[z, T_n] \neq 0$).

Gaussian weight. A straightforward substitution yields

$$-\frac{1}{2}\mathrm{STr}(Y\mathcal{P}Y) \to -\frac{\pi^2}{2}\mathrm{STr}[\hat{\nu}\hat{Q}\mathcal{P}(\hat{\nu}\hat{Q})] = -\frac{\pi^2}{2}\sum_{nm}\nu_n\nu_m P_{|n-m|}\mathrm{Str}Q_nQ_m, \tag{D1}$$

where STr includes the Fock-space trace, while Str is only over internal degrees of freedom.

Fluctuation action. Substituting the ansatz into the Str ln and temporarily neglecting the frequency arguments z, we obtain

$$\begin{aligned}&\mathrm{STr}\ln[-\hat{H}_2 + i\pi\mathcal{P}(\hat{\nu}\hat{Q})]\\ &= \mathrm{STr}\ln[-\hat{H}_2 + i\hat{T}^{-1}\pi\mathcal{P}(\hat{\nu}\hat{Q})\hat{T}]\\ &= \mathrm{STr}\ln\{-\hat{H}_2 + i\pi\mathcal{P}(\hat{\nu}\sigma_3)\\ &\quad + i\pi[\hat{T}^{-1}\mathcal{P}(\hat{\nu}\hat{Q})\hat{T} - \mathcal{P}(\hat{\nu}\sigma_3)]\}\\ &\simeq \mathrm{STr}\ln\{1 + \pi^2\hat{\nu}\sigma_3[\hat{T}^{-1}\mathcal{P}(\hat{\nu}\hat{Q})\hat{T} - \mathcal{P}(\hat{\nu}\sigma_3)]\}\end{aligned}$$

$$\simeq \pi^2 \mathrm{STr}\{\hat{v}\sigma_3[\hat{T}^{-1}\mathcal{P}(\hat{v}\hat{Q})\hat{T} - \mathcal{P}(\hat{v}\sigma_3)]\}$$
$$= \pi^2 \mathrm{STr}[\hat{v}\hat{Q}\mathcal{P}(\hat{v}\hat{Q})], \tag{D2}$$

identical to $(-2\times)$ the Gaussian weight. In the second line we used the cyclic invariance $\mathrm{STr}\ln(\cdots) = \mathrm{STr}\ln[\hat{T}^{-1}(\cdots)\hat{T}]$ and in the fourth the saddle-point equation $[-\hat{H}_2 + i\pi\mathcal{P}(\hat{v}\sigma_3)]^{-1} = -i\pi\hat{v}\sigma_3$.

Frequency action. In a similar manner, we obtain

$$\mathrm{STr}\ln[-\hat{H}_2 + i\pi\mathcal{P}(\hat{v}\hat{Q}) + z]$$
$$\simeq \mathrm{STr}\ln\{\hat{T}[-\hat{H}_2 + i\pi\mathcal{P}(\hat{v}\sigma_3)]\hat{T}^{-1} + z\}$$
$$= \mathrm{STr}\ln[-\hat{H}_2 + i\pi\mathcal{P}(\hat{v}\sigma_3) + \hat{T}^{-1}z\hat{T}]$$
$$\simeq -i\pi\,\mathrm{STr}(\hat{v}\sigma_3\hat{T}^{-1}z\hat{T}) = -i\pi\,\mathrm{STr}(\hat{v}\hat{Q}z), \tag{D3}$$

where in the second line we neglected local fluctuations $P(\hat{v}\hat{T}\sigma_3\hat{T}^{-1}) \simeq \hat{T}P(\hat{v}\sigma_3)\hat{T}^{-1}$, in the third we used cyclic invariance, and in the fourth we used the saddle-point condition. Combining terms, we obtain the effective action (40).

APPENDIX E: WAVE-FUNCTION AND SPECTRAL STATISTICS FROM THE MATRIX MODEL

In this Appendix we provide details on the computation of wave-function and spectral statistics in the deformed $\hat{H}_4$ model. The starting point for both statistics is Eq. (36), with sources $j = J_K$ or $J = J_{I,n}$, respectively, given in Eq. (20). Using the commutativity $[T, \hat{H}_2] = 0$, we represent the action as

$$S[T] = \mathrm{STr}\ln(1 + \hat{G}\mathcal{O}_T) = \sum_{k=1}^{\infty}\frac{(-1)^k}{k}\mathrm{STr}(\hat{G}\mathcal{O}_T)^k,$$

where $\mathcal{O}_T \equiv T^{-1}[z - j(\alpha,\beta)]T$ is an operator in which we need to expand to the order required by the correlation function and we have made the source contribution $j(\alpha,\beta)$ to the matrix $z = \frac{\omega+i\eta}{2}\sigma_3$ explicit again. Concerning the resolvent $\hat{G}^{-1} \equiv i\hat{\kappa}\sigma_3 - \hat{H}_2$, we notice that fluctuation variables commute through the real part of $\hat{G}$ and keep only $i\,\mathrm{Im}\hat{G} = -i\pi\hat{v}$, with local components v_n defined in Eq. (32). Specifically, to zeroth order in the sources and first order in an expansion in $zv_n \sim \omega/\Delta$, the action assumes the form (37).

For the computation of the spectral and wave-function statistics, we need the expansion in sources to first order in β and higher orders in α. With the above definitions, the expansion of the action assumes the form

$$S[T] = -\pi\sum_{k=1}^{\infty}(-iv_n\alpha)^k\left(\frac{1}{k}[Q_{\mathrm{bb}}^{++}]^k + \frac{\beta}{\alpha}[Q_{\mathrm{bb}}^{++}]^{k-1}Q_{\mathrm{ff}}^{--}\right), \tag{E1}$$

where in the terms $k > 2$ we used the approximation $Q_{\mathrm{bf}}^{+-}Q_{\mathrm{fb}}^{-+} \simeq Q_{\mathrm{bb}}^{++}Q_{\mathrm{ff}}^{--}$ valid in the limit $\eta \to 0$ implied in the calculation of wave-function moments [45]. Doing the derivatives in the source parameters, we arrive at

$$\partial_\alpha^{q-1}\partial_\beta\mathcal{Z}|_{\alpha,\beta=0} = (-i\pi v_n)^q q!\langle[Q_{\mathrm{bb}}^{++}]^{q-1}Q_{\mathrm{ff}}^{--}\rangle, \tag{E2}$$

where $\langle\cdots\rangle = \int dQ\, e^{-S_z[Q]}(\cdots)$.

The remaining integral over the four-dimensional matrix Q is conceptually straightforward but technically the hardest part of the calculation. Referring for details to Ref. [45], here we review the main steps. The starting point is a polar coordinate representation $Q = UQ_0U^{-1}$, with Q_0 defined in Eq. (38), and $\hat{\theta} = \mathrm{diag}(i\hat{\theta}_{\mathrm{b}}, \hat{\theta}_{\mathrm{f}})$ containing compact and noncompact angles $0 < \theta_{\mathrm{f}} < \pi$ and $\theta_{\mathrm{b}} > 0$, respectively [45]. The matrix U is block diagonal in causal space and contains four Grassmann variables $\eta^{\pm}$ and $\bar{\eta}^{\pm}$ and two more commuting variables $0 \leqslant \phi$ and $\hat{\chi} < 2\pi$. More specifically, $U = \mathrm{diag}(u_1u_2, v)_{\mathrm{ra}}$, where $u_2 = \mathrm{diag}(e^{i\phi}, e^{i\hat{\chi}})_{\mathrm{bf}}$ and supermatrices $u_1 = e^{-2\hat{\eta}^+}$ and $v = e^{-2i\hat{\eta}^-}$, generated by $\hat{\eta}^{\pm} = \left(\begin{smallmatrix}0 & \bar{\eta}^{\pm}\\ -\eta^{\pm} & 0\end{smallmatrix}\right)_{\mathrm{bf}}$. In this representation, the matrix elements entering the correlation function are given by $Q_{\mathrm{bb}}^{++} = \cosh\theta_{\mathrm{bb}}(1 - 4\bar{\eta}^+\eta^+)$ and $Q_{\mathrm{ff}}^{--} = \cos\theta_{\mathrm{ff}}(1 - 4\bar{\eta}^-\eta^-)$ and the integration measure reads $dQ = \frac{1}{2^6\pi^2}\frac{\sinh\theta_{\mathrm{b}}\sin\theta_{\mathrm{f}}}{(\cosh\theta_{\mathrm{b}} - \cos\theta_{\mathrm{f}})^2}d\phi d\hat{\chi}d\theta_{\mathrm{b}}d\theta_{\mathrm{f}}d\bar{\eta}^+d\eta^+d\bar{\eta}^-d\eta^-$ [45]. The essential advantage of the polar representation is that the action only depends on the radial variables $S_\eta[Q] = -i2\pi\nu(\omega + i\eta)(\cosh\theta_{\mathrm{b}} - \cos\theta_{\mathrm{f}})$.

Wave-function statistics. In the calculation of the wave-function moments, we may set $\omega = 0$. The integration over the noncompact angle is then cut by the parameter η at values $1 \leqslant \cosh\theta_{\mathrm{b}} \lesssim 1/\eta$, while the integration over the compact angles θ_{f} is free. With this simplification, the integration over all variables except the noncompact one θ becomes elementary and one obtains [45]

$$G_{nn}^{+(q-1)}G_{nn}^{-} = 2q(q-1)(-i\pi\nu_n)^q \times\int_0^{\infty}d\theta_{\mathrm{b}}\sinh\theta_{\mathrm{b}}(\cosh\theta_{\mathrm{b}})^{q-2}e^{-2\pi\nu\eta\cosh\theta_{\mathrm{b}}}. \tag{E3}$$

The final integral gives $(2\pi\nu\eta)^{1-q}q!$ and collecting all factors we arrive at

$$I_q = \frac{q!}{\nu^q}\sum_n \nu_n^q. \tag{E4}$$

This result expresses the qth moment of the local wave-function amplitudes through that of the local density of states individually averaged over $\hat{H}_4$ fluctuations. The energies v_n at each individual site are obtained as sums of N random coefficients v_i [cf. Eq. (3)]. For large N, this makes the sum self-averaging, and we replace $I_q \to \langle I_q\rangle_v$ by its average over single-particle energies v_i. Using Eq. (32), we thus obtain

$$I_q = \frac{(-)^{q-1}q}{(\pi\nu)^q}\sum_n(\kappa_n)^q\left\langle\partial_{(\kappa_n)^2}^{q-1}\frac{1}{v_n^2 + (\kappa_n)^2}\right\rangle.$$

The evaluation of this expression now depends on which on-site disorder regime we are in. In regime I, $\delta < N^{-1/2}$ or $|v_n| < 1$, the mean-field broadening assumes the uniform value $\kappa = 1$. In this case, the dependence of I_q on site energies v_n is weak. This implies $\nu \simeq \frac{1}{\pi}\sum_n 1 = D/\pi$. Doing the κ derivatives, we obtain

$$I_q = q!D^{1-q} \quad \text{in regime I}, \tag{E5}$$

which is the RMT result for a matrix of dimension D.

For larger disorder, only a fraction of sites have finite decay width. Using Eq. (33) and assuming self-averaging to replace the n sum to an average over a distribution of site energies of

width δN, the DOS is evaluated as

$$\begin{aligned}\nu &\simeq \frac{1}{\pi}\frac{D}{\sqrt{2\pi N\delta^2}}\int_{-C}^{C} d\upsilon\, e^{-\upsilon^2/2N\delta^2}\frac{\kappa}{\upsilon^2+\kappa^2}\\ &\simeq \frac{1}{\pi}\frac{D}{\sqrt{2\pi N\delta^2}}\int_{-C}^{C} d\upsilon\frac{\kappa}{\upsilon^2+\kappa^2}\\ &= \frac{1}{\pi}\frac{2D}{\sqrt{2\pi N\delta^2}}\arctan(C/\kappa),\end{aligned}$$

where in the second line we used that the distribution of energies is much wider than the tolerance window C. Substituting the values specified in Eq. (33), this leads to

$$\nu = c\frac{D}{\sqrt{N}\delta}, \tag{E6}$$

where c is of order unity and the suppression relative to $\nu = cD$ in regime I accounts for the improbability to find resonant sites.

In the same manner, we obtain

$$\begin{aligned}I_q &\simeq \frac{(-)^{q-1}q}{(\pi\nu)^q}\frac{D}{\sqrt{2\pi N\delta^2}}\kappa^q\partial_{\kappa^2}^{q-1}\int_{-C}^{C} d\upsilon\, e^{-\upsilon^2/2N\delta^2}\frac{1}{\upsilon^2+\kappa^2}\\ &\simeq \frac{(-)^{q-1}q}{(\pi\nu)^q}\frac{D}{\sqrt{2\pi N\delta^2}}\kappa^q\partial_{\kappa^2}^{q-1}\int_{-C}^{C} d\upsilon\frac{1}{\upsilon^2+\kappa^2}\\ &= 2\frac{(-)^{q-1}q}{(\pi\nu)^q}\frac{D}{\sqrt{2\pi N\delta^2}}\kappa^q\partial_{\kappa^2}^{q-1}\frac{1}{\kappa}\arctan(C/\kappa)\\ &\simeq 2\frac{(-)^{q-1}q}{(\pi\nu)^q}\frac{D}{\sqrt{2\pi N\delta^2}}\kappa^q\partial_{\kappa^2}^{q-1}\frac{1}{\kappa}\\ &= \frac{1}{(\pi\nu)^q}\frac{D}{\sqrt{2\pi N\delta^2}}\frac{2q(2q-3)!!}{(2\kappa)^{q-1}},\end{aligned}$$

where $\simeq$ means equality up to some constant $c\sim O(1)$. Insertion of Eq. (E6) leads to Eq. (13). Using Eq. (33), we finally obtain

$$I_q = c^q q!\left(\frac{D}{\sqrt{N}}\right)^{1-q}\times\begin{cases}\delta^{q-1} & \text{in regime II}\\ \delta^{2(q-1)} & \text{in regime III}\end{cases} \tag{E7}$$

for $q\gg 1$. Finally, for a quantitative comparison to numerical simulations in regime III without fitting parameter we trace all constants $c\sim O(1)$ in ν and I_q. Noting that in regime III we can substitute $\arctan(C/\kappa)=\pi/2$, we arrive at

$$I_q = \frac{q(2q-3)!!}{(2\pi\nu\kappa)^{q-1}} = \frac{q(2q-3)!!}{\delta^{2(1-q)}}\left(\frac{\pi D}{4\sqrt{N}}\right)^{1-q}\quad\text{in regime III,} \tag{E8}$$

where in the second equality we used Eq. (C2) for κ.

Level statistics. For the level statistics we need to keep finite ω and differentiate the functional to first order in α and β [Eq. (22)]. Application of Eq. (E2) then leads to [45]

$$\begin{aligned}K(\omega) = \frac{1}{2}\mathrm{Re}\int_0^\infty d\theta_\mathrm{b}\int_{-\pi/2}^{\pi/2} d\theta_\mathrm{f}\\ \times\sinh\theta_\mathrm{b}\sin\theta_\mathrm{f} e^{i\pi\nu\omega(\cosh\theta_\mathrm{b}-\cos\theta_\mathrm{f})},\end{aligned} \tag{E9}$$

where θ_b and θ_f are the noncompact bosonic and compact fermionic angle, respectively. These integrals can be carried out in closed form and yield the two-point correlation function of the Gaussian unitary ensemble (9).

APPENDIX F: LOCALIZATION CRITERION

In this Appendix we demonstrate how the solution of the eigenvalue equation (46) reduces to the criterion (16). We write the sum as

$$\Phi_n = \frac{2\sqrt{\pi}}{\sqrt{\rho}}\sum_{|n-m|=4} a_{nm}\Phi_m,$$

$$a_{nm} = \sqrt{\nu_n\nu_m}\ln\left(\frac{\rho}{(2\pi)^2\nu_n\nu_m}\right)$$

and make the self-consistent assumption that the sum over neighboring sites m is dominated by resonant sites and that the solution Φ_n too is peaked at those sites. Under these conditions it makes sense to consider a zeroth-order approximation $a_{nm}\simeq a^0_{nm}\equiv\sqrt{\nu_n\nu_m}2\ln(\sqrt{\rho}/2\pi\nu_m)$, neglecting site-to-site fluctuations of the logarithm. In a final step we will refine the result by perturbation theory in $\delta a_{nm}\equiv a_{nm}-a^0_{nm}=\sqrt{\nu_n\nu_m}\ln(\nu_m/\nu_n)$. Making the replacement $a_{nm}\to a^0_{nm}$, we observe that the equation is solved by $\Phi_n\propto\sqrt{\nu_n}$, provided

$$1 = \frac{4\sqrt{\pi}}{\sqrt{\rho}}\sum_m \nu_m\ln\left(\frac{\sqrt{\rho}}{2\pi\nu_m}\right), \tag{F1}$$

where the sum extends over the $Z\equiv\binom{N}{4}$ sites in Hamming distance 4 to n (i.e., the parameter Z defines the effective coordination number of the Fock-space lattice). We note that with the above eigenstates the first-order perturbative correction to the unit eigenvalue equation (F1) is given by $\langle\Phi|\delta\alpha|\Phi\rangle\propto\sum_{nm}\nu_n\nu_m\ln(\nu_n/\nu_m)=0$, which we take as a self-consistent justification to work with the zeroth-order approximation. Turning to the consistency equation for the eigenvalue, we again replace the sum over nearest neighbors by an average over their distribution of energies (cf. a similar operation in Appendix C)

$$\sum_m \nu_m f(\nu_m)\simeq Z\langle\nu(\upsilon)f(\nu(\upsilon))\rangle_\upsilon\simeq Z\frac{f\left(\frac{\sqrt{32}\delta}{\sqrt{\pi}}\right)}{\sqrt{32\pi}\delta},$$

$$\langle\cdots\rangle_\upsilon = \frac{1}{\sqrt{2\pi}4\delta}\int d\upsilon\, e^{-\upsilon^2/32\delta^2}(\cdots).$$

Here the second equality is based on the observation that on the subset of active sites $\upsilon<\delta$, where $\nu(\upsilon)$ is nonvanishing, and $\nu(\upsilon)=\frac{\pi}{\delta(\upsilon^2+\delta^{-2})}$ becomes a δ function of width order of δ^{-1} and height $\nu(0)=\pi/\kappa$ with $\kappa=\frac{\sqrt{\pi}}{\sqrt{32}\delta}$ [cf. Eq. (C2)]. The integral collapses to this resonance region, leading to the stated result. (Effectively, this is saying that only resonant sites contribute to the nearest-neighbor sum.)

Application of this auxiliary identity to the eigenvalue equation (F1) leads to

$$1 = \frac{1}{\sqrt{2\rho}}\frac{Z}{\delta}\ln\left(\sqrt{\frac{8\rho}{\pi}}\delta\right), \tag{F2}$$

which is solved by

$$\delta_c = \frac{Z}{\sqrt{2\rho}}W(2Z\sqrt{\pi}), \tag{F3}$$

with W the Lambert W function. For $N \gg 1$, we may approximate $Z = \binom{N}{4} \simeq N^4/24$ and $\rho = \binom{2N}{4} \simeq (2N)^4/4!$. The asymptotic expansion for large arguments $W(x) \simeq \ln(x) + \cdots$ then leads to the estimate (16).

[1] P. W. Anderson, Absence of diffusion in certain random lattices, Phys. Rev. **109**, 1492 (1958).

[2] D. Basko, I. Aleiner, and B. Altshuler, Metal-insulator transition in a weakly interacting many-electron system with localized single-particle states, Ann. Phys. (NY) **321**, 1126 (2006).

[3] I. V. Gornyi, A. D. Mirlin, and D. G. Polyakov, Interacting Electrons in Disordered Wires: Anderson Localization and Low-T Transport, Phys. Rev. Lett. **95**, 206603 (2005).

[4] M. Znidaric, T. Prosen, and P. Prelovsek, Many-body localization in the Heisenberg XXZ magnet in a random field, Phys. Rev. B **77**, 064426 (2008).

[5] A. Pal and D. A. Huse, Many-body localization phase transition, Phys. Rev. B **82**, 174411 (2010).

[6] J. H. Bardarson, F. Pollmann, and J. E. Moore, Unbounded Growth of Entanglement in Models of Many-Body Localization, Phys. Rev. Lett. **109**, 017202 (2012).

[7] M. Serbyn, Z. Papic, and D. A. Abanin, Universal Slow Growth of Entanglement in Interacting Strongly Disordered Systems, Phys. Rev. Lett. **110**, 260601 (2013).

[8] J. A. Kjäll, J. H. Bardarson, and F. Pollmann, Many-Body Localization in a Disordered Quantum Ising Chain, Phys. Rev. Lett. **113**, 107204 (2014).

[9] K. Agarwal, S. Gopalakrishnan, M. Knap, M. Müller, and E. Demler, Anomalous Diffusion and Griffiths Effects Near the Many-Body Localization Transition, Phys. Rev. Lett. **114**, 160401 (2015).

[10] J. Z. Imbrie, Diagonalization and Many-Body Localization for a Disordered Quantum Spin Chain, Phys. Rev. Lett. **117**, 027201 (2016).

[11] J. Z. Imbrie, On many-body localization for quantum spin chains J. Stat. Phys. **163**, 998 (2016).

[12] E. J. Torres-Herrera and L. F. Santos, Extended nonergodic states in disordered many-body quantum systems, Ann. Phys. (Berlin) **529**, 1600284 (2017).

[13] N. Macé, F. Alet, and N. Laflorencie, Multifractal Scalings across the Many-Body Localization Transition, Phys. Rev. Lett. **123**, 180601 (2019).

[14] B. L. Altshuler, Y. Gefen, A. Kamenev, and L. S. Levitov, Quasiparticle Lifetime in a Finite System: A Nonperturbative Approach, Phys. Rev. Lett. **78**, 2803 (1997).

[15] P. G. Silvestrov, Decay of a Quasiparticle in a Quantum Dot: The Role of Energy Resolution, Phys. Rev. Lett. **79**, 3994 (1997).

[16] P. G. Silvestrov, Chaos thresholds in finite Fermi systems, Phys. Rev. E **58**, 5629 (1998).

[17] I. V. Gornyi, A. D. Mirlin, and D. G. Polyakov, Many-body delocalization transition and relaxation in a quantum dot, Phys. Rev. B **93**, 125419 (2016).

[18] I. V. Gornyi, A. D. Mirlin, D. G. Polyakov, and A. L. Burin, Spectral diffusion and scaling of many-body delocalization transitions, Ann. Phys. (Berlin) **529**, 1600360 (2017).

[19] A. Rubio-Abadal, J.-Y. Choi, J. Zeiher, S. Hollerith, J. Rui, I. Bloch, and C. Gross, Many-Body Delocalization in the Presence of a Quantum Bath, Phys. Rev. X **9**, 041014 (2019).

[20] J.-Y. Choi, S. Hild, J. Zeiher, P. Schauß, A. Rubio-Abadal, T. Yefsah, V. Khemani, D. A. Huse, I. Bloch, and C. Gross Exploring the many-body localization transition in two dimensions, Science **352**, 1547 (2016).

[21] M. Schreiber, S. S. Hodgman, P. Bordia, H. P. Lüschen, M. H. Fischer, R. Vosk, E. Altman, U. Schneider, and I. Bloch, Observation of many-body localization of interacting fermions in a quasi-random optical lattice, Science **349**, 842 (2015).

[22] K. Xu, J. J. Chen, Y. Zeng, Y. R. Zhang, C. Song, W. Liu, Q. Guo, P. Zhang, D. Xu, H. Deng, K. Huang, H. Wang, X. Zhu, D. Zheng, and H. Fan, Emulating Many-Body Localization with a Superconducting Quantum Processor, Phys. Rev. Lett. **120**, 050507 (2018).

[23] P. Roushan, C. Neill, J. Tangpanitanon, V. M. Bastidas, A. Megrant, R. Barends, Y. Chen, Z. Chen, B. Chiaro, A. Dunsworth *et al.*, Spectroscopic signatures of localization with interacting photons in superconducting qubits, Science **358**, 1175 (2017).

[24] A. De Luca, B. L. Altshuler, V. E. Kravtsov, and A. Scardicchio, Anderson Localization on the Bethe Lattice: Nonergodicity of Extended States, Phys. Rev. Lett. **113**, 046806 (2014).

[25] G. Biroli and M. Tarzia, Delocalization and ergodicity of the Anderson model on Bethe lattices, arXiv:1810.07545.

[26] K. S. Tikhonov and A. D. Mirlin, Statistics of eigenstates near the localization transition on random regular graphs, Phys. Rev. B **99**, 024202 (2019).

[27] K. S. Tikhonov and A. D. Mirlin, Critical behavior at the localization transition on random regular graphs, Phys. Rev. B **99**, 214202 (2019).

[28] L. Faoro, M. Feigel'man, and L. Ioffe, Non-ergodic extended phase of the quantum random energy model, Ann. Phys. (NY) **409**, 167916 (2019)

[29] V. E. Kravtsov, I. M. Khaymovich, E. Cuevas, and M. Amini, A random matrix model with localization and ergodic transitions, New J. Phys. **17**, 122002 (2015).

[30] X. Leyronas, P. G. Silvestrov, and C. W. J. Beenakker, Scaling at the Chaos Threshold in an Interacting Quantum Dot, Phys. Rev. Lett. **84**, 3414 (2000).

[31] S. Sachdev and J. Ye, Gapless Spin-Fluid Ground State in a Random Quantum Heisenberg Magnet, Phys. Rev. Lett. **70**, 3339 (1993).

[32] A. Kitaev, Talks at KITP on 7 April and 27 May 2015, https://online.kitp.ucsb.edu//online/entangled15/kitaev/; https://online.kitp.ucsb.edu//online/entangled15/kitaev2/ (Kavli Institute for Theoretical Physics, UC Santa Barbara, 2015).

[33] A. M. García-García, B. Loureiro, A. Romero-Bermúdez, and M. Tezuka, Chaotic-Integrable Transition in the Sachdev-Ye-Kitaev Model, Phys. Rev. Lett. **120**, 241603 (2018).

[34] A. R. Kolovsky and D. L. Shepelyansky, Dynamical thermalization in isolated quantum dots and black holes, Europhys. Lett. **117**, 10003 (2017).

[35] N. Rosenzweig and C. E. Porter, Repulsion of energy levels in complex atomic spectra, Phys. Rev. **120**, 1698 (1960).

[36] M. R. Zirnbauer, Localization transition on the Bethe lattice, Phys. Rev. B **34**, 6394 (1986).

[37] I. García-Mata, O. Giraud, B. Georgeot, J. Martin, R. Dubertrand, and G. Lemarié, Scaling Theory of the Anderson Transition in Random Graphs: Ergodicity and Universality, Phys. Rev. Lett. **118**, 166801 (2017).

[38] I. García-Mata, J. Martin, R. Dubertrand, O. Giraud, B. Georgeot, and G. Lemarié, Two critical localization lengths in the Anderson transition on random graphs, Phys. Rev. Res. **2**, 012020 (2020).

[39] T. Micklitz, F. Monteiro, and A. Altland, Nonergodic Extended States in the Sachdev-Ye-Kitaev Model, Phys. Rev. Lett. **123**, 125701 (2019).

[40] V. Oganesyan and D. A. Huse, Localization of interacting fermions at high temperature, Phys. Rev. B **75**, 155111 (2007).

[41] V. E. Kravtsov, B. L. Altshuler, and L. B. Ioffe, Non-ergodic delocalized phase in Anderson model on Bethe lattice and regular graph, Ann. Phys. (NY) **389**, 148 (2018).

[42] G. Biroli and M. Tarzia, Delocalized glassy dynamics and many-body localization, Phys. Rev. B **96**, 201114(R) (2017).

[43] G. Biroli, A. C. Ribeiro-Teixeira, and M. Tarzia, Difference between level statistics, ergodicity and localization transitions on the Bethe lattice, arXiv:1211.7334.

[44] B. L. Altshuler, E. Cuevas, L. B. Ioffe, and V. E. Kravtsov, Nonergodic Phases in Strongly Disordered Random Regular Graphs, Phys. Rev. Lett. **117**, 156601 (2016).

[45] K. B. Efetov, *Supersymmetry in Disorder and Chaos* (Cambridge University Press, Cambridge, 1999).

[46] K. Truong and A. Ossipov, Eigenvectors under a generic perturbation: Non-perturbative results from the random matrix approach, Europhys. Lett. **116**, 37002 (2016).

[47] Y. Y. Atas, E. Bogomolny, O. Giraud, and G. Roux, Distribution of the Ratio of Consecutive Level Spacings in Random Matrix Ensembles, Phys. Rev. Lett. **110**, 084101 (2013).

[48] M. R. Zirnbauer, Anderson localization and nonlinear σ model with graded symmetry, Nucl. Phys. B **265**, 375 (1986).

Chapter 6

Quantum ergodicity in the many-body localization problem

The following consists of a reproduction Ref. [3], co-authored with Masaki Tezuka, Alexander Altland, David A. Huse, and Tobias Micklitz.

Quantum Ergodicity in the Many-Body Localization Problem

Felipe Monteiro,[1] Masaki Tezuka,[2] Alexander Altland,[3] David A. Huse,[4] and Tobias Micklitz[1]
[1]Centro Brasileiro de Pesquisas Físicas, Rua Xavier Sigaud 150, 22290-180 Rio de Janeiro, Brazil
[2]Department of Physics, Kyoto University, Kyoto 606-8502, Japan
[3]Institut für Theoretische Physik, Universität zu Köln, Zülpicher Straße 77, 50937 Cologne, Germany
[4]Department of Physics, Princeton University, Princeton, New Jersey 08544, USA

(Received 23 December 2020; revised 9 April 2021; accepted 28 May 2021; published 15 July 2021)

We generalize Page's result on the entanglement entropy of random pure states to the many-body eigenstates of realistic disordered many-body systems subject to long-range interactions. This extension leads to two principal conclusions: first, for increasing disorder the "shells" of constant energy supporting a system's eigenstates fill only a fraction of its full Fock space and are subject to intrinsic correlations absent in synthetic high-dimensional random lattice systems. Second, in all regimes preceding the many-body localization transition individual eigenstates are thermally distributed over these shells. These results, corroborated by comparison to exact diagonalization for an SYK model, are at variance with the concept of "nonergodic extended states" in many-body systems discussed in the recent literature.

DOI: 10.1103/PhysRevLett.127.030601

Introduction.—Complex quantum systems exposed to external disorder may enter a phase of strong localization. About two decades after the prediction of many-body localization (MBL) [1–3], there is still no strong consensus about the stability of the MBL phase and/or the possible presence of an intermediate phase between MBL and the thermal phase. One class of models where these questions can be explored with more analytic control is confined many-body systems with long-range interactions. Under these conditions, the interaction operator couples all single-particle states, which facilitates the analysis. At the same time, the Hilbert space dimension is still exponentially large in the particle number, which leads to rich physics relevant to systems such as chaotic many-body quantum devices [4–7], small sized optical lattices [8–10], or qubit arrays [11,12].

In recent years, the complex structure of many-body quantum *states* in MBL has become a focus of intensive research. Unlike with single particle problems, where extended wave functions uniformly cover real space, increasing the disorder in a phase of extended many-body states $|\psi\rangle$ leads to a diminished wave function support in Fock space. This phenomenon, which shows, e.g., in a suppression of wave function moments (WFM) $|\langle n|\psi\rangle|^{2q}$ in an occupation number basis $|n\rangle$, has led to the proposal of a phase of "*nonergodic* extended states" [13–16] intermediate between the phases of absent and strong localization. An alternative scenario is that for each realization of the disorder only a subset of states $\{|n\rangle\}$ have finite overlap with the eigenstates of energy E, and in this way define a quantum *energy shell* in Fock space. A uniform (thermal) distribution of the exact eigenstates on this shell would then be the defining criterion for maintained quantum *ergodicity* on the delocalized side of the MBL transition.

At this stage, there is mounting evidence in favor of the second scenario [17–20]. However, in order to firmly characterize the physics of a globally realized many-body ergodic quantum phase, two questions need to be addressed: How can the energy shell be described in quantitative terms? And what is the distribution of quantum states on that shell? As indicated above, wave function statistics can provide at least part of an answer to the first question. In this Letter, we focus on the equally important second part of the problem and demonstrate that the key to its solution lies in concepts of quantum information. Specifically, we will compute pure state entanglement entropies (EE) under a relatively mild set of assumptions. Within this framework we find that to zeroth order wave functions remain thermally distributed over the shell. This establishes a microcanonical distribution, in agreement with the second scenario—maintained ergodicity in all regimes prior to the transition. In addition, the EE contains subleading terms which reflect the characteristic way in which the energy shell is interlaced into Fock space. These contributions sharply distinguish the energy shells of genuine many-body systems from those of phenomenological high dimensional models such as the random energy model (REM) or sparse random states [21]. In this way the combined analysis of WFMs and EEs becomes a sensitive probe into the complex manifestation of wave function ergodicity in many particle systems.

Pure state entanglement entropies.—For a pure state $\rho = |\psi\rangle\langle\psi|$, the entanglement entropy relative to a partitioning $\mathcal{F} = \mathcal{F}_A \otimes \mathcal{F}_B$ of Fock space is defined as the von Neumann entropy, $S_A = -\mathrm{tr}_A(\rho_A \ln \rho_A)$ of the reduced density matrix $\rho_A = \mathrm{tr}_B(|\psi\rangle\langle\psi|)$. The entanglement entropies of pure maximally random states were calculated in the

classic Ref. [22]. More recent work [23] emphasizes the utility of the concept in the context of random matrix models serving as proxies of high-dimensional localizing systems [14]. In these systems, quantum interference shows in a contribution to the entanglement entropy proportional to the ratio of subsystem Fock-space dimensions. A main finding of the present work is that energy-shell correlations distinguishing microscopic systems from random matrix models open a second channel of quantum information and exponentially enhance the suppression of the entanglement below its thermal value. In this way, the entanglement sharply distinguishes between genuine many-body wave functions and wave functions on generic high-dimensional random lattices.

In the rest of this Letter, we will compute the entanglement entropy of pure states prior to the onset of strong localization under a minimal set of assumptions. We will compare our results to the entropies obtained for phenomenological models and to numerical data obtained for a Majorana Sachdev-Ye-Kitaev (SYK) model.

Energy shell.—We begin with a qualitative discussion of the Fock space energy shell. Consider a many-body Hamiltonian $\hat{H} = \hat{H}_2 + \hat{H}_4$, where $\hat{H}_4$ is an interaction operator and $\hat{H}_2$ a one-body operator defined by a single particle spectrum $\{m_i\}$, $i = 1, \ldots, N$ distributed over a range δ. Working in the eigenbasis of $\hat{H}_2$, Fock space is spanned by the $D \equiv 2^N$ occupation number states $n = (n_1, \ldots, n_N)$, $n_i = 0,\ 1$ for spinless fermions. We interpret these states as sites of a hypercubic lattice, carrying local potentials $v_n = \sum(2n_i - 1)m_i$ with rms value $\Delta_2 \equiv N^{1/2}\delta$. Individual states n are connected to a polynomially large number N^α of "nearest neighbors" m by the interaction $\hat{H}_4$. For interaction matrix elements $t_{nm} \sim gN^{-\beta/2}$, the rms eigenvalue of $\hat{H}_4$ scales as $\Delta_4 \sim gN^{(\alpha-\beta)/2}$, with g an N-independent coupling energy for the interaction. These interactions change only an order-one number of occupation numbers, so $|v_n - v_m|$ is of order δ and thus for large N much smaller than the "bandwidth" Δ_2 of $\hat{H}_2$.

In the competition of the operators $\hat{H}_2$ and $\hat{H}_4$, states n may hybridize with states m via the coupling t_{nm}. When the eigenstates of $\hat{H}$ are delocalized in Fock space, this hybridization gives the local spectral density

$$\nu_n(E) \equiv -\frac{1}{\pi}\mathrm{Im}\langle n|(E^+ - \hat{H})^{-1}|n\rangle, \tag{1}$$

a linewidth $\kappa = \kappa(v_n, \delta, g)$ which must be self-consistently determined [24]. The solution of Eq. (1) for a given realization of the disorder contains the essential information on the distribution of the energy shell in Fock space. Specifically, for generic values of the energy E (we set $E = 0$ for concreteness), the strength of the disorder δ defines four regimes of different shell structure:

Regime I: $\delta \ll N^{-1/2}\Delta_4$: the characteristic disorder band width $\delta N^{1/2} = \Delta_2 \ll \Delta_4$ is perturbatively small. In this regime, the spectral density $\nu_n \equiv \nu$ is approximately constant over energy scales $\sim\Delta_2$.

Regime II: $N^{-1/2}\Delta_4 \ll \delta \ll \Delta_4$: the bandwidth of $\hat{H}_2$ exceeds that of the interaction $\hat{H}_4$, but nearest neighbors remain energetically close $|v_n - v_m| \sim \delta \ll \Delta_4$. In this regime, $\kappa \sim \Delta_4$, indicating that the full interaction Hamiltonian enters the hybridization of neighboring sites.

Regime III: $\Delta_4 \ll \delta \ll \delta_c$: only a fraction $\sim(\Delta_4/\delta)^2$ of nearest neighbors remain in resonance, and the broadening is reduced to $\kappa \sim \Delta_4^2/\delta$.

Regime IV: The threshold to localization δ_c is reached when less than one of the $\sim N^\alpha$ neighbors of characteristic energy separation δ falls into the broadened energy window. Up to corrections logarithmic in N (and neglecting potential modifications due to Fock space loop amplitudes) this leads to the estimate $\delta_c \sim N^{\alpha/2}\Delta_4$ for the boundary to the strong localization regime.

The energy shell in the delocalized regimes II and III is an extended cluster of resonant sites embedded in Fock space. It owes its structure to the competition between the large number $\mathcal{O}(N^\alpha)$ of nearest neighbor matrix elements and the detuning of statistically correlated nearest neighbor energies v_n, v_m. In regime II, only a polynomially (in N) small fraction $\kappa/\Delta_2 \overset{II}{\sim} \Delta_4/(\delta N^{1/2})$ of Fock space sites lie in the resonant window defining the energy shell, and in III this fraction is further reduced to $\overset{III}{\sim}\Delta_4^2/(\delta^2 N^{1/2})$, before the shell fragments at the boundary to regime IV.

We also note that *if* a site n lies on the shell, the probability that its neighboring sites of energy $v_m = v_n \pm \mathcal{O}(\delta)$ are likewise on-shell is parametrically enhanced compared to that of generic sites with energy $v_n \pm \mathcal{O}(\Delta_2)$. It is this principle which gives the energy shell of many-body systems a high degree of internal correlations (absent in phenomenological lattice models with statistically independent on-site randomness) [26]. What physical quantities are sensitive to these correlations? And how do quantum states spread over the shell structure? As we are going to discuss next, the pure state entanglement entropy S_A contains the answer to these questions.

Entanglement entropy.—Consider a Fock space (outer product) partitioning defined by $n = (l, m)$ where the N_A-bit vector l labels the states of subsystem A and m those of B with $N_B = N - N_A \gg N_A$. We are interested in the disorder averaged moments $M_r \equiv \langle \mathrm{tr}_A(\rho_A^r)\rangle$, and the entanglement entropy $S_A = -\partial_r M_r|_{r=1}$ of the reduced density matrix $\rho_A = \mathrm{tr}_B(|\psi\rangle\langle\psi|)$ defined by a realization-specific zero-energy eigenstate $\hat{H}|\psi\rangle = 0$. The bookkeeping of index configurations entering the moments $\mathrm{tr}_A(\rho_A^r) = \psi_{l^1m^1}\bar{\psi}_{l^2m^1}\psi_{l^2m^2}\ldots\psi_{l^rm^r}\bar{\psi}_{l^1m^r}$ is conveniently done in a tensor network representation as in Fig. 1. Introducing a multi-index $\mathcal{N} \equiv (n^1, \ldots, n^r)$, and analogously for $\mathcal{N}_{A,B}$, the figure indicates how the index-data

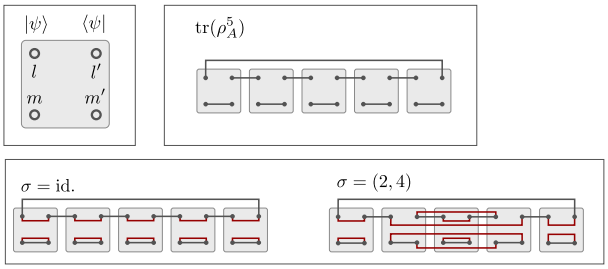

FIG. 1. Top left: graphic representation of the tensor amplitude $\psi_{lm}\bar{\psi}_{l'm'}$. Top right: contraction of indices defining $\mathrm{tr}(\rho_A^5)$. Bottom: averaging enforces pairwise equality of indices n, n' in tensor products $\langle\ldots\psi_n\ldots\bar{\psi}_{n'}\ldots\rangle$, as indicated by red lines. Left: identity pairing of indices within the five factors $\langle \mathrm{tr}_A(\rho_A\rho_A\rho_A\rho_A\rho_A)\rangle$. Right: pairing of indices of the second and fourth factor.

$\mathcal{N}$ and $\mathcal{M}$ carried by ψ and $\bar{\psi}$ is constrained by the summation as $\mathcal{M}_B^i = \mathcal{N}_B^i$ and $\mathcal{M}_A^i = \mathcal{N}_A^{\tau i}$, where $\tau i = (i+1)\mathrm{mod}(r)$. A further constraint, indicated by red lines in the bottom part of the figure, arises from the random phase cancellation under averaging, which in the present notation requires $\mathcal{N}^i \equiv \mathcal{M}^{\sigma i}$, for *some* permutation σ. [The figure illustrates this for the identity, $\sigma = \mathrm{id}.$, and the transposition $\sigma = (2,4)$.] Combining the two constraints, we obtain the representation $M_r = \sum_\sigma \sum_{\mathcal{N}} \prod_i \langle |\psi_{n^i}|^2\rangle \delta_{\mathcal{N}_A,\sigma\circ\tau\mathcal{N}_A}\delta_{\mathcal{N}_B,\sigma\mathcal{N}_B}$. This expression is universal in that it does not require assumptions other than the random phase cancellation. In a less innocent final step we establish contact to the previously discussed local density of states ν_n and compare the two representations $D\nu \equiv \sum_\alpha \delta(E-E_\alpha) = \sum_{n,\alpha}|\psi_{\alpha,n}|^2\delta(E-E_\alpha) = \sum_n \nu_n$ to identify $|\psi_n|^2 = \nu_n/D\nu$. In other words, we identify the moduli $|\psi_n|^2$ of a fixed eigenstate $\psi = \psi_\alpha$ with the realization specific local density of states ν_n at $E = E_\alpha$. For the legitimacy of this replacement for single particle random systems see Ref. [30], and for the SYK model the Supplemental Material [31] and Ref. [25]. With this substitution, we obtain the representation

$$M_r = \sum_\sigma \sum_{\mathcal{N}} \prod_{i=1}^{r} \lambda_{n_i} \delta_{\mathcal{N}_A,(\sigma\circ\tau)\mathcal{N}_A}\delta_{\mathcal{N}_B,\sigma\mathcal{N}_B}, \tag{2}$$

with $\lambda_n \equiv \nu_n/D\nu$. This expression describes two complementary perspectives of quantum states in Fock space: their support on a random energy shell defined by the coefficients $\lambda_n \sim \nu_n$, and random phase cancellations implicit in the combinatorial structure. In the following, we discuss the manifestations of these principles in the above regimes I–IV.

Regime I, maximally random states.—Here, wave functions are uniformly distributed, $\nu_n = \nu$, and the evaluation of Eq. (2) reduces to a combinatorial problem. The latter has been addressed in the string theory literature [37,38] (where high-dimensional pure random states are considered as proxies for black hole micro states.) Inspection of the formula shows that increasing permutation complexity needs to be paid for in summation factors D_B. Keeping only the leading term, $\sigma = \mathrm{id}$, and the next leading single transpositions $\sigma = (ij)$, we obtain $M_r \approx D_A^{1-r} + \binom{r}{2} D_A^{2-r} D_B^{-1}$, and the subsequent differentiation in r yields Page's result [22]

$$S_A - S_{\mathrm{th}} = -\frac{D_A}{2D_B}, \qquad S_{\mathrm{th}} = \ln D_A. \tag{3}$$

Interestingly, higher order terms in the D_A/D_B-expansion vanish in the replica limit [22,37–40], and Eq. (3) is exact for arbitrary $N_A \le N_B$, up to corrections small in $1/D$. (The case $N_A \ge N_B$ follows from exchange $A \leftrightarrow B$.) The result states that to leading order the entropy of the subsystem is that of a maximally random ("thermal") state, S_{th}. The residual term results from wave function interference across system boundaries. Reflecting a common signature of "interference contributions" to physical observables, it is suppressed by a factor proportional to the Hilbert space dimension.

Regime II and III, energy shell entanglement.—The energy shell now is structured and correlations in the local densities $\{\nu_n\}$ lead to a much stronger correction to the thermal entropy. Since these contributions come from the identity permutation (do not involve wave function interference), we ignore for the moment $\sigma \neq \mathrm{id}$, reducing Eq. (2) to $M_r \simeq \sum_l \lambda_{A,l}^r$ with $\lambda_A \equiv \mathrm{tr}_B(\lambda)$. This expression suggests an interpretation of the unit normalized density $\{\lambda_n\}$ as a *spectral measure* $\sum_n \lambda_n = 1$, $\lambda_n \ge 0$ and of λ_A as the reduced density of system A. With this identification, the entropy

$$S_A \approx S_\rho \equiv -\mathrm{tr}_A[\lambda_A \ln(\lambda_A)] \tag{4}$$

becomes the information entropy of that measure.

This is as far as the model-independent analysis goes. Further progress is contingent on two assumptions, which we believe should be satisfied for a wide class of systems in their regimes II and III: First, the exponentially large number of sites entering the computation of the spectral measure justifies a self-averaging assumption,

$$\sum_{n_X} F(v_{n_X}) \approx D_X \langle F(v_X)\rangle_X \equiv \frac{D_X}{\sqrt{2\pi}\Delta_X}\int dv_X \exp\left(-\frac{v_X^2}{2\Delta_X^2}\right) F(v_X), \tag{5}$$

where $X = A, B, AB$ stands for the two subsystems, or the full space, respectively, D_X are the respective Hilbert space dimensions, and $\Delta_X = \delta\sqrt{N_X}$. In other words, we replace the sum over site energies by an average over a single variable whose Gaussian distribution follows from the

central limit theorem. Second, when integrated against the distribution of subsystem energies v_B, the local density of states at zero energy $E \simeq 0$ acts as a smeared δ function, setting the additive energy $v = v_A + v_B \simeq 0$, and effectively smoothing the distribution $\lambda_{A,l}$. Since $\kappa \ll \Delta_2 \sim \Delta_B$, the detailed value of the width of the shell κ is of no significance in this construction.

Under these assumptions, straightforward computations detailed in the Supplemental Material [31] yields, e.g., the density of states as $D\nu = \sum_{AB} \nu_n \approx D\langle \delta_\kappa(v)\rangle_{AB} = D/(\sqrt{2\pi N\delta})$. Applied to the computation of the moments Eq. (2), the averaging procedure obtains the entanglement entropy as [31]

$$S_A - S_{\text{th}} = -\frac{1}{2}\ln\left(\frac{N}{N_B}\right) + \frac{1}{2}\frac{N_A}{N} - \sqrt{\frac{N}{2N_A}\frac{D_A}{2D_B}}. \quad (6)$$

A number of comments on Eq. (6) are needed: Provided the above assumptions on the spectral measure hold, the result has the same level of rigor as Page's formula Eq. (3). The main difference is that (for small subsystems, $N_A \ll N$) the information entropy $S_A - S_{\text{th}} \approx -\frac{1}{4}(N_A/N)^2$ is exponentially enhanced compared to the correction in Eq. (3). Also note that there is no dependence on the disorder strength (see Supplemental Material [31] for more details).

Comparison to phenomenological models.—The entanglement entropy (6) is a universal signature of *correlations* (but not the volume) of the energy shell. Conversely, the WFMs $|\psi_n|^{2q}$ describe the shrinking of the shell volume (but not its correlations). To see that these are independent pieces of information, it is instructive to compare to the random energy model [41], a phenomenological model replacing the one-body randomness by a set of statistically independent Fock state potentials $\{v_n\}$. For increasing δ, the WFMs diminish as in microscopic models [42]. However, we have verified that the EE of REM states coincides with Page's Eq. (3). The same result is obtained for sparse random states [21], as even more phenomenological proxies of many-body states. What is the origin of the difference to Eq. (6)? A genuine many-body model describes many "bodies," representing the microscopic degrees of freedom. The Fock space is an outer product over the single body spaces, and the Hamiltonian contains only operators coupling $\mathcal{O}(1)$ of these degrees of freedom. In this sense the REM is *not* a many-body model, since its nonlocal energy operator acts on the products of all (or most) degrees of freedom simultaneously. Specifically, it lacks the principle of energy subsystem additivity $E = E_A + E_B$, required by Eq. (6). In this way, the entanglement entropy becomes a sensitive indicator of whether quantum states are genuine many-body states or of different origin.

Regime boundaries.—Upon approaching the boundary to the trivially ergodic regime I, the second condition gets compromised, i.e., the width κ of individual states ceases to be small compared to the statistical fluctuations $\sim\Delta_B$. Leaving a detailed analysis of the crossover region to future work, our numerics below shows a collapse of Eq. (6) to Eq. (3) upon crossing the regime boundary. In the opposite MBL regime IV, eigenstates are concentrated on a small number $\mathcal{O}(1)$ of isolated Fock states, and the concept of an energy shell becomes meaningless: to exponential accuracy in N, remote Fock states, even if they are close in energy, have no common matrix elements with individual eigenstates.

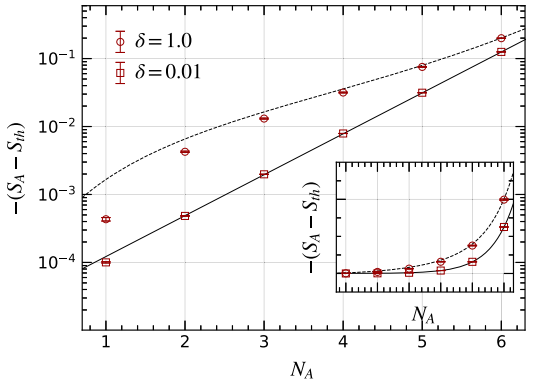

FIG. 2. Numerical entanglement entropies (symbols) vs analytical (lines) for a system of size $N = 15$ in regime I, $\delta = 0.01$ (solid) and III, $\delta = 1$ (dashed). Inset: linear scale representation of the same data.

The entanglement entropy then scales as $S_A \sim s(\delta/\delta_c)N_A/N$, where s is related to the entropy of the distribution of the localized eigenstate in Fock space. For $1 \ll N_A \ll N$, $S_A \ll 1$ stays small down to $\delta \sim \delta_c$, where it jumps to $S_A \sim N_A$ at the localization transition to regime III.

Numerical analysis.—Figure 2 shows a comparison of the analytical predictions of Eqs. (3) and (6) with numerical results obtained for the SYK Hamiltonian [31]. In that case, $\hat{H}_4 = (1/4!)\sum_{i,j,k,l=1}^{2N} J_{ijkl}\hat{\chi}_i\hat{\chi}_j\hat{\chi}_k\hat{\chi}_l$, where $\{\hat{\chi}_l\}$ are Majorana operators [43,44]. The competing one-body operator reads $\hat{H}_2 = \sum_{i=1}^{N} m_i(2c_i^\dagger c_i - 1)$, where $c_i = \frac{1}{2}(\hat{\chi}_{2i-1} + i\hat{\chi}_{2i})$ are complex fermion operators defined by the Majoranas [45,46]. Referring to the Supplemental Material [31] for details, the agreement is very good, and it becomes better with increasing N_A. (We have no certain explanation for the deviations at the smallest values of N_A.)

Discussion.—In this Letter, we applied a combined analysis of the statistics and the entanglement properties of pure quantum states to explore the delocalized phase of disordered many-body systems subject to long-range correlations. Our analysis supports the view that the appealing concept of "nonergodic extended states"—adopted including in publications of the present authors [25,42]—should be abandoned in favor of a qualified interpretation of many-body quantum ergodicity. Its key element is the support set

$\{n\}$ of states of a given energy, the quantum analog of an energy shell. We have shown how the entanglement properties of pure quantum states reveal ergodicity and in addition characteristic correlations distinguishing the energy shells of genuine many-body systems from those of phenomenological proxies.

What is the scope of the above findings? Referring to the Supplemental Material [31] for a more detailed discussion, the freedom to adjust the exponents α, β entering the definition of the model Hamiltonian, implies that our result applies to a wide class of *effectively* long-range interacting systems, among them realizations whose interaction operators are short range in a microscopic ("real space") basis but long range in the eigenbasis of $\hat{H}_2$. It is tempting to speculate on generalizations to yet wider system classes. To this end, we note that the derivation of Eq. (6) relies on a number of necessary conditions: subsystem additivity $E \simeq E_A + E_B$ (requiring that the coupling energy between the subsystems is negligibly small in the limit of large system sizes), statistically independent distribution of the energies $E_{A,B}$, and dependence of the spectral density (measure) on no more than the single conserved quantity, energy. Whether these criteria are not only required but actually sufficient to stabilize the result is an interesting question left for forthcoming research [47]. However, regardless of the scope of Eq. (6), we reason that the combination of wave function statistics and pure state entanglement defines the suitable diagnostic to characterize the ergodic phase of many-body quantum chaotic systems.

D. A. H. thanks Vir Bulchandani and Sarang Gopalakrishnan for helpful discussions. F. M and T. M. acknowledge financial support by Brazilian agencies CNPq and FAPERJ. A. A. acknowledges partial support from the Deutsche Forschungsgemeinschaft (DFG) within the CRC network TR 183 (Project Grant No. 277101999) as part of projects A03. The work of M. T. was supported in part by JSPS KAKENHI Grants No. JP17K17822, No. JP20K03787, and No. JP20H05270. D. A. H. is supported in part by DOE Grant No. DE-SC0016244.

[1] B. L. Altshuler, Y. Gefen, A. Kamenev, and L. S. Levitov, Quasiparticle Lifetime in a Finite System: A Nonperturbative Approach, Phys. Rev. Lett. **78**, 2803 (1997).
[2] D. Basko, I. Aleiner, and B. L. Altshuler, Metal-insulator transition in a weakly interacting many-electron system with localized single-particle states, Ann. Phys. (Amsterdam) **321**, 1126 (2006).
[3] I. V. Gornyi, A. D. Mirlin, and D. G. Polyakov, Interacting Electrons in Disordered Wires: Anderson Localization and Low-T Transport, Phys. Rev. Lett. **95**, 206603 (2005).
[4] P. G. Silvestrov, Decay of a Quasiparticle in a Quantum Dot: The Role of Energy Resolution, Phys. Rev. Lett. **79**, 3994 (1997).
[5] P. G. Silvestrov, Chaos thresholds in finite Fermi systems, Phys. Rev. E **58**, 5629 (1998).
[6] I. V. Gornyi, A. D. Mirlin, and D. G. Polyakov, Many-body delocalization transition and relaxation in a quantum dot, Phys. Rev. B **93**, 125419 (2016).
[7] I. V. Gornyi, A. D. Mirlin, D. G. Polyakov, and A. L. Burin, Spectral diffusion and scaling of many-body delocalization transitions, Ann. Phys. (Amsterdam) **529**, 1600360 (2017).
[8] A. Rubio-Abadal, J.-Y. Choi, J. Zeiher, S. Hollerith, J. Rui, I. Bloch, and C. Gross, Many-Body Delocalization in the Presence of a Quantum Bath, Phys. Rev. X **9**, 041014 (2019).
[9] J.-Y. Choi, S. Hild, J. Zeiher, P. Schauß, A. Rubio-Abadal, T. Yefsah, V. Khemani, D. A. Huse, I. Bloch, and C. Gross, Exploring the many-body localization transition in two dimensions, Science **352**, 1547 (2016).
[10] M. Schreiber, S. S. Hodgman, P. Bordia, H. P. Lüschen, M. H. Fischer, R. Vosk, E. Altman, U. Schneider, and I. Bloch, Observation of many-body localization of interacting fermions in a quasi-random optical lattice, Science **349**, 842 (2015).
[11] K. Xu, J. J. Chen, Y. Zeng, Y. R. Zhang, C. Song, W. Liu, Q. Guo, P. Zhang, D. Xu, H. Deng, K. Huang, H. Wang, X. Zhu, D. Zheng, and H. Fan, Emulating Many-Body Localization with a Superconducting Quantum Processor, Phys. Rev. Lett. **120**, 050507 (2018).
[12] P. Roushan *et al.*, Spectroscopic signatures of localization with interacting photons in superconducting qubits, Science **358**, 1175 (2017).
[13] A. De Luca, B. L. Altshuler, V. E. Kravtsov, and A. Scardicchio, Anderson Localization on the Bethe Lattice: Nonergodicity of Extended States, Phys. Rev. Lett. **113**, 046806 (2014).
[14] V. E. Kravtsov, I. M. Khaymovich, E. Cuevas, and M. Amini, A random matrix model with localization and ergodic transitions, New J. Phys. **17**, 122002 (2015).
[15] B. L. Altshuler, E. Cuevas, L. B. Ioffe, and V. E. Kravtsov, Nonergodic Phases in Strongly Disordered Random Regular Graphs, Phys. Rev. Lett. **117**, 156601 (2016).
[16] V. E. Kravtsov, B. L. Altshuler, and L. B. Ioffe, Non-ergodic delocalized phase in Anderson model on Bethe lattice and regular graph, Ann. Phys. (Amsterdam) **389**, 148 (2018).
[17] K. S. Tikhonov and A. D. Mirlin, Statistics of eigenstates near the localization transition on random regular graphs, Phys. Rev. B **99**, 024202 (2019).
[18] K. S. Tikhonov and A. D. Mirlin, Critical behavior at the localization transition on random regular graphs, Phys. Rev. B **99**, 214202 (2019).
[19] K. S. Tikhonov and A. D. Mirlin, From Anderson localization on random regular graphs to many-body localization, arXiv:2102.05930.
[20] K. S. Tikhonov and A. D. Mirlin, Eigenstate correlations around many-body localization transition, Phys. Rev. B **103**, 064204 (2021).
[21] G. De Tomasi and I. M. Khaymovich, Multifractality Meets Entanglement: Relation for Nonergodic Extended States, Phys. Rev. Lett. **124**, 200602 (2020).
[22] D. N. Page, Average Entropy of a Subsystem, Phys. Rev. Lett. **71**, 1291 (1993).

[23] M. Haque, P. A. McClarty, and I. M. Khaymovich, Entanglement of mid-spectrum eigenstates of chaotic many-body systems—deviation from random ensembles, arXiv:2008.12782.
[24] Self-consistency enters via the condition $\kappa_n = \pi \sum_m |J_{nm}|^2 \nu_n$, where $|J_{nm}|$ are the matrix elements of the interaction operator (see also Ref. [25]).
[25] F. Monteiro, T. Micklitz, M. Tezuka, and A. Altland, A minimal model of many-body localization, Phys. Rev. Research **3**, 013023 (2021).
[26] Random matrix models such as the Rosenzweig-Porter model [27–29] too may develop structured energy shells comprising multiple interlaced "mini bands." Yet, the absence of a tensor product structure makes these different from the shells of genuine many-body systems.
[27] N. Rosenzweig and C. E. Porter, Repulsion of energy levels in complex atomic spectra, Phys. Rev. **120**, 1698 (1960).
[28] E. Cuevas and V. E. Kravtsov, Two-eigenfunction correlation in a multifractal metal and insulator, Phys. Rev. B **76**, 235119 (2007).
[29] G. De Tomasi, M. Amini, S. Bera, I. M. Khaymovich, and V. E. Kravtsov, Survival probability in generalized Rosenzweig Porter random matrix ensemble, SciPost Phys. **6**, 014 (2019).
[30] V. N. Prigodin, Spatial Structure of Chaotic Wave Functions, Phys. Rev. Lett. **74**, 1566 (1995).
[31] See Supplemental Material at http://link.aps.org/supplemental/10.1103/PhysRevLett.127.030601 which includes Refs. [32–36], for providing details on the analytical calculation of the entanglement entropy and on the numerical calculations for the SYK model.
[32] K. B. Efetov, *Supersymmetry in Disorder and Chaos* (Cambridge University Press, Cambridge, England, 1999).
[33] A. D. Mirlin, Statistics of energy levels and eigenfunctions in disordered systems, Phys. Rep. **326**, 259 (2000).
[34] A. Altland and D. Bagrets, Quantum ergodicity in the SYK model, Nucl. Phys. **B930**, 45 (2018).
[35] K. S. Tikhonov and A. D. Mirlin, Many-body localization transition with power-law interactions: Statistics of eigenstates, Phys. Rev. B **97**, 214405 (2018).
[36] N. Macé, F. Alet, and N. Laflorencie, Multifractal Scalings across the Many-Body Localization Transition, Phys. Rev. Lett. **123**, 180601 (2019).
[37] G. Penington, S. H. Shenker, D. Stanford, and Z. Yang, Replica wormholes and the black hole interior, arXiv:1911.11977.
[38] H. Liu and S. Vardhan, Entanglement entropies of equilibrated pure states in quantum many-body systems and gravity, Phys. Rev. X Quantum **2**, 010344 (2021).
[39] S. K. Foong and S. Kanno, Proof of Page's Conjecture on the Average Entropy of a Subsystem, Phys. Rev. Lett. **72**, 1148 (1994).
[40] J. Sanchez-Ruiz, Simple proof of page's conjecture on the average entropy of a subsystem, Phys. Rev. E **52**, 5653 (1995).
[41] C. L. Baldwin, C. R. Laumann, A. Pal, and A. Scardicchio, The many-body localized phase of the quantum random energy model, Phys. Rev. B **93**, 024202 (2016).
[42] T. Micklitz, F. Monteiro, and A. Altland, Nonergodic Extended States in the SYK Model, Phys. Rev. Lett. **123**, 125701 (2019).
[43] S. Sachdev and J. Ye, Gapless Spin-Fluid Ground State in a Random Quantum Heisenberg Magnet, Phys. Rev. Lett. **70**, 3339 (1993).
[44] A. Kitaev, https://online.kitp.ucsb.edu/online/entangled15/kitaev/ and https://online.kitp.ucsb.edu/online/entangled15/kitaev2/ (2015).
[45] A. M. García-García, B. Loureiro, A. Romero-Bermúdez, and M. Tezuka, Chaotic-Integrable Transition in the Sachdev-Ye-Kitaev Model, Phys. Rev. Lett. **120**, 241603 (2018).
[46] A. R. Kolovsky and D. L. Shepelyansky, Dynamical thermalization in isolated quantum dots and black holes, Eur. Phys. Lett. **117**, 10003 (2017).
[47] (to be published).

Chapter 7

Closing Remarks

One of the central premises of quantum statistical mechanics is that all systems eventually reach thermal equilibrium. The formalization of this concept for closed quantum systems is non-trivial, with the best formulation taking the form of the ETH. However, open questions remain, such as understanding the conditions under which ETH holds for various quantum systems, and exploring how it breaks down into the transition to the MBL phase. Another important question, which we addressed in this thesis, is the potential existence of an intermediate NEE phase between the thermal and localized phases, where states are extended but feature non-ergodic amplitude distributions. Addressing these complex quantum many-body systems presents significant challenges, both theoretically and in terms of practical analytical and numerical approaches. To explore these complexities, the SYK model significantly facilitates numerical and analytical computations. Since the SYK is known to be fully ergodic, in order to address the questions regarding the breakdown of ergodicity into many-body localization, we introduced two modifications to the SYK model. The aim was to probe the transition from ergodic to localized states, with a particular focus on understanding the role of non-ergodic extended states.

In this thesis, we explored the eigenstate properties and energy distributions of two systems, both being comprised of an ergodic SYK Hamiltonian modified with a localization-inducing perturbation. Utilizing both analytical methods and numerical simulations, we investigated the energy and eigenstate statistical properties, as well as entanglement entropy characteristics. While the numerical investigations pertain to two specific models, H_a and H_b, the analytical insights extend to a broader class of systems, particularly those exhibiting long-range interactions in Fock space. The study underscores the importance of incorporating wave-function statistics and entanglement properties in the analysis of ergodic systems, going beyond the conventional focus on energy statistics.

Our main findings were an extension of Page's result on entanglement entropy, applied to disordered many-body systems undergoing a transition to the MBL phase. We demonstrated how quantum interference plays a crucial role in contributing to the entanglement entropy in such systems, especially those with long-range interactions. This contribution is highlighted in the context of localizing systems represented by random matrix models. Additionally, our research offers new perspectives on "non-ergodic extended states" in quantum systems, challenging traditional views and providing insights into wave function ergodicity and eigenstate distribution over energy shells. A key distinction was made between the energy shells of genuine many-body systems and those in high-dimensional random lattice models, based on their entanglement entropies.

A natural extension for future research lies in exploring the dynamics of quantum systems in the NEE regime. This research direction aims to uncover how the unique structural characteristics of the NEE phase, distinguished by its restricted wave function support in Fock space, manifest in time-dependent processes. Central to this investigation will be the examination of quantum relaxation dynamics, transport

properties, and the response to external perturbations within the NEE regime. Utilizing numerical techniques such as time-dependent density matrix renormalization group or continuous-time quantum Monte Carlo methods, alongside analytical approaches grounded in random matrix theory and eigenstate thermalization hypothesis, this research could provide crucial insights into the temporal behavior of disordered quantum systems. A particular focus could be the exploration of how the NEE regime influence the onset of quantum chaos, the spreading of entanglement, and the thermalization processes, potentially leading to a deeper understanding of the phase diagram of disordered quantum systems.

References

[1] T. Micklitz, Felipe Monteiro, and Alexander Altland. Nonergodic Extended States in the Sachdev-Ye-Kitaev Model. *Phys. Rev. Lett.*, 123(12):125701, September 2019.

[2] F. Monteiro, T. Micklitz, Masaki Tezuka, and Alexander Altland. Minimal model of many-body localization. *Phys. Rev. Research*, 3(1):013023, January 2021.

[3] Felipe Monteiro, Masaki Tezuka, Alexander Altland, David A. Huse, and Tobias Micklitz. Quantum Ergodicity in the Many-Body Localization Problem. *Phys. Rev. Lett.*, 127(3):030601, July 2021.

[4] D.M. Basko, I.L. Aleiner, and B.L. Altshuler. Metal–insulator transition in a weakly interacting many-electron system with localized single-particle states. *Annals of Physics*, 321(5):1126–1205, 2006.

[5] I. V. Gornyi, A. D. Mirlin, and D. G. Polyakov. Interacting electrons in disordered wires: Anderson localization and low-T transport. *Phys. Rev. Lett.*, 95(20):206603, November 2005.

[6] John Z. Imbrie. On Many-Body Localization for Quantum Spin Chains. *J Stat Phys*, 163(5):998–1048, June 2016.

[7] Tomaž Prosen, Jan Šuntajs, Janez Bonča, and Lev Vidmar. Quantum chaos challenges many-body localization. *Phys. Rev. E*, 102(6):062144, December 2020.

[8] D. A. Abanin, J. H. Bardarson, G. De Tomasi, S. Gopalakrishnan, V. Khemani, S. A. Parameswaran, F. Pollmann, A. C. Potter, M. Serbyn, and R. Vasseur. Distinguishing localization from chaos: Challenges in finite-size systems. *Annals of Physics*, 427:168415, April 2021.

[9] A. De Luca, B. L. Altshuler, V. E. Kravtsov, and A. Scardicchio. Anderson localization on the bethe lattice: Nonergodicity of extended states. *Phys. Rev. Lett.*, 113(4):046806, July 2014.

[10] K. S. Tikhonov and A. D. Mirlin. Critical behavior at the localization transition on random regular graphs. *Phys. Rev. B*, 99(21):214202, June 2019.

[11] Lara Faoro, Mikhail V. Feigel'man, and Lev Ioffe. Non-ergodic extended phase of the Quantum Random Energy model. *Annals of Physics*, 409:167916, 2019.

[12] V. E. Kravtsov, I. M. Khaymovich, E. Cuevas, and M. Amini. A random matrix model with localization and ergodic transitions. *New J. Phys.*, 17(12):122002, December 2015.

[13] Subir Sachdev and Jinwu Ye. Gapless spin-fluid ground state in a random quantum Heisenberg magnet. *Phys. Rev. Lett.*, 70(21):3339–3342, May 1993.

[14] Alexey Kitaev. http://online.kitp.ucsb.edu/online/ entangled15/kitaev/ .... /kitaev2/ (Talks at KITP on April 7th and May 27th 2015).

[15] Jordan S. Cotler, Guy Gur-Ari, Masanori Hanada, Joseph Polchinski, Phil Saad, Stephen H. Shenker, Douglas Stanford, Alexandre Streicher, and Masaki Tezuka. Black holes and random matrices. *J. High Energ. Phys.*, 2017(5):118, May 2017.

[16] Hrant Gharibyan, Masanori Hanada, Stephen H. Shenker, and Masaki Tezuka. Onset of random matrix behavior in scrambling systems. *J. High Energ. Phys.*, 2018(7):124, July 2018.

[17] Antonio M. García-García and Jacobus J. M. Verbaarschot. Spectral and thermodynamic properties of the Sachdev-Ye-Kitaev model. *Phys. Rev. D*, 94(12):126010, December 2016.

[18] David J. Luitz, Nicolas Laflorencie, and Fabien Alet. Many-body localization edge in the random-field Heisenberg chain. *Phys. Rev. B*, 91(8):081103, February 2015.

[19] Don N. Page. Average Entropy of a Subsystem. *Phys. Rev. Lett.*, 71(9):1291–1294, August 1993.

[20] Mark Srednicki. Chaos and quantum thermalization. *Phys. Rev. E*, 50(2):888–901, August 1994.

[21] J. M. Deutsch. Quantum statistical mechanics in a closed system. *Phys. Rev. A*, 43(4):2046–2049, February 1991.

[22] Marcos Rigol, Vanja Dunjko, and Maxim Olshanii. Thermalization and its mechanism for generic isolated quantum systems. *Nature*, 452(7189):854–858, April 2008.

[23] Adam M. Kaufman, M. Eric Tai, Alexander Lukin, Matthew Rispoli, Robert Schittko, Philipp M. Preiss, and Markus Greiner. Quantum thermalization through entanglement in an isolated many-body system. *Science*, 353(6301):794–800, 2016.

[24] Alexander Wietek and Andreas M. Läuchli. Sublattice coding algorithm and distributed memory parallelization for large-scale exact diagonalizations of quantum many-body systems. *Phys. Rev. E*, 98(3):033309, September 2018.

[25] Francesca Pietracaprina, Nicolas Macé, David J. Luitz, and Fabien Alet. Shift-invert diagonalization of large many-body localizing spin chains. *SciPost Phys.*, 5(5):045, November 2018.

[26] Fritz Haake, Sven Gnutzmann, and Marek Kusiba. *Quantum Signatures of Chaos*. Springer Series in Synergetics. Springer, Cham, Switzerland, fourth edition edition, 2018.

[27] M. L. Mehta. *Random Matrices*. Elsevier, Amsterdam, 3rd ed edition, 2004.

[28] Vadim Oganesyan and David A. Huse. Localization of interacting fermions at high temperature. *Phys. Rev. B*, 75(15):155111, April 2007.

[29] Y. Y. Atas, E. Bogomolny, O. Giraud, and G. Roux. Distribution of the Ratio of Consecutive Level Spacings in Random Matrix Ensembles. *Phys. Rev. Lett.*, 110(8):084101, February 2013.

[30] Alexander Altland and Dmitry Bagrets. Quantum ergodicity in the SYK model. *Nuclear Physics B*, 930:45–68, May 2018.

[31] Alexander D. Mirlin. Statistics of energy levels and eigenfunctions in disordered systems. *Physics Reports*, 326(5):259–382, March 2000.

[32] Konstantin Efetov. *Supersymmetry in Disorder and Chaos*. Cambridge University Press, Cambridge, 1996.

[33] Kevin Truong and Alexander Ossipov. Eigenvectors under a generic perturbation: Non-perturbative results from the random matrix approach. *EPL*, 116(3):37002, November 2016.

[34] Geoff Penington, Stephen H. Shenker, Douglas Stanford, and Zhenbin Yang. Replica wormholes and the black hole interior, April 2020.

[35] Hong Liu and Shreya Vardhan. Entanglement Entropies of Equilibrated Pure States in Quantum Many-Body Systems and Gravity. *PRX Quantum*, 2(1):010344, March 2021.

[36] Antonio M. García-García, Bruno Loureiro, Aurelio Romero-Bermúdez, and Masaki Tezuka. Chaotic-Integrable Transition in the Sachdev-Ye-Kitaev Model. *Phys. Rev. Lett.*, 120(24):241603, June 2018.

[37] Andrey R. Kolovsky and Dima L. Shepelyansky. Dynamical thermalization in isolated quantum dots and black holes. *EPL*, 117(1):10003, February 2017.

[38] K. S. Tikhonov and A. D. Mirlin. Many-body localization transition with power-law interactions: Statistics of eigenstates. *Phys. Rev. B*, 97(21):214205, June 2018.

[39] Nicolas Macé, Fabien Alet, and Nicolas Laflorencie. Multifractal Scalings Across the Many-Body Localization Transition. *Phys. Rev. Lett.*, 123(18):180601, October 2019.

[40] Masudul Haque, Paul A. McClarty, and Ivan M. Khaymovich. Entanglement of mid-spectrum eigenstates of chaotic many-body systems – deviation from random ensembles. *arXiv:2008.12782 [cond-mat]*, August 2020.

Appendix A

Supplementary Material to: "Non-ergodic extended states in the SYK model"

A.1 SUSY Matrix integral in a nutshell

In this section we provide a concise yet self contained derivation of the supersymmetric matrix integral representation for the computation of SYK Green functions.

Generating function

The general starting point for such constructions is the Gaussian integral identity for the inverse elements of $N \times N$-matrices

$$M^{-1}_{nm} = \int D(\bar{\psi}, \psi)\, e^{-\bar{\psi} M \psi} \psi^{\sigma}_{m} \bar{\psi}^{\sigma}_{n}, \tag{A.1}$$

where the $2N$ dimensional 'graded' vector $\psi = (\psi^{\mathrm{b}}, \psi^{\mathrm{f}})^{T}$ contains N-component vectors of commuting and Grassmann variables, $\sigma = \mathrm{b}, \mathrm{f}$, respectively. It is set up such that

the matrix determinants generated by the commuting and the Grassmann integral, respectively, cancel out. The advantage of this design over the alternative replica formalism for the generation of determinant-free representations is that no spurious analytic continuations are involved, which provides a more reliable basis for non-perturbative calculations.

Referring to our discussion in the main text, we represent moments of the wave functions as,

$$I_q = \frac{1}{2i\pi\nu_0}\lim_{\delta\to 0}(2i\delta)^{q-1}\sum_n G^{+(q-1)}_{nn}G^{-}_{nn},$$
$$G^{\pm}_{nn'} = \Big\langle n|(\pm i\delta - \hat{H})^{-1}|n'\Big\rangle, \tag{A.2}$$

where we noted that products of only retarded Green functions do not contribute to the connected average of observables and may be discarded. We now use Eq. (A.1) with the identification $M = \mathrm{diag}(-i[G^+]^{-1}, i[G^-]^{-1}) = -i\sigma_3(i\delta\sigma_3 - \hat{H})$ to generate these moments. To this end we introduce

$$\mathcal{Z}(\alpha,\beta) = \int D(\bar{\psi},\psi)e^{-\bar{\psi}\left(i\delta\sigma_3 - \hat{H} - j(\alpha,\beta)\right)\psi}, \tag{A.3}$$

where $\psi = \{\psi^{s,\sigma}_n\}$ now is a $4D$ component supervector, carrying the Fock-space index n, and the causal index $s = \pm$ in addition to $\sigma = \mathrm{b}, \mathrm{f}$. The source matrix $j(\alpha,\beta) = (\alpha\pi^{\mathrm{b}}\otimes\pi^{+} + \beta\pi^{\mathrm{f}}\otimes\pi^{-})\otimes|n\rangle\langle n|$ contains projectors $|n\rangle\langle n|$ in Fock- space and $\pi^{\sigma/s}$ onto subspaces of specific grading/causality, respectively. It is now straightforward to verify that the product of resolvents appearing in Eq. (A.2) is represented as

$$G^{+(q-1)}_{nn}G^{-}_{nn} = \frac{1}{(q-1)!}\partial_\beta\partial^{q-1}_\alpha\mathcal{Z}|_{\alpha,\beta=0}. \tag{A.4}$$

Effective action

Inserting the SYK-Hamiltonian, Eqs. (1),(2) in the main text, the average over couplings J generates a term quartic in the superfields,

$$\mathcal{Z}(\alpha,\beta) = \int D(\bar{\psi},\psi) e^{-\bar{\psi}\hat{O}\psi - \frac{3J^2}{N^3}\sum_a (\bar{\psi}X_a\psi)(\bar{\psi}X_a\psi),} \tag{A.5}$$

where $\hat{O} \equiv i\delta\sigma_3 - \hat{H}_V - j(\alpha,\beta)$, and $\sum_a$ is a sum over all ordered index quadruples $a = (i,j,k,l)$, $i<j<k<l$. We reorganize the quartic term as $(\bar{\psi}X_a\psi)(\bar{\psi}X_a\psi) = -\mathrm{STr}\left(\psi\bar{\psi}X_a\psi\bar{\psi}X_a\right)$, where the 'dyads' $\psi\bar{\psi}$ represent the composite fields indicated in shading in Fig. 2 of the main text. A Hubbard-Stratonovich decoupling in it via a set of $4D$-dimensional supermatrix fields $A_a = \{A_{a,nn'}^{ss',\sigma\sigma'}\} \sim \{\psi_n^{s\sigma}\bar{\psi}_{n'}^{s'\sigma'}\}$ leads to

$$\mathcal{Z}(\alpha,\beta) = \int DA e^{-\frac{1}{2N}\sum_a \mathrm{STr}(X_aA_a)^2 + \mathrm{STr}\ln\left(\hat{O} + i\frac{c_N\gamma}{\mathcal{N}}\sum_a A_a\right),} \tag{A.6}$$

where $c_N \equiv 4!\mathcal{N}/(2N)^4$, $\mathcal{N} \equiv \binom{2N}{4}$, $\gamma = \frac{J}{2}(2N)^{1/2}$, and the Gaussian integral over ψ has been carried out. We next observe that the 'STr ln' in (A.6) couples only to the linear combination $Y \equiv \frac{1}{\mathcal{N}}\sum_a A_a$. This motivates a variable change $A_a \mapsto Y + A_a$, where $\sum_a A_a = 0$. Enforcing the constraint via Lagrange multipliers, it is straightforward to carry out the Gaussian integral over A_a (see Ref. [30] for a few more details) and to arrive at

$$\mathcal{Z}(\alpha,\beta) = \int DY\, e^{-\frac{1}{2}\mathrm{STr}(Y\mathcal{P}^{-1}Y) + \mathrm{STr}\ln\left(\hat{O} + ic_N\gamma Y\right)}, \tag{A.7}$$

where $\mathcal{P}Y \equiv \frac{1}{\mathcal{N}}\sum_a X_aYX_a^\dagger$. The action of the functional integral defines Eq. (3) of the main text, where we approximated $c_N = 1$ and the source has been suppressed, $j(\alpha,\beta) = 0$. (The precise value of $c_N = 1 + \mathcal{O}(N^{-1})$ only enters the comparison with numerics for small system sizes $N = \mathcal{O}(10^1)$.)

Wave-function statistics

Upon projection onto the Fock-space homogeneous mode, Eq. (A.7) reduces to the effective action of the Rosenzweig-Porter model (see discussion in main text)

$$S[T] = \mathrm{STr}\ln\left(i\delta\sigma_3 - \hat{H}_V - j(\alpha,\beta) + i\gamma\kappa\, Q\right), \tag{A.8}$$

where $Q = T\sigma_3 T^{-1}$. Using the the commutativity of the fluctuations T with $\hat{H}_V$ and cyclic invariance of the 'STr-ln' this expression can be represented as $S[T] = \mathrm{STr}\ln\left(1 + G_V\mathcal{O}_T\right)$, where $G_V^{-1} \equiv i\gamma\kappa\,\sigma_3 - \hat{H}_V$, and $\mathcal{O}_T \equiv T^{-1}\left[i\delta\sigma_3 - j(\alpha,\beta)\right]T$ is an operator in which we need to expand to the order required by the correlation function. For example, to linear order in δ one arrives at the action of the zero-dimensional σ-model $S_\delta[Q] = \pi\nu_0\delta\mathrm{STr}\left(\sigma_3 Q\right)$, where we employed the saddle point solution $\mathrm{tr}_{\mathcal{F}} G_V = -iY_0 = -i\kappa\sigma_3$. In a similar fashion, the source term gives a contribution $S_j[T] = -\sum_{k=1}^{\infty} g_n^k\left(\frac{\alpha^k}{k}[Q_{\mathrm{bb}}^{++}]^k + \beta\alpha^{k-1}[Q_{\mathrm{bb}}^{++}]^{k-1}Q_{\mathrm{ff}}^{--}\right)$, where $g_n \equiv \frac{-i\pi\nu_0}{D(\kappa^2+v_n^2)}$, and we approximated $Q_{\mathrm{bf}}^{+-}Q_{\mathrm{fb}}^{-+} \simeq Q_{\mathrm{bb}}^{++}Q_{\mathrm{ff}}^{--}$ [31]. Doing the derivatives in the source parameters, we then obtain

$$\partial_\alpha^{q-1}\partial_\beta\mathcal{Z}|_{\alpha,\beta=0} = g_n^q q!\,\langle\left[Q_{\mathrm{bb}}^{++}\right]^{q-1}Q_{\mathrm{ff}}^{--}\rangle, \tag{A.9}$$

We finally need to average over the soft mode fluctuation implied by the average $\langle ...\rangle = \int dQ\, e^{-S_\delta[Q]}(\dots)$. Referring for details of this to Ref. [32] we here sketch the principal steps of this calculation. The starting point is a 'polar coordinate' representation, $Q = UQ_0U^{-1}$, where $Q_0 = \left(\begin{smallmatrix}\cos\hat{\theta} & i\sin\hat{\theta}\\ -i\sin\hat{\theta} & -\cos\hat{\theta}\end{smallmatrix}\right)$ is a matrix in causal space and we introduced the diagonal supermatrix $\hat{\theta} = \mathrm{diag}(i\hat{\theta}_{\mathrm{b}}, \hat{\theta}_{\mathrm{f}})$ containing compact and non-compact angles $0 < \theta_{\mathrm{f}} < \pi$ and $\theta_{\mathrm{b}} > 0$, respectively [32]. U is a diagonal matrix in causal space which contains the four Grassmann variables $\eta^{\pm}, \bar{\eta}^{\pm}$, and two more commuting variables $0 \le \phi, \chi < 2\pi$. In this representation, the matrix elements entering the correlation

function are given by $Q^{++}_{\rm bb} = \cosh\theta_{\rm bb}(1-4\bar\eta^+\eta^+)$ and $Q^{--}_{\rm ff} = \cos\theta_{\rm ff}(1-4\bar\eta^-\eta^-)$, and the integration measure reads $dQ = \frac{1}{2^6\pi^2}\frac{\sinh\theta_{\rm b}\sin\theta_{\rm f}}{(\cosh\theta_{\rm b}-\cos\theta_{\rm f})^2}d\phi d\chi d\theta_{\rm b}d\theta_{\rm f}d\bar\eta^+d\eta^+d\bar\eta^-d\eta^-$ [32]. The essential advantage of the polar representation is that the action only depends on the 'radial variables' $S_\delta[Q] = 2\pi\nu_0\delta(\cosh\theta_{\rm b}-\cos\theta_{\rm f})$. This shows how the integration over the non-compact angle is cut by the parameter δ at values $1 \le \lambda \equiv \cosh\theta_{\rm b} \lesssim 1/\delta$, while the integration over the compact angles $\theta_{\rm f}$ is free. With these structures in place, it is straightforward to obtain

$$G^{+(q-1)}_{nn}G^{-}_{nn} \simeq 2q(q-1)g_n^q\int_0^\infty d\lambda\,\lambda^{q-2}e^{-2\pi\nu_0\delta\lambda}. \tag{A.10}$$

Doing the final integral and collecting all factors we arrive at Eq. (6) in the main text.

Level-level correlations

The two level correlation function $K(\omega) = \nu_0^{-2}\langle\nu(\omega/2)\nu(-\omega/2)\rangle$ probing spectral statistics in the middle of the band can be obtained in similar ways. Starting from the representation,

$$K(\omega) = \frac{1}{\pi^2\nu_0^2}\langle{\rm Im\,tr}\,G(\tfrac{\omega}{2}){\rm Im\,tr}\,G(-\tfrac{\omega}{2})\rangle, \tag{A.11}$$

we introduce a source matrix $j(\alpha,\beta) = (\alpha\pi^{\rm b}\otimes\pi^+ + \beta\pi^{\rm f}\otimes\pi^-)$ into the action generalized for finite frequency differences, $i\delta\sigma_3 \to (\omega/2+i\delta)\sigma_3$ in Eq.(3) of the main text. From this representation, the function K is obtained as $K(\omega) = \frac{1}{2\pi^2\nu_0^2}{\rm Re}\,\partial^2_{\alpha\beta}\mathcal{Z}|_{\alpha,\beta=0}$. Proceeding as in the computation of the wave-function moments, one obtains [32]

$$K(\omega) = \frac{1}{2}{\rm Re}\int_1^\infty d\lambda_{\rm b}\int_{-1}^1 d\lambda_{\rm f}\,e^{i\pi\nu_0(\lambda_{\rm b}-\lambda_{\rm f})}, \tag{A.12}$$

where $\lambda_{\rm b} \equiv \lambda$ is the non-compact bosonic angle introduced above and $\lambda_{\rm f}$ the compact fermionic angle. These integrals can be carried out in closed form, and yield the two-point correlation function of the Gaussian Unitary Ensemble, $K(s) = 1 - \frac{\sin^2(\pi s)}{(\pi s)^2} + \delta(s)$, with $s = \omega\nu_0$. This demonstrates that the presence of an inhomogeneous diagonal in the Green functions affects the wave function moments, but not the spectral correlation functions [33]. The reason for this is that the wave function moments — formally obtained as powers of Green function matrix elements — respond more sensitively to the presence of a fluctuating diagonal than the spectral correlation function — obtained via tracing over single Green functions.

Appendix B

Supplementary Material to: "A minimal model of many body localization"

B.1 Derivation of the action (??)

We here derive the action Eq. (**??**) from the averaged functional (**??**). We start by rewriting the quartic term as $(\bar{\psi}\hat{X}_a\psi)^2 = \mathrm{STr}((\psi\bar{\psi}\hat{X}_a)^2)$. To decouple this non-linearity, we multiply the functional with the unit normalized Gaussian integral $1 = \int DA\, \exp\Big(-\frac{1}{2}\sum_a \mathrm{STr}(A_a\hat{X}_a)^2\Big)$, where $DA \equiv \prod_a dA_a$, and $A_a = \{A_{nn'}^{ss',\sigma\sigma'}\}$ are $4D$-dimensional matrices. A shift $A_a \to A_a + w\psi\bar{\psi}$ then removes the quartic term, and the subsequent integration over ψ leads to

$$\mathcal{Z}[j] = \int DA\, e^{-\frac{1}{2}\sum_a \mathrm{STr}(A_a\hat{X}_a)^2 - \mathrm{STr}\log\left(\hat{G}^{-1} + w\sum_a A_a\right)},$$

where $\hat{G}^{-1} = z - \hat{H}_2$, and we changed $A_a \mapsto \hat{X}_a A_a \hat{X}_a$. We now observe that the nonlinear part of the action couples only to the combination $\sum_a A_a$. This motivates

the definition, $A_a = \frac{i}{\rho}(Y + Y_a)$, where the factor of i is included for later convenience, and $\sum_a Y_a = 0$. Adding a Lagrange multiplier $\frac{i}{\rho}\sum_a \mathrm{STr}(Y_a\Lambda)$ to enforce the constraint, we are led to consider the functional $\mathcal{Z}[j] = \int DY D\Lambda \exp(-S[Y,\Lambda])$, with action

$$S[Y,\Lambda] = -\frac{1}{2\rho^2}\sum_a \mathrm{STr}((Y+Y_a)P_a(Y+Y_a)) + \frac{i}{\rho}\sum_a \mathrm{STr}(\Lambda Y_a) + \mathrm{STr}\log\Big(\hat{G}^{-1} + iwY\Big),$$

where $\rho = \binom{2N}{4}$ and we defined the operator $\hat{P}_a B = \hat{X}_a B \hat{X}_a$. Note that $\hat{P}_a$ is self-inverse, $\hat{P}_a^2 B = \hat{X}_a^2 B \hat{X}_a^2 = B$, and hermitian in the sense that $\mathrm{STr}(C\hat{P}_a B) = \mathrm{STr}(\hat{P}_a C B)$. We now do the Gaussian integrals over Y_a to obtain,

$$S[Y,\Lambda] = -\mathrm{STr}\Big(\frac{\rho}{2}\Lambda\mathcal{P}\Lambda + i\Lambda Y\Big) + \mathrm{STr}\log\Big(\hat{G}^{-1} + iwY\Big),$$

where $\mathcal{P} = \frac{1}{\rho}\sum_a \hat{P}_a$. The Gaussian integration over Λ may now be performed and after rescaling $Y \to \rho^{1/2}Y$, and defining $\gamma = w\rho^{1/2} = \frac{J}{2}(2N)^{1/2}$ we obtain the action $S[Y] = -\frac{1}{2}\mathrm{STr}(Y\mathcal{P}^{-1}Y) + \mathrm{STr}\log\Big(z - \hat{H}_2 + i\gamma Y\Big)$. In a final step, we perform a linear transformation $\mathcal{P}^{-1}Y \to Y$, and recall that in our units $J^2 = 2/N$ and $\gamma = 1$, to arrive at Eq. (**??**).

B.2 The operator $\mathcal{P}$

In this Appendix, we discuss the action of the operator $\mathcal{P}$ states $|n\rangle\langle n|$ diagonal in the occupation number basis. To this end, note that for a state $|n\rangle = |n_1, \ldots, n_i, \ldots, n_N\rangle$, the action of the Majorana operator $\hat{\chi}_{2i} = c_i + c_i^\dagger$ produces the state $|n_i\rangle \equiv \hat{\chi}_{2i}|n\rangle = |n_1, \ldots, \bar{n}_i, \ldots, n_N\rangle$, where $\bar{n}$ is 0 for $n = 1$, and vice versa. Similarly, $\hat{\chi}_{2i-1}|n\rangle = i(-)^{n_i}|n_i\rangle$. Except for n_i all other occupation numbers remain unchanged, and no superpositions of states are generated. The adjoint action thus generates $\hat{\chi}_{2i}|n\rangle\langle n|\hat{\chi}_{2i} =$

$\hat{\chi}_{2i-1}|n\rangle\langle n|\hat{\chi}_{2i-1} = |n_i\rangle\langle n_i|$, which we interpret as nearest neighbor hopping in Fock space. Notice that $(\hat{\chi}_{2i}\hat{\chi}_{2i-1})|n\rangle\langle n|(\hat{\chi}_{2i-1}\hat{\chi}_{2i}) = |n\rangle\langle n|$ leaves the state unchanged.

With these structures in place, it is straightforward to describe the action of $\mathcal{P}|n\rangle\langle n| = \frac{1}{\rho}\sum_a \hat{X}_a|n\rangle\langle n|\hat{X}_a$. The summation contains contributions changing the particle number $|n|$ by $0, 2$ and 4. With $\mathcal{P}_{n,m} = \langle m|(\mathcal{P}|n\rangle\langle n|)|m\rangle$, the diagonal contribution, $\mathcal{P}_0$ is obtained from the $\binom{N}{2}$ terms of the structure $\hat{\chi}_{2i}\hat{\chi}_{2i+1}\hat{\chi}_{2\beta}\hat{\chi}_{2\beta+1}$. Similar counting for the contributions changing $|n|$ by two and four gives the matrix elements stated in the main text,

$$\mathcal{P}_0 = \frac{N(N-1)}{2\rho}, \quad \mathcal{P}_2 = \frac{4(N-2)}{\rho}, \quad \mathcal{P}_4 = \frac{16}{\rho}, \tag{B.1}$$

and it is verified that

$$\begin{aligned}
&\sum_m \mathcal{P}_{m,n} \\
&= \binom{N}{0}\frac{N(N-1)}{2\rho} + \binom{N}{2}\frac{4(N-2)}{\rho} + \binom{N}{4}\frac{16}{\rho} \\
&= 1.
\end{aligned} \tag{B.2}$$

B.3 Saddle point equations

In this Appendix we address the solution of the saddle point equation Eq. (**??**). The non-trivial element in this equation is the quantity $\kappa_n \equiv \pi(\mathcal{P}\hat{\nu})_n$ in the denominator. In terms of this quantity, Eq. (**??**) becomes the simple algebraic equation (**??**). A closed yet site non-local equation for κ is obtained by acting on Eq. (**??**) with the

operator $\mathcal{P}$,

$$\begin{aligned}\kappa_n &= \sum_m \mathcal{P}_{|n-m|}\mathrm{Im}\frac{1}{v_m - i\kappa_m} \\ &= \sum_m \mathcal{P}_{|n-m|}\mathrm{Re}\int_0^\infty dt\, e^{iv_m t-\kappa_m t},\end{aligned}$$

where in the second line switch to a temporal Fourier representation to facilitate the treatment of the argument v_m. The solution of this equation relies on two conceptual elements, first the ansatz Eq. (**??**) and second a replacement of the sum over the ρ neighboring sites m by a Gaussian average over energies v_m. Specifically, we note that up to corrections small in N^{-1}, the neighbor sites m are separated by Hamming distance 4 from n and each change in n_i changes $v_n \mapsto v_n \pm 2v_i$. This means that $v_m = v_n + v$, where we assume v to be Gaussian distributed with width $\sqrt{4}2\delta = 4\delta$. Substituting the ansatz $\kappa_m = \kappa\Theta(C - |v_m|)$ into the equation, and splitting the integral over v into regions with $C - |v_m| = C - |v_n + v|$ smaller and larger than zero, respectively, we obtain after shifting $v \mapsto v - v_n$

$$\begin{aligned}\kappa_n &= \frac{1}{\sqrt{32\pi}\delta}\mathrm{Re}\int_0^\infty dt \\ &\times \left(\int dv\, e^{-\frac{(v-v_n)^2}{32\delta^2}} + \int_{-C}^{C} dv\, e^{-\frac{(v-v_n)^2}{32\delta^2}}\left(e^{-\kappa t} - 1\right)\right) e^{ivt}.\end{aligned}$$

With $\mathrm{Re}\int_0^\infty dt\, e^{ivt} = \pi\delta(v)$, the first and the third term in the second line cancel out, and the t-integration of the second term gives

$$\kappa_n = \frac{\sqrt{\pi}}{\sqrt{32}\delta}\int_{-C}^{C} dv\, e^{-\frac{(v-v_n)^2}{32\delta^2}}\frac{\kappa}{\pi(v^2+\kappa^2)}, \tag{B.3}$$

where the notation emphasizes that the κ-dependent term effectively represents a δ-function $\delta_\kappa(v) = \frac{\kappa}{\pi(v^2+\kappa^2)}$ in v, smeared over scales $\sim \kappa$. This expression defines the mean field amplitude κ_n at site n in dependence of the tolerance window C for the

energy v_n, and κ itself. We now explore for which configurations (C, κ) it represents a self consistent solution.

The details of this analysis depend on wether we work with weakly (I, II) or strongly (III, IV) distributed on-site energies.

Strong on-site disorder III, IV: Anticipating that all solutions satisfy $\kappa \ll 1$, the width of $\delta_\kappa(v)$ is much smaller than that of the Gaussian weight, δ. The function δ_κ thus collapses the integral, and we obtain

$$\kappa_n = \frac{\sqrt{\pi}}{\sqrt{32}\delta} e^{-\frac{v_n^2}{32\delta^2}}. \tag{B.4}$$

This is consistent with our ansatz with $C = 2\delta$ and $\kappa \sim \delta^{-1}$.

Narrow on-site disorder I, II: In this regime, we test for the validity of the ansatz with $C = 1$ and $\kappa = 1$. First assume $|v_n| > 1 = C \gg \delta$. In this case, the ansatz requires exponentially suppressed κ, the δ_v-function again becomes effective, and the integral collapses to $\kappa_n = \frac{\sqrt{\pi}}{\sqrt{32}\delta} \exp\left(-\frac{v_n^2}{32\delta^2}\right)$ consistent with the assumed smallness of κ. Conversely, for $|v_n| < 1 = C$, the ansatz requires $\kappa = 1$. The function $\delta_\kappa = \delta_1$ is now much wider than the width of the Gaussian, $\sim \delta$, and the integration boundaries can be extended to infinity. Doing the integral, we obtain $\kappa_n \equiv \kappa = 1/\kappa$, or $\kappa = 1$, consistent with Eq. (**??**).

B.4 Effective matrix theory

In this appendix we discuss the derivation of Eqs. (**??**) and (**??**) from Eq. (**??**). In Eq. (**??**), we substitute $Y \to \pi\hat{\nu}\hat{Q}$ with $Q_n = T_n \sigma_3 T_n^{-1}$. The expansion of the action in fluctuations then comprises three parts: the Gaussian weight, the expansion of the 'Str log' in site-to-site fluctuations, and the expansion of the 'Str log' in small frequency arguments, z (reflecting the non-commutativity, $[z, T_n] \neq 0$.)

Gaussian weight: A straightforward substitution yields

$$\begin{aligned} &-\frac{1}{2}\mathrm{STr}(Y\mathcal{P}Y) \to -\frac{\pi^2}{2}\mathrm{STr}(\hat{\nu}\hat{Q}\mathcal{P}(\hat{\nu}\hat{Q})) \\ &= -\frac{\pi^2}{2}\sum_{nm}\nu_n\nu_m P_{|n-m|}\mathrm{Str}Q_nQ_m, \end{aligned} \tag{B.5}$$

where 'STr' includes the Fockspace trace, while 'Str' is only over internal degrees of freedom.

Fluctuation action: Substituting the ansatz into the 'Str log' and temporarily neglecting the frequency arguments, z, we obtain

$$\begin{aligned} &\mathrm{STr}\log\Big(-\hat{H}_2 + i\pi\mathcal{P}(\hat{\nu}\hat{Q})\Big) \\ &= \mathrm{STr}\log\Big(-\hat{H}_2 + i\hat{T}^{-1}\pi\mathcal{P}(\hat{\nu}\hat{Q})\hat{T}\Big) \\ &= \mathrm{STr}\log\Big(-\hat{H}_2 + i\pi\mathcal{P}(\hat{\nu}\sigma_3) + i\pi[\hat{T}^{-1}\mathcal{P}(\hat{\nu}\hat{Q})\hat{T} - \mathcal{P}(\hat{\nu}\sigma_3)]\Big) \\ &\simeq \mathrm{STr}\log\Big(1 + \pi^2\hat{\nu}\sigma_3[\hat{T}^{-1}\mathcal{P}(\hat{\nu}\hat{Q})\hat{T} - \mathcal{P}(\hat{\nu}\sigma_3)]\Big) \\ &\simeq \pi^2\mathrm{STr}(\hat{\nu}\sigma_3[\hat{T}^{-1}\mathcal{P}(\hat{\nu}\hat{Q})\hat{T} - \mathcal{P}(\hat{\nu}\sigma_3)]) \\ &= \pi^2\mathrm{STr}(\hat{\nu}\hat{Q}\mathcal{P}(\hat{\nu}\hat{Q})), \end{aligned} \tag{B.6}$$

identical to $(-2\times)$ the Gaussian weight. In the second line we used the cyclic invariance $\mathrm{STr}\log(\dots) = \mathrm{STr}\log\Big(\hat{T}^{-1}(\dots)\hat{T}\Big)$, and in the fourth the saddle point equation $(-\hat{H}_2 + i\pi\mathcal{P}(\hat{\nu}\sigma_3))^{-1} = -i\pi\hat{\nu}\sigma_3$.

Frequency action: In a similar manner, we obtain

$$\begin{aligned} &\mathrm{STr}\log\Big(-\hat{H}_2 + i\pi\mathcal{P}(\hat{\nu}\hat{Q}) + z\Big) \\ &\simeq \mathrm{STr}\log\Big(\hat{T}(-\hat{H}_2 + i\pi\mathcal{P}(\hat{\nu}\sigma_3))\hat{T}^{-1} + z\Big) \\ &= \mathrm{STr}\log\Big(-\hat{H}_2 + i\pi\mathcal{P}(\hat{\nu}\sigma_3) + \hat{T}^{-1}z\hat{T}\Big) \\ &\simeq -i\pi\mathrm{STr}(\hat{\nu}\sigma_3\hat{T}^{-1}z\hat{T}) = -i\pi\mathrm{STr}(\hat{\nu}\hat{Q}z), \end{aligned} \tag{B.7}$$

where in the second line, we neglected local fluctuations $P(\hat{\nu}\hat{T}\sigma_3\hat{T}^{-1}) \simeq \hat{T}P(\hat{\nu}\sigma_3)\hat{T}^{-1}$, in the third used cyclic invariance, and in the fourth the saddle point condition.

Combining terms, we obtain the effective action (**??**).

B.5 Wave function and spectral statistics from matrix model

In this section we provide details on the computation of wave-function and spectral statistics in the deformed $\hat{H}_4$ model. The starting point for both statistics is Eq. (**??**), with sources $j = J_K$ or $J = J_{I,n}$, respectively, given in Eq. (**??**). Using the commutativity $[T, \hat{H}_2] = 0$ we represent the action as

$$S[T] = \mathrm{STr}\log\left(1 + \hat{G}\mathcal{O}_T\right) = \sum_{k=1}^{\infty} \frac{(-1)^k}{k} \mathrm{STr}(\hat{G}\mathcal{O}_T)^k,$$

where $\mathcal{O}_T \equiv T^{-1}\left[z - j(\alpha,\beta)\right]T$ is an operator in which we need to expand to the order required by the correlation function, and we have made the source contribution, $j(\alpha,\beta)$, to the matrix $z = \frac{\omega+i\eta}{2}\sigma_3$ explicit again. Concerning the resolvent, $\hat{G}^{-1} \equiv i\hat{\kappa}\,\sigma_3 - \hat{H}_2$, we notice that fluctuation variables commute through the real part of $\hat{G}$, and keep only $i\,\mathrm{Im}\hat{G} = -i\pi\hat{\nu}$, with local components ν_n defined in Eq. (**??**). Specifically, to zeroth order in the sources, and first order in an expansion in $z\nu_n \sim \omega/\Delta$, the action assumes the form (**??**).

For the computation of the spectral and wave function statistics, we need the expansion in sources to first order in β and higher orders in α. With the above definitions, the expansion of the action assumes the form

$$S[T] = -\pi \sum_{k=1}^{\infty} (-i\nu_n\alpha)^k \left(\frac{1}{k}[Q_{\mathrm{bb}}^{++}]^k + \frac{\beta}{\alpha}[Q_{\mathrm{bb}}^{++}]^{k-1}Q_{\mathrm{ff}}^{--}\right), \tag{B.8}$$

where in the terms $k > 2$ we used the approximation $Q^{+-}_{\rm bf} Q^{-+}_{\rm fb} \simeq Q^{++}_{\rm bb} Q^{--}_{\rm ff}$ valid in the limit $\eta \to 0$ implied in the calculation of wave function moments [32]. Doing the derivatives in the source parameters, we arrive at

$$\partial_\alpha^{q-1} \partial_\beta \mathcal{Z}|_{\alpha,\beta=0} = (-i\pi\nu_n)^q \, q! \, \langle \left[Q^{++}_{\rm bb} \right]^{q-1} Q^{--}_{\rm ff} \rangle, \tag{B.9}$$

where $\langle ... \rangle = \int dQ \, e^{-S_z[Q]} (\dots)$.

The remaining integral over the four-dimensional matrix Q is conceptually straightforward but technically the hardest part of the calculation. Referring for details to Ref. [32], we here review the main steps. The starting point is a 'polar coordinate' representation $Q = U Q_0 U^{-1}$ with Q_0 defined in Eq. (**??**), $\hat{\theta} = {\rm diag}(i\hat{\theta}_{\rm b}, \hat{\theta}_{\rm f})$ containing compact and non-compact angles $0 < \theta_{\rm f} < \pi$ and $\theta_{\rm b} > 0$, respectively [32]. The matrix U is block-diagonal in causal space and contains four Grassmann variables $\eta^{\pm}, \bar{\eta}^{\pm}$, and two more commuting variables $0 \leq \phi, \hat{\chi} < 2\pi$. More specifically, $U = {\rm diag}(u_1 u_2, v)_{\rm ra}$, where $u_2 = {\rm diag}(e^{i\phi}, e^{i\hat{\chi}})_{\rm bf}$ and supermatrices $u_1 = e^{-2\hat{\eta}^+}$, $v = e^{-2i\hat{\eta}^-}$, generated by $\hat{\eta}^{\pm} = \left(\begin{smallmatrix} 0 & \bar{\eta}^{\pm} \\ -\eta^{\pm} & 0 \end{smallmatrix} \right)_{\rm bf}$. In this representation, the matrix elements entering the correlation function are given by $Q^{++}_{\rm bb} = \cosh\theta_{\rm bb}(1 - 4\bar{\eta}^+\eta^+)$ and $Q^{--}_{\rm ff} = \cos\theta_{\rm ff}(1 - 4\bar{\eta}^-\eta^-)$, and the integration measure reads $dQ = \frac{1}{2^6\pi^2} \frac{\sinh\theta_{\rm b} \sin\theta_{\rm f}}{(\cosh\theta_{\rm b} - \cos\theta_{\rm f})^2} d\phi d\hat{\chi} d\theta_{\rm b} d\theta_{\rm f} d\bar{\eta}^+ d\eta^+ d\bar{\eta}^- d\eta^-$ [32]. The essential advantage of the polar representation is that the action only depends on the 'radial variables' $S_\eta[Q] = -i2\pi\nu(\omega + i\eta)(\cosh\theta_{\rm b} - \cos\theta_{\rm f})$.

Wave function statistics: In the calculation of the wave function moments, we may set $\omega = 0$. The integration over the non-compact angle is then cut by the parameter η at values $1 \leq \cosh\theta_{\rm b} \lesssim 1/\eta$, while the integration over the compact angles $\theta_{\rm f}$ is free. With this simplification, the integration over all variables except the non-compact one,

θ, becomes elementary, and one obtains [32]

$$G_{nn}^{+(q-1)}G_{nn}^{-} = 2q(q-1)\,(-i\pi\nu_n)^q \\ \times \int_0^\infty d\theta_{\rm b}\,\sinh\theta_{\rm b}\,(\cosh\theta_{\rm b})^{q-2}\,e^{-2\pi\nu\eta\cosh\theta_{\rm b}}. \tag{B.10}$$

The final integral gives $(2\pi\nu\eta)^{1-q}q!$ and collecting all factors we arrive at

$$I_q = \frac{q!}{\nu^q}\sum_n \nu_n^q. \tag{B.11}$$

This result expresses the qth moment of the local wave function amplitudes through that of the local density of states individually averaged over $\hat{H}_4$ fluctuations. The energies v_n at each individual site are obtained as sums of N random coefficients v_i (cf. Eq. (**??**)). For large N, this makes the sum self averaging, and we replace $I_q \to \langle I_q\rangle_v$ by its average over single particle energies, v_i. Using Eq. (**??**), we thus obtain

$$I_q = \frac{(-)^{q-1}q}{(\pi\nu)^q}\sum_n(\kappa_n)^q\left\langle \partial_{(\kappa_n)^2}^{q-1}\frac{1}{v_n^2+(\kappa_n)^2}\right\rangle.$$

The evaluation of this expression now depends on which on-site disorder regime we are in. In regime I, $\delta < N^{-1/2}$, or $|v_n| < 1$, the mean field broadening assumes the uniform value $\kappa = 1$. In this case, the dependence of I_q on site energies, v_n, is weak. This implies $\nu \simeq \frac{1}{\pi}\sum_n 1 = D/\pi$. Doing the κ derivatives, we obtain

$$I_q = q!D^{1-q}, \qquad \text{regime I}, \tag{B.12}$$

which is the RMT result for a matrix of dimension D.

For larger disorder, only a fraction of sites have finite decay width. Using Eq. (**??**) and assuming self averaging to replace the n-sum to an average over a distribution of

site energies of width δN, the DoS is evaluated as

$$\begin{aligned}\nu &\simeq \frac{1}{\pi}\frac{D}{\sqrt{2\pi N\delta^2}}\int_{-C}^{C} dv\, e^{-\frac{v^2}{2N\delta^2}}\frac{\kappa}{v^2+\kappa^2}\\ &\simeq \frac{1}{\pi}\frac{D}{\sqrt{2\pi N\delta^2}}\int_{-C}^{C} dv\,\frac{\kappa}{v^2+\kappa^2}\\ &= \frac{1}{\pi}\frac{2D}{\sqrt{2\pi N\delta^2}}\arctan(C/\kappa),\end{aligned}$$

where in the second line we used that the distribution of energies is much wider than the tolerance window C. Substituting the values specified in Eq. (**??**), this leads to

$$\nu = c\frac{D}{\sqrt{N}\delta}, \tag{B.13}$$

where c is of order unity and the suppression relative to $\nu = cD$ in regime I accounts for the improbability to find resonant sites.

In the same manner, we obtain

$$\begin{aligned}I_q &\simeq \frac{(-)^{q-1}q}{(\pi\nu)^q}\frac{D}{\sqrt{2\pi N\delta^2}}\kappa^q\partial_{\kappa^2}^{q-1}\int_{-C}^{C} dv\, e^{-\frac{v^2}{2N\delta^2}}\frac{1}{v^2+\kappa^2}\\ &\simeq \frac{(-)^{q-1}q}{(\pi\nu)^q}\frac{D}{\sqrt{2\pi N\delta^2}}\kappa^q\partial_{\kappa^2}^{q-1}\int_{-C}^{C} dv\,\frac{1}{v^2+\kappa^2}\\ &= 2\frac{(-)^{q-1}q}{(\pi\nu)^q}\frac{D}{\sqrt{2\pi N\delta^2}}\kappa^q\partial_{\kappa^2}^{q-1}\frac{1}{\kappa}\arctan(C/\kappa)\\ &\simeq 2\frac{(-)^{q-1}q}{(\pi\nu)^q}\frac{D}{\sqrt{2\pi N\delta^2}}\kappa^q\partial_{\kappa^2}^{q-1}\frac{1}{\kappa}\\ &= \frac{1}{(\pi\nu)^q}\frac{D}{\sqrt{2\pi N\delta^2}}\frac{2q(2q-3)!!}{(2\kappa)^{q-1}},\end{aligned}$$

where '$\simeq$' here means equality up to some constant $c \sim \mathcal{O}(1)$. Insertion of Eq. (B.13) leads to Eq. (**??**). Using Eq. (**??**), we finally obtain

$$q \gg 1: \qquad I_q = c^q q! \left(\frac{D}{\sqrt{N}}\right)^{1-q} \begin{cases} \delta^{q-1}, & \text{II}, \\ \delta^{2(q-1)}, & \text{III}. \end{cases} \tag{B.14}$$

Finally, for a quantitative comparison to numerical simulations in regime III without fitting parameter we trace all constants $c \sim \mathcal{O}(1)$ in ν and I_q. Noting that in regime III we can substitute $\arctan(C/\kappa) = \pi/2$ we arrive at,

$$I_q = \frac{q(2q-3)!!}{(2\pi\nu\kappa)^{q-1}} = \frac{q(2q-3)!!}{\delta^{2(1-q)}} \left(\frac{\pi D}{4\sqrt{N}}\right)^{1-q}, \qquad \text{III} \tag{B.15}$$

where in the second equality we used Eq. (B.4) for κ.

Level-statistics: For the level statistics we need to keep finite ω, and differentiate the functional to first order in α and β (Eq. (**??**)). Application of Eq. (B.9) then leads to [32]

$$K(\omega) = \frac{1}{2}\mathrm{Re}\int_0^\infty d\theta_\mathrm{b} \int_{-\pi/2}^{\pi/2} d\theta_\mathrm{f} \times \sinh\theta_\mathrm{b} \sin\theta_\mathrm{f} e^{i\pi\nu\omega(\cosh\theta_\mathrm{b} - \cos\theta_\mathrm{f})}, \tag{B.16}$$

where θ_b and θ_f are the non-compact bosonic and compact fermionic angle, respectively. These integrals can be carried out in closed form, and yield the two-point correlation function of the Gaussian Unitary Ensemble (**??**).

B.6 Localization criterion

In this Appendix we demonstrate how the solution of the eigenvalue Equation (**??**) reduces to the criterion (**??**). We write the sum as

$$\Phi_n = \frac{2\sqrt{\pi}}{\sqrt{\rho}} \sum_{|n-m|=4} a_{nm}\Phi_m,$$
$$a_{nm} = \sqrt{\nu_n\nu_m}\log\left(\frac{\rho}{(2\pi)^2\nu_n\nu_m}\right),$$

and make the self consistent assumption that the sum over neighboring sites m is dominated by resonant sites, and that the solution, Φ_n, too, are peaked at those sites. Under these conditions it makes sense to consider a zeroth order approximation $a_{nm} \simeq a^0_{nm} \equiv \sqrt{\nu_n\nu_m}2\log\left(\sqrt{\rho}/2\pi\nu_m\right)$, neglecting site-to-site fluctuations of the logarithm. In a final step we will refine the result by perturbation theory in $\delta a_{nm} \equiv a_{nm} - a^0_{nm} = \sqrt{\nu_n\nu_m}\log\left(\nu_m/\nu_n\right)$. Making the replacement $a_{nm} \to a^0_{nm}$, we observe that the equation is solved by $\Phi_n \propto \sqrt{\nu_n}$, provided that

$$1 = \frac{4\sqrt{\pi}}{\sqrt{\rho}} \sum_m \nu_m \log\left(\frac{\sqrt{\rho}}{2\pi\nu_m}\right), \tag{B.17}$$

where the sum extends over the $Z \equiv \binom{N}{4}$ sites in Hamming distance 4 to n (i.e. the parameter Z defines the effective coordination number of the Fock space lattice.) We note that with the above eigenstates the first order perturbative correction to the unit eigenvalue Eq. (B.17) is given by $\langle\Phi|\delta\alpha|\Phi\rangle \propto \sum_{nm}\nu_n\nu_m\log(\nu_n/\nu_m) = 0$, which we take as a self consistent justification to work with the zeroth order approximation. Turning to the consistency equation for the eigenvalue, we again replace the sum over nearest neighbors by an average over their distribution of energies (cf. a similar operation in

Appendix B.3):

$$\sum_m \nu_m f(\nu_m) \simeq Z\langle \nu(v) f(\nu(v))\rangle_v \simeq Z\frac{f\left(\frac{\sqrt{32}\delta}{\sqrt{\pi}}\right)}{\sqrt{32\pi}\delta},$$
$$\langle \dots \rangle_v = \frac{1}{\sqrt{2\pi}4\delta}\int dv\, e^{-\frac{v^2}{32\delta^2}}(\dots).$$

Here, the second equality is based on the observation that on the subset of active sites, $v < \delta$, where $\nu(v)$ is non-vanishing, and $\nu(v) = \frac{\pi}{\delta(v^2+\delta^{-2})}$ becomes a δ-function of width $\sim \delta^{-1}$ and height $\nu(0) = \pi/\kappa$ with $\kappa = \frac{\sqrt{\pi}}{\sqrt{32}\delta}$ (cf. Eq. (B.4)). The integral collapses to this resonance region, leading to the stated result. (Effectively, this is saying that only resonant sites contribute to the nearest neighbor sum.)

Application of this auxiliary identity to the eigenvalue equation Eq. (B.17) leads to

$$1 = \frac{1}{\sqrt{2\rho}}\frac{Z}{\delta}\log\left(\sqrt{\frac{8\rho}{\pi}}\delta\right), \tag{B.18}$$

which is solved by

$$\delta_c = \frac{Z}{\sqrt{2\rho}}W\left(2Z\sqrt{\pi}\right), \tag{B.19}$$

with W the Lambert-W function.

For $N \gg 1$, we may approximate $Z = \binom{N}{4} \simeq N^4/24$ and $\rho = \binom{2N}{4} \simeq (2N)^4/4!$. The asymptotic expansion for large arguments, $W(x) \simeq \log(x) + \dots$ then leads to the estimate Eq. (**??**) in the main text.

Appendix C

Supplementary Material to: "Quantum ergodicity in the many-body localization problem"

C.1 Entanglement entropy and local density of states

In this section we discuss the derivation of Eq. (2) describing the entanglement entropy in terms of the local density of states. The construction parallels a similar one for the wave functions of single particle systems [32, 31], (see also Ref. [2] for a recent extension to Fock space), and we limit ourselves to an outline of the main construction steps.

Moments of the reduced density matrix from Fock space resolvents

Working in a first quantized representation—where the Hamiltonian $\hat{H}$ is considered as a high dimensional matrix—our starting point is a representation of the reduced

density matrix, $M_r(A) = \langle \mathrm{Tr}_A(\rho_A^r)\rangle$, in terms of retarded/advanced resolvent operators, $G_E^{\pm} = (E \pm i\eta - \hat{H})^{-1}$. Introducing a formal Lehmann representation in term of exact eigenstates, it is straightforward to verify the likewise exact relation

$$M_r = \frac{(2i)^{r-2}}{\pi\nu_E} \lim_{\eta\to 0} \eta^{n-1} \langle \mathrm{tr}_A \left(\left(\mathrm{tr}_B[G_E^+] \right)^{r-1} \mathrm{tr}_B[G_E^-] \right) \rangle, \tag{C.1}$$

where ν_E is the density of states at energy E.

Construction of the matrix integral

Following Efetov's supersymmetry approach [32, 31], we next represent the Green function matrix elements in Eq. (C.1) as Gaussian integrals. This representation is obtained from the auxiliary formula $M^{-1}_{nm} = \int D(\bar{\psi},\psi)\, e^{-\bar{\psi}M\psi} \psi^\sigma_m \bar{\psi}^\sigma_n$, where M is a general $L \times L$ matrix and the $2L$ dimensional 'graded' vector $\psi = (\psi^{\mathrm{b}}, \psi^{\mathrm{f}})^T$ contains L-commuting components ψ^{b}_n, and an equal number of Grassmann components ψ^{f}_n. The double integral over these variables cancels unwanted determinants $\det(M)$, while the pre-exponential factors, either commuting or anti-commuting, $\sigma = \mathrm{b}, \mathrm{f}$, isolate the inverse matrix element. With the identification $M = \mathrm{diag}(-i[G^+]^{-1}, i[G^-]^{-1}) = \eta - i\sigma_3\hat{H}$, we are then led to consider the generating function

$$\mathcal{Z}[j] = \int D(\bar{\psi},\psi) \left\langle e^{-\bar{\psi}\left(i\eta\sigma_3 - \hat{H}\right)\psi + S_J} \right\rangle, \tag{C.2}$$

where we focus on the band center $E = 0$, the average $\langle ... \rangle$ is with respect to random coefficients of the Hamiltonian $\hat{H}$, σ_3 is a Pauli matrix distinguishing between advanced and retarded components, and $S_J = \sum_n \left(j_n\psi_n + \bar{\psi}_n \bar{j}_n \right)$, with

$$j_n = (\alpha_n \pi^{\mathrm{rr}} + \beta_n \pi^{\mathrm{aa}}) \otimes \pi^{\mathrm{bb}},$$
$$\bar{j}_n = (\bar{\alpha}_n \pi^{\mathrm{rr}} + \bar{\beta}_n \pi^{\mathrm{aa}}) \otimes \pi^{\mathrm{bb}}.$$

is a source term from which the required products are obtained by differentiation ($\partial_{\alpha_{n_i}} \equiv \partial_{\alpha_n}|_{n=n_i}$):

$$\sum_{\sigma\in S_{r-1}} G^R_E(n^1, m^{\sigma(1)})...G^R_E(n^{r-1}, m^{\sigma(r-1)})G^A_E(n^r, m^r) = \prod_{l=1}^{r-1} \partial_{\bar{\alpha}_{m^l}}\partial_{\alpha_{n^l}}\partial_{\bar{\beta}_{m^r}}\partial_{\beta_{n^r}}\mathcal{Z}[j].$$

Here, $\pi^{rr/aa}$ and π^{bb} are projectors onto the subspaces of retarded/advanced and commuting variables, respectively. With this identity, and using the permutation symmetry of Green function matrix elements under trace, we obtain

$$M_r = c_r \lim_{\eta\to 0} \eta^{r-1} \sum_{\{n^l\}} \prod_{l=1}^{r-1} \partial_{\bar{\alpha}_{m^l}}\partial_{\alpha_{n^l}}\partial_{\bar{\beta}_{m^r}}\partial_{\beta_{n^r}}\mathcal{Z}[j], \tag{C.3}$$

where $c_r \equiv (2i)^{r-2}/(\pi\nu_E(r-1)!)$ and the differentiation arguments m^i are fixed as $m^l = (n^{l+1}_A, n^l_B)$, $l = 1\dots r-1$, and $m^r = (n^1_A, n^r_B)$. Using the notation in the man text this can be summarized as $\mathcal{M}^i_B = \mathcal{N}^i_B$ and $\mathcal{M}^i_A = \mathcal{N}^{\tau i}_A$, where $\tau i = (i+1)\mathrm{mod}(r)$.

Effective action

We now average over the random parameters of the interaction Hamiltonian and then apply constructions steps standard in the theory of disordered electronic systems[32, 31] and transferred to the SYK context in Refs. [30, 2]. In regimes I-III, this procedure maps the generating function onto the integral $\mathcal{Z}[j] = \int \mathcal{D}Q\, e^{-S[Q]+S_J[Q]}$, where $Q = Q\otimes 1_{\mathrm{Fock}}$ is a 4×4 matrix in the spaces of advanced/retarded and commuting/anticommuting indices and

$$S_\eta[Q] = \pi\eta\,\mathrm{STr}(\hat{\nu}Q\sigma_3), \quad S_J[Q] = -i\pi\mathrm{STr}\left(\bar{j}\hat{\nu}Qj\right). \tag{C.4}$$

Here 'STr' refers to the graded trace over Fock and internal degrees of freedom, and $\hat{\nu}$ is a diagonal matrix in Fock space with the local density of states as its diagonal elements, $(\hat{\nu})_n = \nu_n$.

Moments

Performing the $2r$-fold derivative, we arrive at

$$\mathcal{M}_r(A) = c_r \lim_{\eta\to 0} \eta^{r-1} \sum_{\sigma\in S_r} \sum_{\mathcal{N}} \nu_{n^1} ... \nu_{n^r}$$
$$\times \langle Q^{\mathrm{rr}}_{\mathrm{bb}} ... Q^{\mathrm{rr}}_{\mathrm{bb}} Q^{\mathrm{aa}}_{\mathrm{bb}} \rangle \delta_{\mathcal{N}_A, \sigma\circ\tau(\mathcal{N}_A)} \delta_{\mathcal{N}_B, \sigma(\mathcal{N}_B)}, \tag{C.5}$$

where the average $\langle ... \rangle$ is over the action Eq. (C.4). In a final step, we perform the matrix integral to obtain

$$c_r \eta^{r-1} \langle [Q^{\mathrm{rr}}_{\mathrm{bb}}]^{r-1} Q^{\mathrm{aa}}_{\mathrm{bb}}] \rangle = \frac{1}{(D\nu)^r}, \tag{C.6}$$

In this way, the identification of wave function moduli with coefficients of the local density of states fundamental to Eq. (2) of the main text is established.

C.2 Entanglement entropy in regimes II/III

Leading contribution

Central to the analysis of the wave function moments is the reduced spectral density, $\lambda_{A,l} = \frac{1}{D\nu} \langle \delta_\kappa(v_l + v_B) \rangle_B$. Performing the Gaussian average Eq. (5) of the main text, we obtain $D\nu = D\langle \delta_\kappa(v) \rangle_{AB} = \frac{D}{\sqrt{2\pi N \delta}}$ and similarly $\lambda_{A,l} = \frac{1}{D_A} \frac{\Delta}{\Delta_B} \exp(-v_l^2/2\Delta_B^2)$.

As discussed in the main text, the leading contribution to the entanglement entropy comes from the identity permutation

$$M_r^{\rm id}(A) = D_A D_B^r \langle \lambda_A^r \rangle_A. \tag{C.7}$$

Substituting the above result for λ_A and performing the Gaussian average, we obtain

$$M_r^{\rm id}(A) = \frac{D_A^{1-r} N_A^{r/2}}{\sqrt{1 + r N_A/N_B}}. \tag{C.8}$$

Subleading contribution

Single transpositions $\sigma = (ij)$, give the subleading contribution to the entanglement entropy. Inspection of Eq.(2) of the main text (see also the index configuration defined by the right part of the bottom panel of Fig.1) shows that they provide a contribution $M_r^\sigma = \sum_{l_1,l_2} \sum_{m_1,\ldots,m_{r-1}} \lambda_{l_1 m_1} \nu_{l_2 m_1} \lambda_{l_1 m_2} \ldots \lambda_{l_1 m_{r-1}}$ to the rth moment. Following the same recipe as above, we substitute $\lambda_{l,m} = (D\nu)^{-1}\delta(v_m + v_l)$ and the index summations by Gaussian averages over the energy variables $v_m \to v_A$ and $v_l \to v_B$. It is then straightforward to obtain

$$M_r^\sigma = \frac{D_A^{2-r}}{D_B} \frac{N^{r/2}}{\sqrt{N_A}} \frac{N_B^{(2-r)/2}}{\sqrt{2N_B + (r-1)N_A}}. \tag{C.9}$$

Noting that there are $\binom{r}{2}$ such terms, the differentiation in r yields the entropy Eq.(6).

Remaining contributions

In regime I, the leading and subleading contributions discussed above give the Page entropy Eq. (3) in the main text [19]. Permutations that are not the identity or single transpositions vanish. This cancellation has been discussed in the string theory

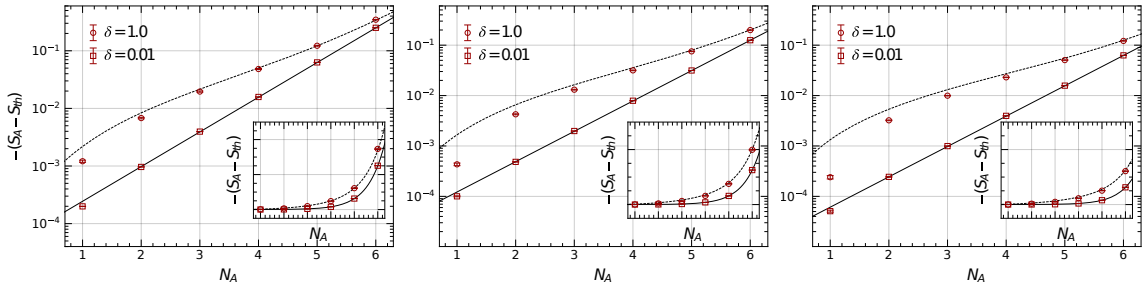

Fig. C.1 Numerical entanglement entropies (symbols) vs. analytical (lines) for a system of size $N = 14$ (left), 15 (middle), 16 (right) in regime I, $\delta = 0.01$ (solid) and III, $\delta = 1$ (dashed). Inset: linear scale representation of the same data.

literature [34, 35], and the arguments presented there also apply to regimes II & III. (Basically, the combinatorial factor for contributions with a given number of transpositions are the Narayana numbers and vanish for more than one transposition in the replica limit.) We thus conclude that Eq. (6) describes the entanglement entropy in regime III, at the same level of rigor as Page's result in regime I.

Comment on crossover to Regime I

The crossover between Page's result and our Eq. (5) can be worked out, but requires a more elaborate analysis of above integrals without approximating the local density of states by a δ-function. We leave this analysis for future work.

C.3 Exact diagonalization

We numerically calculated the reduced density matrix and the average entanglement entropy for generic eigenstates (in the center of the band) of the SYK Hamiltonian $\hat{H} = \hat{H}_4 + \hat{H}_2$, where $\hat{H}_4 = \frac{1}{4!}\sum_{i,j,k,l=1}^{2N} J_{ijkl}\hat{\chi}_i\hat{\chi}_j\hat{\chi}_k\hat{\chi}_l$, and the free particle contribution [36, 37] $\hat{H}_2 = \frac{1}{2}\sum_{i,j=1}^{2N} J_{ij}\hat{\chi}_i\hat{\chi}_j$. Matrix elements $\{J_{ijkl}\}$ and $\{J_{ij}\}$ are drawn from Gaussian distributions with vanishing mean and variances $\langle|J_{ijkl}|^2\rangle = 6J^2/(2N)^3$ and $\langle|J_{ij}|^2\rangle = \delta^2/2N$. The many body band width, Δ_4, of the interaction operator and the distribution

width, Δ_2, of the on-site random potential then read $\Delta_4 = \sqrt{\frac{3J^2}{4N^3}\binom{2N}{4}}$ and $\Delta_2 = \sqrt{\frac{\delta^2}{2N}\binom{2N}{2}}$, respectively. For our calculations, we generate at least 100 realizations of the Hamiltonians (H_4, H_2), taking the average of the entanglement entropy over eigenstates corresponding to energies within the middle 1/7th of the spectrum, unless otherwise mentioned. Here, the even and odd fermion parity sectors are diagonalized separately. We further improve the statistics by averaging over all $\binom{N}{N_A}$ Fock space bi-partitions.

In Fig. 2 and Fig. C.2 (see below), the error bar shows the standard deviation of the results over the realizations of the Hamiltonians. The two parity sectors are treated as separate samples. We observe an increasing ratio of this error bar to the value of $S_{\text{th}} - S_A$ for diminishing subsystem size N_A. The reason is the exponential diminishing of $S_{\text{th}} - S_A$ with decreasing N_A, which leads to relatively larger numerical fluctuations around this value. We have no certain explanation for the observation that in regime III (and I) results for smallest N_A lie outside the estimated error bar (see also Fig. C.1).

A subtlety in these calculations is that the SYK Hamiltonian conserves fermion parity. Considering the density matrix ρ defined by an eigenstate with definite parity, the partial trace leads to a block diagonal structure $\rho_A = \text{tr}_B \rho = \begin{pmatrix} \rho_A^e & \\ & \rho_A^o \end{pmatrix}$ with matrices ρ_A^e and ρ_A^o acting in the even and odd fermion parity subspaces of the subsystem A Hilbert space. A trace over the two-dimensional parity sector defines the (normalized) reduced density matrix $\text{tr}_P \rho_A = \rho_A^e + \rho_A^o$. One can then convince oneself that $\text{tr}_P \rho_A$ has the same entropy as the reduced density matrix of a pure state in the 2^{N-1} system with broken fermion parity conservation. This can be also verified by comparing our results in the fully ergodic phase to Page's prediction for a Fock space of dimension $D = 2^{N-1}$, as shown (by the dashed line) in Fig. 2 of the main text.

Variation of entanglement entropy with disorder

Our analytical analysis predicts the formation of a δ-independent plateau of the entanglement entropy in regime III. In Fig. C.2 we show the numerically calculated entanglement entropy for the system sizes $N = 14, 15, 16$, as a function of δ, and for different partitions N_A. For the limited system sizes accessible to exact diagonalization, the observation of a true plateau seems out of reach. However, one can see the formation of the plateau around $\delta = 1$ which becomes more pronounced with increasing N_A and N. At the same time, the value $\delta = 1$ defines the "center" of regime III. This follows from the recent work Ref. [2] by some of the present authors, where the regimes I-IV were characterized in terms of their WFMs. (On the same basis, $\delta = 0.01$ is well within regime I.) While we cannot exclude a coincidence, the respective regime centers as determined by wave function statistics show the best agreement between numerics and analytics for the entropies.

C.4 Generalization

Within the above class of strong interaction coupled models, there is some freedom in the specific realization of the $\hat{H}_2$ eigenstates. Broadly speaking, this setup is realized in 3 types of settings: *i*) The system may not have any other geometry beyond that specified by the matrix elements of $\hat{H}_4$, as in a SYK model. *ii*) The single-particle eigenstates of $\hat{H}_2$ may be localized in a d-dimensional real-space, and the couplings in $\hat{H}_4$ are such that the long-range couplings dominate (e.g., a power-law in space that decays slowly enough) [38]. In these first two cases, as we take the limit of large N, the sparsity of the interactions can be adjusted with N to set α, but we require $\alpha > 0$. *iii*) The single-particle eigenstates of $\hat{H}_2$ may be all delocalized in real space. In this case, even local interactions couple all-to-all and for density-density interactions,

for example, we will have $\alpha = 4$. In all three cases, as we take the limit of large N, the strength of the interactions can be adjusted with N to set β. Our analysis does not apply to models of MBL with only short-range interactions (see e.g. the recent numerical study Ref. [39] on the multifractal scalings across the MBL transition). At the same time, it does not specifically exclude this case, and it seems natural that the ergodicity picture extends to it. However the corroboration of that belief requires further study. (For very recent work on the entanglement entropy of extended random systems, see Ref. [40].)

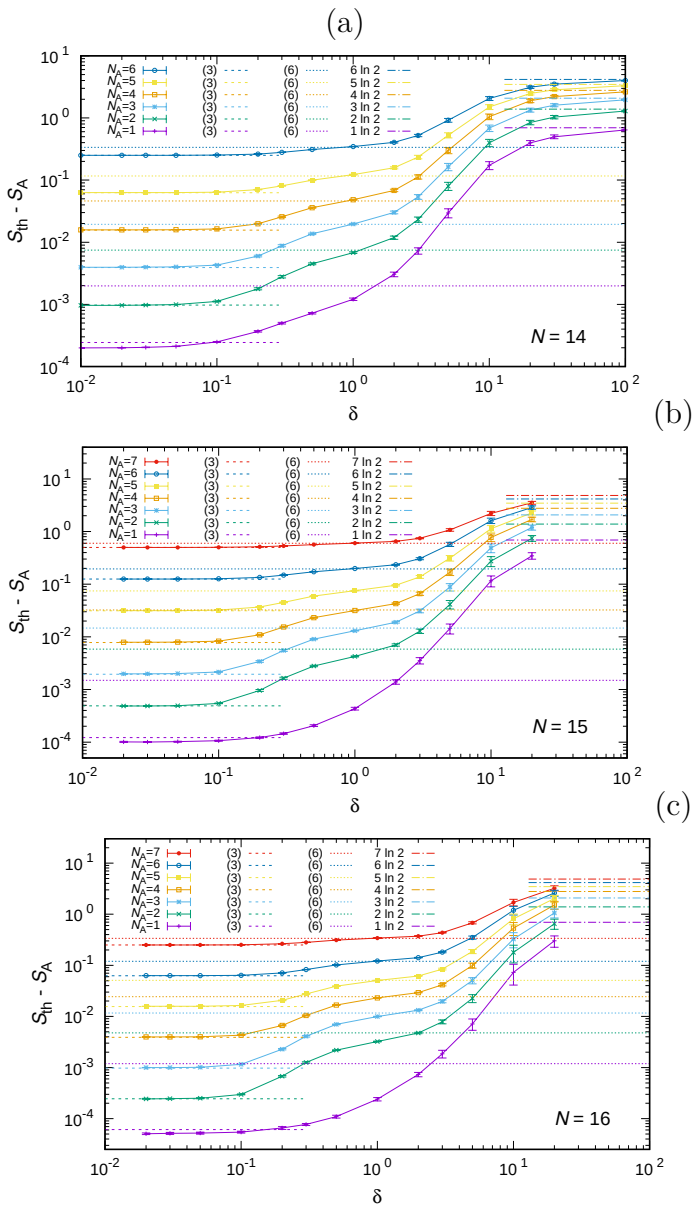

Fig. C.2 Entanglement entropy as a function of the disorder strength δ for different partitions N_A, (a) $N = 14$, 104 realizations of the Hamiltonian and 1171 eigenvectors (1/7 of the entire spectrum) are used. (b) $N = 15$, 100 realizations of the Hamiltonian and 100 eigenvectors ($\sim 0.6\%$) are used. (c) $N = 16$, at least 12 realizations of the Hamiltonian and 20 eigenvectors ($\sim 0.06\%$) are used.